Study of the effect of Diamond-Like Carbon coatings deposition process parameters on their tribomechanical and corrosion properties for different metallic substrates

Authors: Alejandro Chicahuala Casabone
Martín Clarke

Director: Lisandro Escalada, PhD.

Co-directors: Daniel Heim, PhD.
Christian Forsich, PhD.

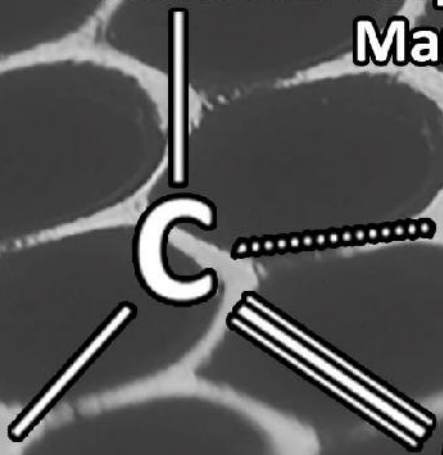

FACULTAD DE INGENIERÍA

UNIVERSIDAD NACIONAL de MAR DEL PLATA

Recubrimientos de carbono símil diamante depositados en diferentes sustratos metálicos. Estudio de su comportamiento tribomecanico y su resistencia a la corrosión en basea los parámetros del proceso de deposición

Autores: Alejandro Chicahuala Casabone
Martín Clarke

Director: Dr. Lisandro Escalada

Co-directores: Dr. Daniel Heim
Dr. Christian Forsich

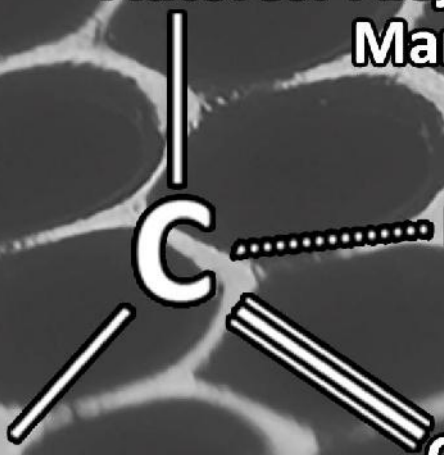

FACULTAD DE INGENIERÍA

UNIVERSIDAD NACIONAL de MAR DEL PLATA

ACKNOWLEDGEMENTS

Our project could not have been done without the help and support of many people and institutions.

Firstly, we would like to thank immensely to our final project director, PhD Lisandro Escalada, and our former director, nowadays soon-to-be retired, PhD Silvia Simison. With their guidance and support all along the way, we could finish this project and sorted out the many difficulties we faced along the path. They supported us via video conference call during our stay in Wels, personally in our return, and once again virtually during the current COVID-19 pandemic lockout. Additionally, Silvia handled the arrangements for our stay in Wels, and made possible for us to live that wonderful adventure. We are forever grateful for this.

We want to thank our co-directors as well, PhD Daniel Heim and PhD Christian Forsich, in charge of the Surface and Coatings Technology department of FHÖO Wels. They helped us immensely in everything we needed, helped us to design the project layout, handled every supply needed, explained us the details of every test and made us feel welcome every day of our stay.

We are extremely grateful with everyone in FHÖO Wels, especially with the International Office and the Surface and Coatings Technology (Tribolab) department staff. Angela and Kamilla from the International Office do their job amazingly, providing every international student with everything needed, and functioning as a coordination with the different departments of FHÖO Wels. Together with Silvia, they handled every detail needed for our transfer to Wels, such as accommodation and legal paperwork, and provided us with every information needed during our stay. Our colleagues in the Tribolab, Bernd Rübig, Christian Mairhoffer and Daniel Peterbauer, were so supportive with us, explained us in detail every test method we needed, and were great company on our everyday activities. We would like to make a special mention for Christian, who designed the immersion test device used in this project as part of his own Bachelor thesis project.

We would like to thank Rübig GmbH. immensely. They funded our stay during the six months we lived in Wels, provided us with every sample used for this project and did the nitriding pre-process in the samples needed as well. We were able to have a guided tour in their facilities as well, thanks to our partner in the Tribolab, Dipl. Bernd Rübig, which we enjoyed so much.

Thanks so much to every professor and colleague in the Engineering Faculty of Universidad Nacional de Mar del Plata. Without them, we would not have been able to present this project. The learning process during all these years was very complete, we acquired so many concepts that we applied during the elaboration of our work.

Finally, we would like to thank all our friends and family, especially to Ana and Teddy, Martín's parents, and Alicia and Daniel, Alejandro's parents. Their unconditional love and

support either in good or bad times is the most important fuel to complete our goals. We would not be the persons we are today without them, and they are one of the most important parts of our achievements.

Index

Abstract

DLC coatings have attracted the interest of many researches due to their unique combination of properties. They are often used in various applications as protective coatings because of their excellent low friction, high wear resistance and chemical inertness. The focus of this work was to analyse tribological, mechanical and anti-corrosive properties of coatings varying in chemical composition, substrate material, surface treatment and deposition process parameters. One of the mail goals was to evaluate a possible effect of the silicon doping on the corrosive behaviour of the coated samples regarding a possible change in the coating electrical conductivity, but due to the 2020 COVID-19 pandemic this study was not possible to complete.

In the present work, thick (~30µm) and thin (~3µm) Silicon doped DLC (a:C:H:Si) and a Silicon free DLC (a:C:H) were deposited on nitrided or non-nitrided low alloyed and stainless steels, with a thin or thick Silicon interlayer.

The DLC coatings properties were characterized with the following techniques: nanoindentation, scratch test, calogrinding and pin on disk were used for tribomechanical characterization; Raman spectroscopy and confocal microscopy were used to characterize the DLC coating molecular structure and its superficial roughness; corrosion behaviour was analysed after immersion and salt spray chamber tests were performed, optical microscopy, confocal microscopy, scanning electron microscopy and energy dispersive spectroscopy were used for a qualitative analysis of the corrosion properties of the DLC coatings.

In order to effectively compare the different exhibited behaviours regarding corrosion behaviour, the materials selection weighted property index method (WPIM) was applied. The coating thickness and its silicon content resulted the ruling factors to achieve the best corrosion resistance. This effect was mainly related to their synergistic effect in decreasing the passing-through defect density of the DLC coating. The substrate's corrosion resistance also plays a major role, since plasma nitrided AISI 304 coated samples only suffered corrosion damage on the nitriding edge effect zone, a plasma nitriding process generated defect.

With the Raman spectra results of the DLC coatings it was possible to estimate their molecular structure. The silicon doped coatings had lower hydrogen content and sp^3 bonds fraction, but since silicon substitution promotes the formation of Si-C and C-C sp^3 bonds, an increase in the coating hardness was measured. Additionally, the lower bias voltage in the silicon doped coating's deposition process was related to a decrease in the coating's defect density.

Besides the hardness increasing effect of the silicon doping variable, the scratch testing adherence results and their fractographic behaviour was studied. The adherence

between the substrate and the DLC coating increased with the coating’s thickness, due to an increased load carrying capacity, and its superficial roughness, mainly related to the substrate roughness increase after the plasma nitriding process.

Resumen Extendido

El presente trabajo fue realizado en el marco de una colaboración entre la Facultad de Ingeniería de la Universidad Nacional de Mar del Plata y la Universidad de Ciencias Aplicadas de Alta Austria. El proyecto fue gestado y dirigido inicialmente por la Dra. Silvia Simison, que luego fue sucedida por el Dr. Lisandro Escalada, ambos miembros del departamento de Ingeniería de Bioprocesos e Interfases de INTEMA. El foco de este trabajo se centra en analizar las propiedades tribomecánicas, estructurales y anti-corrosivas de recubrimientos de carbono símil diamante, o DLC por sus siglas en inglés (Diamond-like Carbon), depositado sobre sustratos metálicos al variarse distintos parámetros de su proceso de deposición química de vapor asistida por plasma, o PACVD por sus siglas en inglés (Plasma-Assisted Chemical Vapour Deposition).

Nosotros, Alejandro Chicahuala Casabone y Martín Clarke, en ese entonces alumnos de la carrera de Ingeniería en Materiales, vivimos por un período de 6 meses en Wels, Austria. Durante esta primera etapa del proyecto realizamos tareas de laboratorio asociadas a las investigaciones del departamento de Tecnología de Recubrimientos y Superficies de la Universidad de Alta Austria, dirigido por el Dr. Daniel Heim y el Dr. Christian Forsich, además de las correspondientes a nuestro propio proyecto final, enfocándonos en sacar el máximo provecho de diversas técnicas y equipos que no estaban disponibles en nuestra universidad. En la segunda etapa del proyecto, en Argentina, procesamos un gran volumen de datos obtenidos durante la etapa anterior, los analizamos y llevamos a cabo ensayos con técnicas adicionales, cuyo objetivo era el de estudiar la resistencia a la corrosión de los distintos recubrimientos. Lamentablemente, parte de estos ensayos se realizaron de manera acotada o no fue posible realizarlos debido a la cuarentena resultante de la pandemia global del virus COVID-19, que imposibilitó el acceso a los laboratorios de INTEMA por un largo período de tiempo. Finalmente, se logró dar forma al presente escrito, que es la prueba fehaciente de la culminación de nuestros estudios, y pone de manifiesto todos los conocimientos prácticos y teóricos adquiridos durante la carrera de Ingeniería en Materiales.

A continuación, se presenta una breve introducción a los recubrimientos DLC y se exponen, de igual manera, los resultados de este trabajo.

El diamante es el material que posee las propiedades más extremas de cualquier sólido tridimensional real, tal como la más alta densidad atómica, la más alta dureza, el mayor módulo elástico y la mayor conductividad térmica a temperatura ambiente. Además, tiene alta resistividad eléctrica, es químicamente inerte, posee transparencia óptica y muy bajo coeficiente de fricción en diversos sistemas tribológicos. El carbono símil diamante, o DLC, es un material amorfo que consiste de una red desordenada de átomos de carbono con una

mezcla de enlaces hibridizados sp^2 y sp^3. El contenido de enlaces sp^3 le confiere a este material propiedades mecánicas y físicas que, en ciertos aspectos, se asemejan a las del diamante. La gran ventaja de este tipo de materiales radica en las técnicas de deposición a temperatura ambiente de grandes áreas, con bajo costo asociado, y para geometrías complejas. De esta forma se obtienen películas delgadas que pueden ser depositadas sobre todo tipo de sustratos, presentando propiedades deseables como bajo coeficiente de fricción y alta resistencia al desgaste. Estas características hacen de este tipo de recubrimientos una alternativa atractiva para diversas aplicaciones industriales que van desde partes automotrices y dispositivos microelectrónicos de alto rendimiento, hasta cuchillas de afeitar y acabado superficial con fines decorativos.

Las desventajas del DLC radican en la generación de elevadas tensiones residuales compresivas en la película, que provocan su delaminación, y la falta de afinidad química con diversos sustratos, que se traduce en problemas de adherencia. Sin embargo, la naturaleza amorfa de este tipo de recubrimientos permite desarrollar aleaciones al dopar con elementos como H, Cr, Al, N, Si, etc. El silicio, particularmente, es muy utilizado a nivel industrial, tanto para generar una intercapa enlazante entre el sustrato y el DLC, que mejora la adherencia, como elemento dopante en la estructura molecular del film, que reduce las tensiones residuales del recubrimiento, mejora la adherencia, aumenta la dureza y reduce el coeficiente de fricción en ambientes húmedos. Adicionalmente, uno de los objetivos iniciales del presente trabajo era estudiar el posible efecto del dopaje con silicio sobre la conductividad eléctrica del recubrimiento, y, por ende el efecto que podría tener sobre la resistencia a la corrosión de los sustratos recubiertos. Este efecto sería analizado con mediciones de Espectroscopía de Impedancia Electroquímica, una de las técnicas que como se mencionó anteriormente, no pudieron ser completadas.

Se estudian recubrimientos DLC finos y gruesos, de ~3µm y ~30µm respectivamente, con y sin dopaje con silicio, que poseen una intercapa de silicio fina o gruesa como interfase entre el recubrimiento y el sustrato. Además, se utilizan como sustratos dos materiales con una marcada diferencia respecto de su resistencia a la corrosión: acero inoxidable AISI 304 y acero de baja aleación SAE 4140. A su vez, se comparan los posibles efectos que un pretratamiento de nitrurado por plasma sobre ambos sustratos podría tener sobre las propiedades resultantes.

Las distintas propiedades de las películas DLC fueron caracterizadas con las siguientes técnicas:

- Propiedades tribomecánicas:
    - Nanoindentación (dureza)
    - Prueba de resistencia al rayado (adherencia)
    - Calotest (espesor de película)

    - Pin on disk (Desgaste y coeficiente de fricción)
- Espectroscopía Raman (estructura molecular)
- Microscopía Confocal (rugosidad)
- Microscopía Óptica (complementario a diversas técnicas de las listadas)
- Ensayo de Inmersión y Ensayo en Cámara de Niebla Salina (resistencia a la corrosión)
- Microscopía electrónica de barrido y espectroscopía de energía dispersiva (composición de productos de corrosión)

Para poder comparar efectivamente los resultados del análisis cualitativo de la resistencia a la corrosión de los distintos sustratos recubiertos, se aplicó el método de selección de materiales por índice de propiedades ponderadas, WPIM por sus siglas en inglés (Weighted Property Index Method).

Los espectros Raman resultantes de la técnica permitieron estimar la estructura molecular de los recubrimientos DLC. Las películas dopadas con silicio resultaron en un menor contenido de hidrógeno y una menor fracción total de enlaces sp^3 que las muestras libres de silicio. Dado que el silicio promueve la formación de enlaces Si-C y C-C sp^3, se encontró un aumento de dureza respecto de los recubrimientos sin silicio, incluso aunque estos últimos resultaran tener una fracción de enlaces sp^3 aproximada mayor. Las diferencias en el contenido de hidrógeno fueron relacionadas con la potencia de reactor del proceso de deposición asociada al dopaje con silicio, 150W para dopar con silicio y 500W para DLC libre de silicio. Este parámetro podría, a su vez, estar vinculado con la densidad total de defectos pasantes, menor para las películas dopadas con silicio.

Los recubrimientos gruesos dopados con silicio resultaron en la mayor resistencia a la corrosión de todas las combinaciones de variables posibles. Este efecto se relaciona principalmente a un efecto sinérgico de estas variables frente a la reducción de la densidad de defectos pasantes en la película DLC, generados durante su proceso de deposición. La resistencia a la corrosión del sustrato también resultó afectar en gran medida la respuesta del sistema recubierto al medio corrosivo, dado que los sustratos de acero AISI 304 nitrurados, cuya resistencia a la corrosión aumenta si se evita el fenómeno de sensibilización, sólo sufrieron daño por corrosión preferencial en un defecto de borde generado por la geometría de la pieza durante el nitrurado por plasma del sustrato.

Por último, la adherencia de los recubrimientos y el comportamiento fractográfico de sus modos de falla fueron estudiados. La adherencia entre el sustrato y el recubrimiento DLC fue mayor tanto en recubrimientos gruesos como sobre sustratos nitrurados, como consecuencia de un aumento en la capacidad de carga de las películas más gruesas y a un

aumento de la rugosidad superficial asociado a la expansión volumétrica diferencial de los granos de ambos aceros debida a la difusión de nitrógeno.

1 Introduction

Carbon is unique among all the elements in the diversity of short, medium and long-range configurations it forms with itself and with other elements[1]. Carbon-based solid materials exhibit exceptional properties such as super-high hardness and thermal conductivity, like in diamond (sp^3, fourfold tetrahedral bonding), or unusual softness and lubricity, like in graphite (sp^2, threefold planar bonding)[2].

Diamond is known to possess the most extreme properties of any real three-dimensional solid, such as highest atomic density, highest hardness, highest Young's modulus, highest room temperature thermal conductivity, high electrical resistivity, chemical inertness, optical transparency, wide band gap, and low wear rate in various tribological systems. But diamond is inconvenient as a coating material, because its growth temperature is high[2,3].

Diamond-like carbon, or DLC, is a name attributed to a variety of amorphous carbon materials that consist of a disordered network of carbon atoms with a mixture of both sp^3 and sp^2 coordinated bonds. The significant fraction of sp^3 type carbon bonds gives them attractive physical and mechanical properties that are, to a certain extent, like those of diamond. These carbon-based materials were first discovered by Schmellenmeier in 1950, who described the deposited coating as "amorphous carbon with a high hardness". However, these results did not attract much attention until approximately 20 years later.

DLC coatings have the huge advantage over diamond of having room temperature, rather low cost and large-area vacuum deposition methods. These advantages are what gives them a wide range of applications. These carbon-based coatings can be deposited as thin films on different types of substrates and display desirable properties of both diamond and graphite such as low friction coefficient and high wear resistance. DLCs can be produced by numerous different methods such as plasma assisted chemical vapour deposition (PACVD), magnetron sputtering, vacuum arc evaporation, ion beam and pulsed laser deposition (PLD). Depending on the deposition method used, the properties of coatings can vary substantially[2,3].

DLC coatings are not only scientifically fascinating, but also attractive for numerous industrial applications, due to the variety of available deposition techniques, together with their excellent mechanical properties, wear prevention and minimization of energy losses, and the possibility of tailoring the properties to specific requirements by varying the deposition conditions, film structure or doping them with different elements or compounds. DLC films can be customized to meet multifunctional application needs not only of advanced mechanical systems, but also of optical, electrical and biomedical systems. The DLC industrial application range from high end microelectronics, automotive and general mechanic parts to everyday

devices, like razor blades, magnetic media or decorative pieces. Additionally, when the DLC deposition on metallic substrates is combined with different types of surface treatments, like nitriding, it can enhance its properties or provide additional functionality[3].

However, DLC coatings have a series of drawbacks. Two of the main ones are that its thin films tend to have a large compressive stress, and that it is not mechanically tough. Nevertheless, the amorphous character of DLC means that it can be alloyed with elements such as H, Si, Ti, Cr, Al, N, B that can lower residual stresses and improve the tribological properties of the coating. In the case of metallic substrates, several surface treatments, like nitriding, can further enhance residual stress relieving and improving the adhesion.

In the near future, the DLC related studies aim to improve the applicability of the film by overcoming several technological issues like:

- A better control of the compressive stress to enable deposition of thicker films.
- Improvement of field emission properties.
- Increasing the homogeneity of the DLC films completely eliminating the inclusion of nano and micro particles.
- Increasing the purity of DLC films to meet the standards of the semiconductor industry.

Since the DLC related field of study is relatively recent, their study is expected to increase, leading to new combination of properties[1].

1.1 Scope and Motivation

As time goes by the modern mechanical systems are expected to operate efficiently in increasingly more demanding conditions. Materials for the most demanding tribological applications tend to be expensive and difficult to manufacture. DLC coatings enable the use of many cheaper materials to for high-end applications. These coatings can supply the base material with many appealing properties, such as longer life service, resistance to corrosion, ability to tolerate greater loads and low friction, among many others.

DLC coatings are being increasingly used in various systems because of their wear prevention properties and minimization of energy losses. However, many modern applications require good tribological and mechanical performance in chemically aggressive environments. DLC coatings are chemically inert, but coating failures or imperfections that connect a corrosive environment with the substrate material could result in a corrosion damage mechanism. Additionally, the influence of the coating's electrical properties on its corrosion

resistance hasn't been widely researched and could contribute to corrosion related failures. These failures could result in catastrophic economic and human damage for several industrial applications. This motivated the mechanical, chemical and tribological characterization of several types of DLC with differences in their electrical properties and the relation they could have with the DLC corrosive behaviour.

This project was done within a collaboration between the University of Applied Sciences of Upper Austria (FHÖO) and the National University of Mar del Plata (UNMdP). PhD Lisandro Escalada and PhD Silvia Simison, members of the INTEMA division of Interphases and Bioprocesses Engineering department, directed the research and guided us all the way. The Surface and Coatings Technology department of FHÖO directed by PhD Daniel Heim with the collaboration of PhD Christian Forsich has been studying PACVD-produced DLC films for several years, with the aid of Rübig Gmbh, a company dedicated to the production of industrial vacuum furnaces, heat and plasma pre-treatments, die forging, research and development, among others.

During a time lapse of 6 months, we lived in Wels, Austria, where one of four FHÖO campuses is located, where we started this Materials Engineering career final project. Different types of DLC coatings were deposited on two types of steel substrate by varying some of the deposition process variables. In order to study these variables effects on the mechanical, tribological and corrosion properties of the coated steels, a series of tests were made, including: calotesting, scratch test, nanoindentation, pin on disk, salt spray test, immersion test, confocal microscopy, scanning electron microscopy, energy dispersive spectroscopy and optical microscopy. In our return to Argentina, chemical characterization of the coatings by Raman spectroscopy took place. Electrochemical measurements of the coated steels could not be made due to the 2020 COVID-19 pandemic.

1.2 Goals of the Final Project

The main objective of the final project was to observe and compare the mechanical, tribological and anti-corrosive properties of different DLC systems by varying the type of steel substrate to be coated, its thermal pre-treatment and deposition process parameters like the coating's silicon doping, its thickness and the thickness of a silicon interlayer interphase between the DLC and the substrate. The aim of this project is to analyse which parameter, or combination of parameters, have a bigger impact upon the combination of mechanical and anti-corrosive properties of the DLC.

The main points of this research were:

- Mechanical and tribological characterization of the proposed DLC systems.

- Study of the DLC coated samples behaviour while exposed to a corrosive environment.

- Comparative study of the relationships between the process parameters and the DLC mechanical, tribological and anti-corrosive properties.

- Selection of the most promising set of DLC parameters for coating in corrosive environments applications.

It is intended to develop an understanding of the effect that the proposed variables have on the DLC properties in order to contribute to this novel technology development.

2 Literature Review

2.1 Diamond-like Carbon Coatings' State of the Art

Carbon atoms can be arranged in different multi-atomic structures (allotropes). Diamond and graphite are the most known allotropes, but there are many others, such as fullerene, graphene, nanotubes and amorphous carbon[3].

In the diamond structure, carbon atoms are fully arranged in sp^3 bonds. This arrangement gives diamonds a perfectly symmetric structure, which provides properties such as extremely high hardness, excellent thermal conductivity, high electrical resistivity, chemical inertness, optical transparency, wide band gap, and low wear rate in various tribological systems. Graphite has strong anisotropic properties in one direction, in which carbon atoms are arranged in sp^2 bonds forming layers, while in the perpendicular direction, only weak Van der Waals forces act keeping the layers together. This results in low hardness, low electrical resistivity and high wear rate, combined with a low friction due to solid lubrication.

DLC can be either an amorphous carbon (a-C) or hydrogenated amorphous carbon (a-C:H) thin film material with a mixture of sp^2 and sp^3 carbon bonds. Hydrogen stabilizes the amorphous lattice, preventing the collapse in a graphitic phase. These materials are used as coatings, and present a series of very interesting properties, such as elevated hardness, chemical inertness, tuneable electrical resistivity and optical properties, biocompatibility, and excellent tribological behaviour, due to the combination of low wear rate and auto lubrication, which results in a notable decrease of friction coefficient[3].

2.1.1 Classification of DLC Coatings

The different types of DLC compositions can be seen in the sp^3 carbon, sp^2 carbon and hydrogen ternary phase diagram (**Figure 1**)[4].

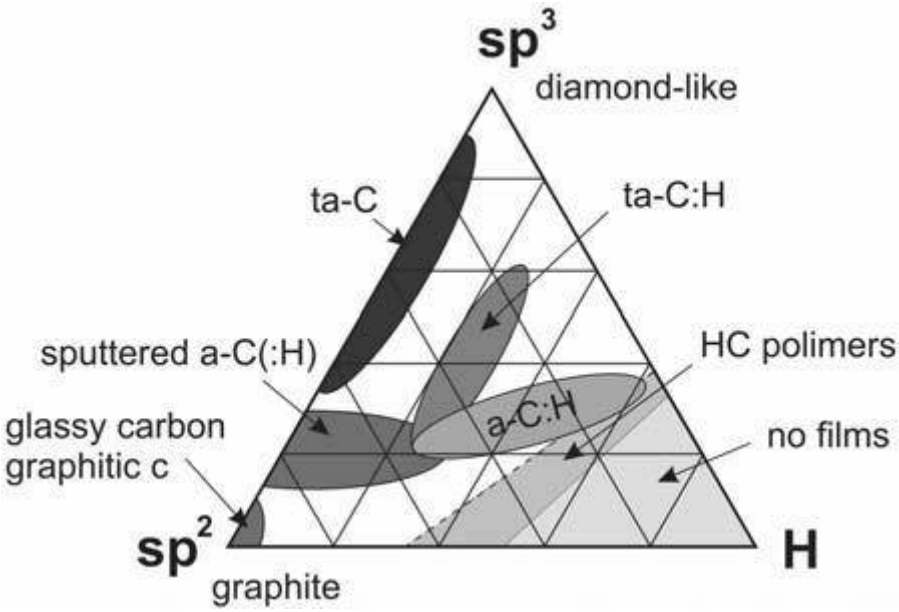

Figure 1. *Ternary phase diagram of the sp^2 carbon, sp^3 carbon and hydrogen (H) system[4].*

The phase diagram consists of three main regions[4]:

- *Hydrogen-free a-C region*:

This region is located along the left axis, where combinations of sp^3 and sp^2 carbon fractions with very low or no hydrogen are shown. The sp^2 a-C is typically glassy carbon, or a-C made by pyrolysis of hydrocarbon polymers or by evaporation and, is not DLC. At high sp^3 content there is a specific type of a-C designated as tetrahedral amorphous carbon or ta-C. The higher sp^3 fraction on ta-C grants very high hardness and Young modulus, while the thickness is greatly limited due to the high residual stresses present in the material[3]. With a lower fraction of sp^3 bonds, and typically made by sputtering, a-C DLCs are formed. These DLCs present a majority of sp^2 bonds, which means that the hardness and elastic modulus is not as high as ta-C. Besides, residual tensions are also greatly lower[5].

- *Solid state / gas delimitation region*:

In the surroundings of the lower right vertex, the hydrogen content is large enough to prevent the material to form a fully connected lattice, instead, it presents only gas molecules. This area is limited by the compositions of C_2H_2 on the sp^2-H axis and $(CH_2)_n$ on the sp^3-H axis.

- *a-C:H region*:

Between the first regions lies the a-C:H DLC region. Typically produced by plasma-enhanced chemical vapour deposition (PECVD) or sputtering, this type of DLC can range from a 20% hydrogen content up to 60% and is the most common type of DLC. By modifying the deposition process a denser a-C:H can be produced which is called highly tetrahedral hydrogenated amorphous carbon, or “ta-C:H”.

In order to improve the DLC coating’s properties, several modifications to its chemistry, deposition technique and parameters or coating architecture can be made.

2.1.2 Modification of DLC Coatings

Most of the DLC modifications have been made to reduce its typically high internal compressive stress, to reduce its surface energy, for further lowering, its already low, friction coefficient, or to modify its electrical properties[5]. The three main methods for modifying DLC coatings are: process parameter variation during the deposition process, doping with additional elements and the introduction of a bonding layer between the DLC coating and the substrate[3]. In the present work the changes in the behaviour and properties of DLC coatings with differences in its doping and bonding layers are studied.

2.1.2.1 Doping

Doping consists in alloying the DLC with different elements during the coating deposition process. The amount and type of the incorporated elements strongly influence the film structure and its general properties[3]. Figure 2 presents schematically the effect that different elements have on the DLC coating properties[4]. The addition of doping elements can be done either from the gas phase or the solid phase. Reactive gasses can be added to the carbon plasma flux such as nitrogen, hydrogen, carbon-containing gases (e.g. C_2H_2), fluorine-containing gases (e.g. CF_4), or silicon-containing gases (e.g. Hexamethyldisiloxane or HMDSO). The gas phase can additionally be activated by plasma or ion sources[3].

In the present work silicon doped DLC, or Si-DLC, are synthesised and characterized.

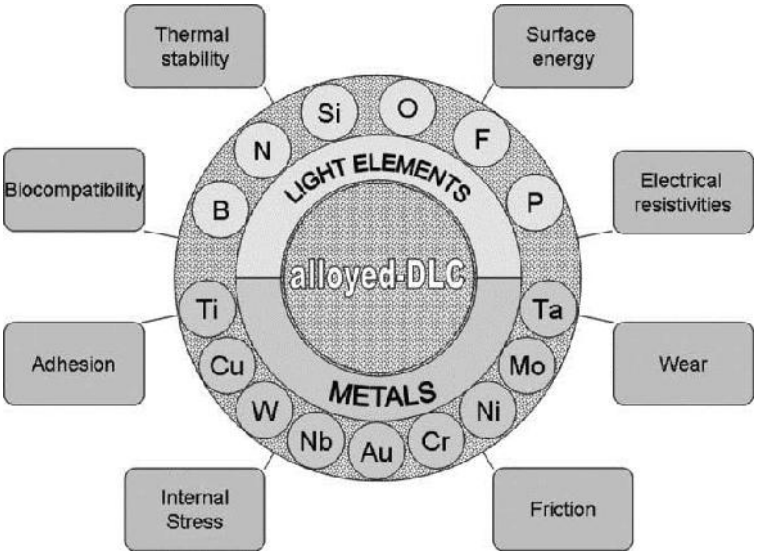

Figure 2. *Typical doping elements and their effects on the DLC coating properties[4].*

Silicon Doped DLC (Si-DLC)

The addition of silicon into DLC films stabilizes the sp^3 bonding, reduces the stress, makes the friction coefficient independent of the relative humidity, improves adhesion to metal substrates and surface roughness, and increases thermal stability and optical gap[6,7]. However, the silicon addition influence on the nanomechanical properties is rather controversial, as hardness and elastic modulus have been reported either to increase, decrease or remain unchanged.

Although the effect of silicon addition on the DLC structure is not yet completely understood, some proposed structural models are gradually gaining followers. These models suggest that the DLC coating hardness and residual stresses are related to the degree of three-dimensional inter-links of sp^2 carbon bonded clusters. These 3-D inter-links are the sp^3 carbon bonds, and since silicon can only have sp^3 hybridized bonds, its addition to the amorphous carbon network might increase the inter-links[8].

Si-DLC tend to have much lower friction coefficient than silicon-free DLC. Some investigators relate this difference to the formation of silicon-rich oxide debris on the Si-DLC surface that acts as a solid lubrication, lowering the friction coefficient, while others have found that on humid environments, Si-DLC films have an extremely low friction due to water lubrication effect: the absorbed water molecules on SiOH groups in the film surfaces reduce shear strength between the Si-DLC surface and the abrasive counterpart in contact[7].

Some researchers have reported that Si-DLC coatings present improved corrosion resistance due to the formation of a passive silicon oxide film. On the other hand, others have reported that an increase in the sp^3 bonds in the DLC, which can be achieved by silicon addition, reduces electrochemical corrosion and increases the electrochemical protection

efficiency. Although this increase in sp^3 sites causes high internal stress that would normally reduce corrosion resistance, silicon stabilizes the sp^3 bonds, reducing the stress[9].

Regarding the DLC electrical properties, it was one of the initial goals of this work to evaluate if silicon-free DLC's exhibited differences in their corrosion behaviour when compared with silicon doped ones that could be related to changes in the film electrical conductivities.

2.1.2.2 Bonding Layers

There are three main problems related to the direct DLC deposition onto metallic substrates: the carbon diffuses into the metals delaying DLC nucleation, the formation of graphite by the iron's catalytic effect can be detrimental to adhesion and the difference in the thermal expansion coefficients of the coating and the steels result in poor adhesion and high residual stress[10].

To overcome these problems, different types of bonding layers have been studied, such as silicon interlayers or nitrided layers (**Figure 3**). These layers can, for example, have a stress relieving effect, reduce structure film mismatching and promote stronger chemical bonds at the interfaces[11]. In the present work the mentioned types of bonding layers are analysed regarding their effect on the DLC coatings deposition onto steel substrates.

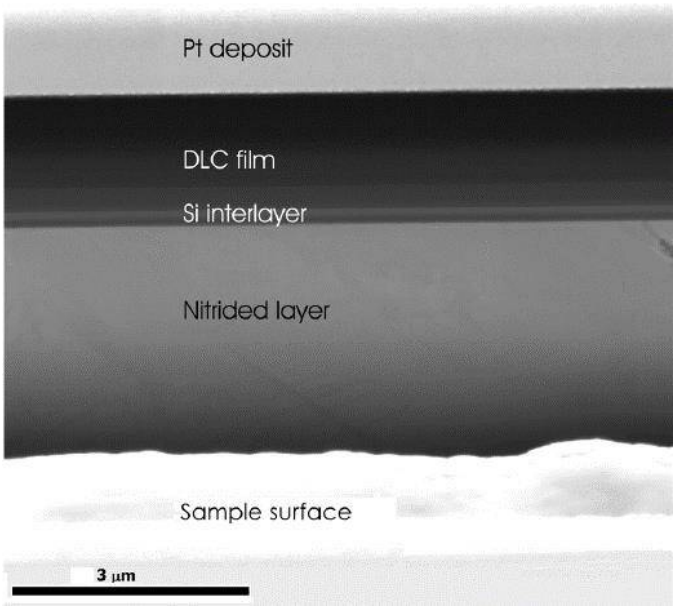

Figure 3. *FIB-SEM image of the cross-section of a DLC coated sample with both, a silicon interlayer and a nitrided layer[10].*

Silicon Interlayer

The use of silicon-containing interlayers in current industrial processes is a well-known approach for improving DLC adhesion on steels. Silicon has both, a chemical affinity with the metallic atoms present in the alloy and with the carbon atoms constituting the DLC[11]. The formation of Si-Fe bonds in the steel/silicon-interlayer interphase and Si-C bonds in the silicon-interlayer/DLC interphase, has been reported by several researchers to explain the adhesion improvements[12].

Nitrided Layer

The nitriding process is a diffusion treatment used in steels to improve their superficial hardness, by enabling the diffusion of nitrogen atoms into their surface to a certain thickness that is determined by the conditions used in the process, such as temperature, exposition time or pressure. When nitrogen diffuses into the surface zone, it is at first dissolved interstitially in the iron matrix. This forms a layer, constituted mainly by specific types of iron nitrides denominated ε phase and γ' phase, that improves the surface wear characteristics. With the formation of this iron nitride layer, nitrogen diffuses inward and combines with nitride-forming elements to form nitride compounds. The precipitation of these compounds occurs in grain boundaries and specific crystallographic planes resulting in an increase in the nitride compound layer hardness[13].

The generation of a nitrided interphase between the steel substrate and the DLC coating, which has a graded compositional and hardness profile, has been proven to improve adhesion[10].

2.1.3 Plasma-enhanced Chemical Vapor Deposition of DLC

The methods for producing DLC coatings are broadly divided into two types: Physical Vapor Deposition (PVD) and Chemical Vapor Deposition (CVD)[14]. The PVD technique uses evaporation, sputtering, and other physical processes to produce vapours from solid materials, while in the CVD technique a precursor gas flows into a chamber and deposition of thin films on the surface occurs due to the chemical reaction in vapor phase, activated either by heat or radiation[15].

Depending on the activation energy used in the CVD process, such as temperature, photon or plasma, it can be categorized into several groups, namely thermal CVD, laser/photo CVD, and plasma CVD. Thermal CVD typically requires high temperature in the ranges of 800-2000°C, which can be produced by methods such as hot plate heating and radiant heating. In the case of laser photo CVD procedures, photons are produced using either a high-

power laser or ultraviolet radiation. However, in plasma CVD, or plasma-enhanced CVD (PECVD), the reaction is activated by the use of inert gas plasma. The utilization of plasma decreases the deposition temperature to a great degree in comparison with other methods such as thermal CVD. Deposition can occur at room temperature, which opens the possibility of coating polymers and other materials with low melting temperatures or undesirable thermal effects[15].

Plasma is a partially or fully ionized gaseous state of matter and generally is a mixture of electrons, charged particles, and neutral atoms in about equal numbers, and therefore, the plasma state has extremely high energy and it has no net charge[15,16].

In the PECVD process, an external energy source is required for the ionization of atoms and molecules (creation of the plasma), a pressure reduction system (maintain the plasma state), and finally, the existence of a reaction chamber. One method for plasma production is the heating of the gas, however, ionization temperatures are extremely high, and this can be a limitation. The other way of plasma production is the utilization of electrical energy, at various frequency discharges which can be subcategorized into audio frequency (10-20 kHz), radio frequency (13.56 MHz), and microwave frequency (2.45 GHz), resulting in various types of produced plasma. When a plasma produced by any of these techniques is utilized, the deposition species undergo fragmentation which forces them to become free radicals and ions. Neutral molecules are ionized or exited when the electrons and ions in the plasma interact with them, so they become chemically reactive. The collision of a charged ion with a neutral atom results in improved chemical reactivity and production of implantation reactions of atoms, radical generation, and polymer-forming or etching reactions[15].

PECVD techniques are used to produce a stable DLC coating, as it is required to form a certain amount of sp^3 bonds, which can be achieved by ionic bombardment on the workpiece surface. In **Figure 4** a scheme of a PECVD reactor is shown. Plasma activates carbon precursors, allowing the reaction on the substrate surface, as well as collide against its surface due to its accelerated cations. These impacts provide an amount of energy enough to form sp^3 bonds between carbon atoms, while reducing sp^2 bonds and the amount of hydrogen in the DLC, becoming less polymeric and acquiring a diamond-like structure.

Both the working pressure and polarization voltage rule the energy of the colliding ions, which must be maximized in order to obtain a decent amount of sp^3 bonds. The best conditions are high voltage and low pressure: a high voltage implies a higher acceleration of ions, as it increases the electric field and thus the collision energy, while a low pressure increases the mean free path, as there is less species in the plasma flow to collide against, allowing more collisions to the workpiece.

The correct carbon gas choice is crucial for the process. The main issue to determine which gas to use is the H/C ratio, which should be as low as possible, although not lower than

1. This requirement is fulfilled in gases like acetylene and benzene. They both have advantages and disadvantages: while benzene is purer, it is liquid in room temperature, which adds a new phase to the process, and it is carcinogenic as well. When the process is run to produce doped DLC, additional gases are used, such as silane for a-C:H:Si DLC. Besides, a noble gas such as argon is used for stabilizing the process[2].

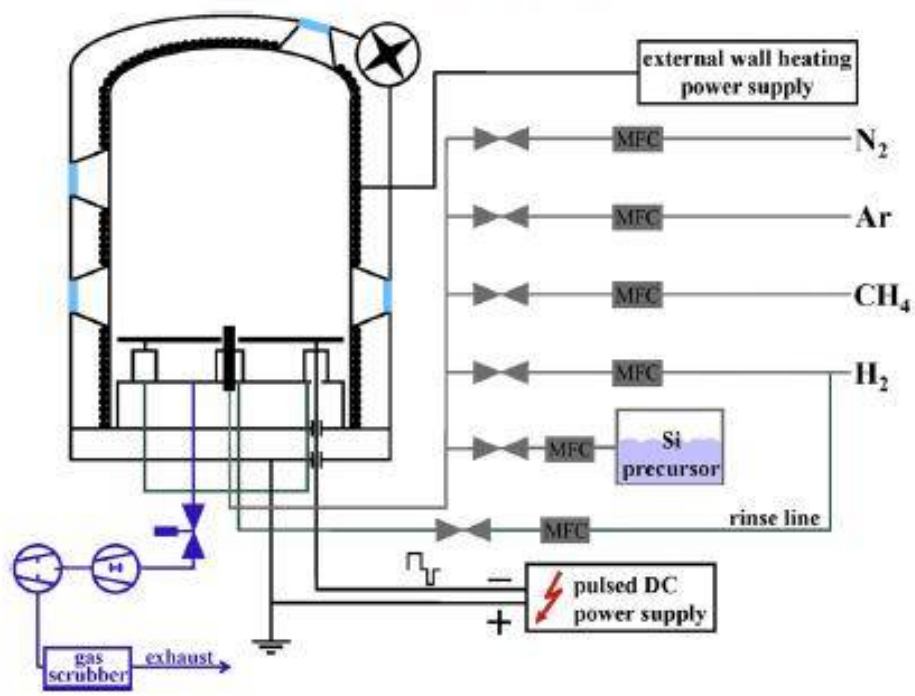

Figure 4. *PACVD reactor scheme[17].*

2.1.3.1 Plasma Nitriding

There are different nitriding techniques, such as liquid or gas nitriding, that are usually carried out in the temperature range between 400-600ºC. Nevertheless, this is a critical temperature range for the stainless steels, since at this temperature range they can suffer a phenomenon regarded as “sensitization”. This phenomenon happens when a stainless steel is held at a temperature in the range of 425-815°C and chromium carbides precipitate at the grain boundaries. This precipitation happens because the carbides are insoluble at these temperatures. In order for the carbide to precipitate, it must obtain chromium from the surrounding metal. This means that there is a chromium depleted zone around the grain boundaries that is prone to intergranular corrosion. This is why the nitriding on high chromium steels should be done in low temperatures, around 400ºC[18]. Hence, plasma nitriding is used for nitriding stainless steels, as its temperature range has quite a lower minimum, ranging between, 350-580ºC[13].

In plasma nitriding, elemental nitrogen is forced into the samples surface in a vacuum environment with the aid of a low-energy plasma. This element is introduced to the sample via

an ionized gas mixture of nitrogen, hydrogen and a carbon gas such as methane or carbon dioxide.

Plasma nitriding method presents some advantages compared to others, such as lower process duration, lower energy use, non-emission of pollutants, lower distortion and dimensional changes, no finishing latter process, lower final cost, possibility to remove the oxide films before nitriding and homogeneity and uniformity of samples with complex geometry, among others[13].

Despite these overwhelming advantages, there is an associated phenomenon with this technique, known as edge effect, that results in a nonuniform surface when treating samples with complex geometries, where the central and peripheral regions of the workpiece show different colours. This is the consequence of the sample submission to a high cathodic potential in order to produce plasma directly on their surface. As a result of distortions in the electric field around the corners and edges, the shape of the plasma sheath, which is associated to the geometry of the samples, determines ion flux distribution and creates erosion rings, characterized by different colours and discontinuous hardness. This occurs mainly in the treatment of materials containing a high percentage of alloy elements like chromium, which produces nitrides, as in the case of stainless steels[19].

Even when the nitriding process in stainless steels is done at temperatures low enough to avoid the sensitization phenomenon, due to edge effects this temperature can slightly raise in the borders. Thus, the solubility limit of nitrogen in the austenitic phase of the workpiece can be reached, producing a dissolution of the metastable γ_N phase, and precipitating CrN compounds. This way, a deficit of both chromium and nitrogen occur in the surrounding region of the rings, which results in a poorer corrosion resistance of the affected area[19].

2.1.4 Applications

The properties DLC coatings have makes them a suitable material for a wide range of industries. It is mostly used for applications where high wear resistance is needed. DLCs are used in industries like automotive, metallurgy, biomedical, aerospace and knives, among others. Some of these applications are briefly explained in the following paragraphs.

Biocompatibility, as well as the easiness to dope its surface to change or add some properties, are very alluring attributes for the medical industry. Nevertheless, its use in this industry is still in development phase due to its adhesion issues. There have been a series of studies, such as implants placed on sheep and rabbits, as well as cell behaviour studies by growing different cell types in vitro on DLC and studying the cell response[2]. Another future possible application that has been studied is to apply the coating in stents.

The excellent tribological properties found a very suitable use in the blade industry. Non doped DLCs are used where low contact pressures are applied and heat generation is low. An example of this use is the coating of textile industry knives, where the blade is needed to cut multiple layers of fibres. Without the coating, the blade must be sharpened frequently, but once the DLC is applied, this necessity is greatly reduced. Another example is its use in knives for cutting vinyl coated wallpapers, where the DLC coating reduces the cutting friction, increasing the knife durability by 100 times[20].

Aerospace industry applies DLC for many uses, one of which is the deployment of satellite solar panels. These panels must stay fixed close to the satellite body during two critical stages, the take-off and the satellite release, while during the deployment the panel must be able to slip open. This means that the hold-down device must allow the panels to stay fixed in both positions, opened and closed, and this is achieved by applying mechanical loads. DLC is optimal for this application, as it can act both as a solid lubricant to aid the deployment, as well as a cold-welding prevention when the panels are folded[21].

2.2 Corrosion

Corrosion is a phenomenon that affects many of the things we can see and use in our daily lives. From rust in our cars, fences or cooking utensils to expensive repairs to home plumbing or water heating systems. While many times this is only an aesthetic or domestic issue, it can imply huge economic or social losses in several industries. For example, there have been aeronautical accidents in which part of the fuselage tore away during flight due to combined effects of atmospheric corrosion and mechanical cyclic stress.

This phenomenon is the degradation of materials caused by a reaction with the environment surrounding them. Every metal is unstable under given circumstances and develop damage in the shape of pits, superficial oxides, etc. Most metals are not found in nature freely, but as minerals, and the same energy spent to reach a more stable state is the one that gets freed when chemical corrosion reactions occur. This is why it can be said that corrosion is the mechanism through which metals return to its combined state in chemical compounds as found in nature. There are not materials that resist corrosion in every environment, but there are materials more suitable for each specific application.

Almost every corrosion process involves charge transfer in aqueous solutions. There are two reactions involved in the corrosion process, the anodic reaction and cathodic reaction. In the anodic reaction or oxidation, metals increase its valence number liberating electrons and forming part of the aqueous solution when they are solvated by water molecules or corrosion product compounds. In the cathodic reaction or reduction, a metal or non-metal reduces its valence number, consuming electrons. For example, in **Figure 5** we can see a

metal dissolving into cations after the reduction of Hydrogen takes place by taking electrons from the metal.

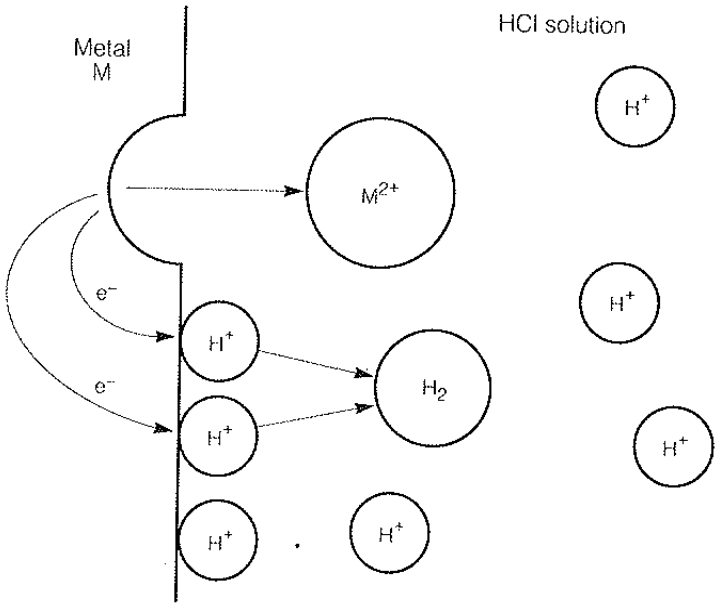

Figure 5. Diagram of corrosion process of a metal in a HCl solution[18].

Electrochemical reactions can produce metallic oxides and hydroxides, instead of forming metal cations solvated by the environment. In some metals, such as iron, nickel or chromium, a phenomenon called passivation occurs. When this happens, corrosion products form a thin, resistant and continuous metallic oxide superficial layer. This layer prevents electric contact between the metal and the environment, which helps to reduce drastically the corrosion rate, meaning that this layer protects the metal. This occurs in the appropriate potential and pH conditions, in which corrosion, and so the formation of the oxide layer, is thermodynamically stable.

The most common corrosive environments do not possess the conditions needed to passivate low alloy steels, but chromium can form the protective layer under the same conditions and working parameters. Chromium by itself is a difficult metal to use, as it is too fragile and difficult to produce. This is why chromium and steel alloys are used, as it can take advantage of both materials, passivating the alloy thanks to chromium when at least 12% is present, and steel plays the role of a structural metal. These alloys are commonly known as stainless steels.

Another way to protect metals from corrosion attack is by coating it. Coatings can be metallic, polymeric or ceramic. It acts as a physical barrier between the metal and the environment, avoiding their contact and reduction and oxidation reactions to happen. Coatings are not perfect anyways, as they present defects, areas in which there is no continuity of the coating lattice. In these areas, localized corrosion can occur. This corrosion type differs from

general corrosion for appearing in certain areas of the structure, leading to a lower loss of material than general corrosion. Anyways, the corrosion rate in the damaged areas is higher, so the penetration and collapse of the workpiece is also faster[18].

2.2.1 Low-Alloy Steels Corrosion

Low-alloy steels comprise a category of ferrous materials that exhibit mechanical properties superior to those of ordinary carbon steels as the result of additions of such alloying elements as chromium, nickel, and molybdenum. Their total alloy content can range from 0.5 to 1% and up to levels just below that of stainless steels. The primary function of the alloying elements is to increase hardenability in order to optimize mechanical properties and toughness after heat treatment, however, some alloying additions are also used to reduce environmental degradation under certain specified service conditions. Regarding corrosion in aqueous environments in this type of steel, additions of nickel, chromium, silicon, and phosphorus promote the formation of relatively insoluble protective corrosion products. Chlorine and chlorides, commonly found in aqueous environments containing salts, have a deleterious effect on the protective rust layer on low-alloy steels[22].

2.2.2 Austenitic Stainless Steels Corrosion

The stainless steels are iron-base alloys containing at least 10.5% chromium. With increasing chromium content and the presence or absence of some ten to fifteen other elements, stainless steels can provide and extraordinary range of corrosion resistance. They are categorized in five distinct families according to their crystal structure and strengthening mechanism.

The austenitic stainless steels have a face-centred cubic crystal structure, achieved by the addition of austenite phase stabilizers like nickel, manganese and nitrogen. Austenite is characterized as nonmagnetic, and it is usually relatively low in yield strength with high ductility, rapid work-hardening rates, and excellent toughness.

In carbon steels, alloy steels, and most other metals the formation of a relatively protective barrier of true oxide separates their surface from the surrounding atmosphere. The degree of protection afforded by such an oxide layer is a function of its thickness, its continuity, its coherence and adhesion to the metal, and the diffusivities of oxygen and metal in the oxide. In stainless steels the formation of a passive oxide film at low temperatures takes place. When conditions are favourable for maintaining passivity, stainless steels exhibit extremely low corrosion rates. If passivity is destroyed under conditions that do not permit restoration of the passive film, the stainless steel will corrode much like a carbon or low-alloy steel.

When a local discontinuity of the passive film takes place, and the film is unable to heal, a localized form of corrosion can occur. Pitting is a localized attack that can produce penetration of a stainless steel with almost negligible wight loss to the total structure. Chloride is the most common agent for pitting initiation since it produces a local chemical breakdown of the passive film. Once a pit is formed, it in effect becomes a crevice, the local chemical environment is substantially more aggressive than the bulk environment. Crevice corrosion can be considered a severe form of pitting. Any crevice, whether the result of a metal-to-metal joint, a gasket, fouling or deposits, tends to restrict oxygen access, concentrate the chloride ion, and reduce the pH, resulting in attack[22].

2.3 Experimental Characterization Techniques

2.3.1 Surface characterization

2.3.1.1 Raman Spectroscopy

This is a non-destructive chemical analysis technique, that brings valuable and detailed information about the sample analysed, regarding chemical structure, phase, polymorphy, crystallinity and molecular interactions. The method relies in the interaction of light and the chemical bonds of the material of the sample.

A source of monochromatic light, generally a laser near the infrared or near the ultraviolet range, is directed towards the sample. The light interacts with the molecular vibrations, phonons or other excitations in the system, and the molecule scatters the incident light. Most of this scattered light is of the same wavelength as the original beam (known as the Rayleigh scatter), but a small part of it is scattered at different wavelengths, depending on the chemical structure of the sample (known as the Raman scatter). The Rayleigh scatter is filtered out while the Raman scatter is collected for analysis (**Figure 6**).

This collected light forms a Raman spectrum that features a number of peaks that show the intensity and wavelength position of the scattered light, where each peak corresponds to a unique molecular bond vibration, or groups of bonds[23].

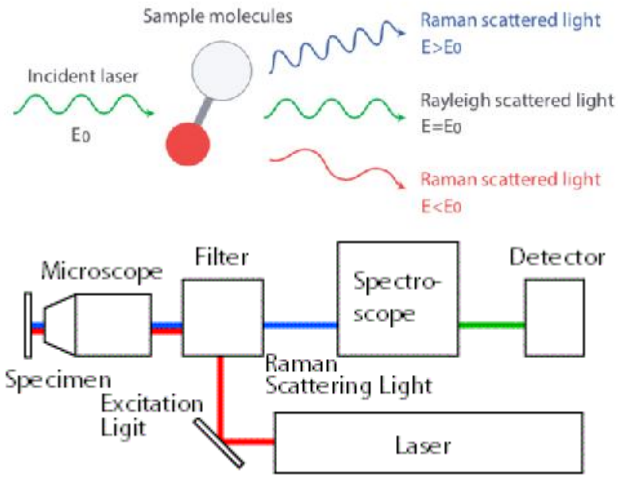

Figure 6. *Raman spectroscopy methodology[24].*

Pure DLC spectrum consists mainly of two peaks: G peak at around 1580cm^{-1} and D peak at around 1350cm^{-1}. D peak originates due to the breathing mode on carbon aromatic rings, and G peak corresponds to the stretch of the sp2 sites on the C-C bonds in the rings, or alkene chains[25].

The key Raman parameters to monitor carbon bonding are the intensity ratio of the D and G peaks, I(D)/I(G), the full width at half maximum of the G peak, FWHM(G), and the displacement of the G peak position from its theoretical value, Displacement(G) or Disp(G). In amorphous carbons I(D)/I(G) is a measure of the size of the sp^2 phase organized in rings. If I(D)/I(G) is negligible, then the sp^2 phase is mainly organized in chains. On the other hand, FWHM(G) and Disp(G) both measure disorder, however, FWHM(G) is mainly sensitive to structural disorder, while Disp(G) is mainly sensitive to topological disorder. Structural disorder arises from bond angle and bond length distortions. Topological disorder arises from the size and shape distribution of sp^2 clusters.

Another issue involved in intensity ratios is the radio frequency power used in the formation of the DLC coatings. An increase in process power affects the I(D)/I(G), and hence, the sp^3 fraction, due to the higher ionization levels of CH_4. The new CH_n radicals will increase the sp^2 clusters, which lends to a higher intensity on the D peak. This also increases the hydrogen concentration in the coating, as there is additional atomic hydrogen produced during the coating process, which increases internal stresses in the film[26].

2.3.1.2 Calotesting

This technique is a quick process that measures a coating thickness. It consists in a holder for the sample to be tested and a steel ball of known diameter that is rotated by a rotating shaft connected to a motor whilst a diamond suspension is applied to the contact area. The ball is rotated for a short amount of time and wears a crater trough the coatings. Then the

inner and outer diameters of the crater are measured using an optical microscope and then the thickness of the coating is calculated using a simple equation shown in **Figure 7**[27].

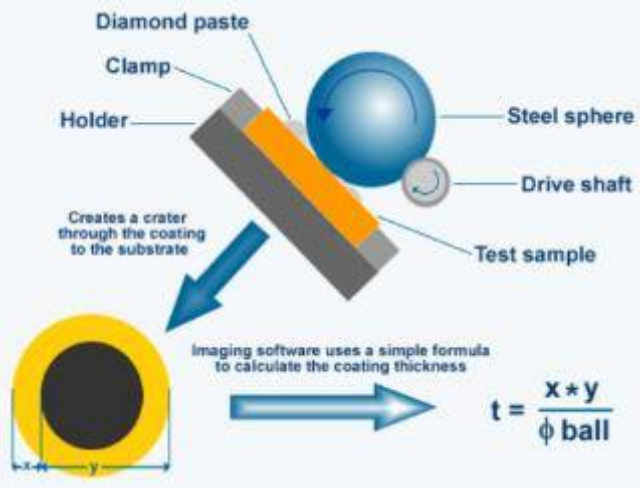

Figure 7. *Calotesting technique and thickness calculation equation*[28].

2.3.1.3 Nanoindentation

This test is most commonly used for the measurement of hardness and elastic modulus, while it is also useful to acquire other properties, such as hardening exponents, creep parameters and residual stresses. Its principal components are the test material, the sensors and actuators used to apply and measure the mechanical load and indenter displacement, and the indenter tip. The tip is made of diamond, in a sharp, symmetric shape such as a pyramid. During a typical nanoindentation test, force and displacement are recorded as the indenter tip is pressed into the test material's surface with a prescribed loading and unloading profile. These parameters form the load-displacement curve (or P-h curve), and the differences from one material to another in the curve reflect the differences in mechanical properties between the materials. Multiple measurements can be made at numerous points of the surface and spatially map its mechanical properties[29,30].

2.3.2 Tribological characterization

2.3.2.1 Pin-on-Disk

The test consists of a sphere which is attached to a stiff elastic arm that is weighted down onto a sample with a precisely known weight (**Figure 8**). The sample is rotated at a selected speed. The elastic arm ensures a nearly fixed contact point and a stable position in the friction track formed by the sphere on the sample. The kinetic friction coefficient is determined during the test by measuring the deflection of the elastic arm. Wear rates for the sphere and the disk are calculated from the material loss during the test measured with a

confocal microscope. Since the device is equipped with an environmental chamber it is also possible to control and measure the effect of humidity and temperature[31].

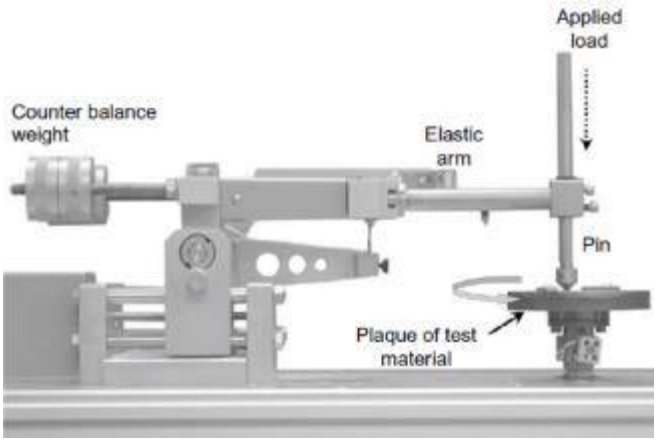

Figure 8. *Pin-on-Disc tribometer equipment[31].*

2.3.2.2 Scratch Test

This test is used to evaluate the adhesion strength of the deposited coatings. In this technique, a diamond stylus is drawn in a straight line over the coating under an increasing normal load, during a stipulated length (**Figure 9**). If enough load is applied, coating will show the initial signs of failure at a designated load by producing cracking on the coating (known as LC1 or critical load 1), and substrate will be firstly revealed at another designated load, producing spalling on the coated piece surface (known as LC2 or critical load 2). These failures occur as a result of the detachment of the coating from the substrate[17,32].

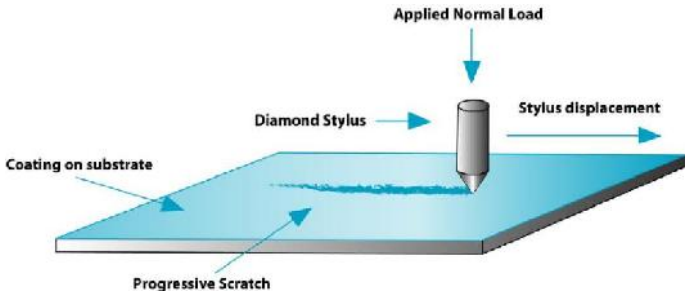

Figure 9. *Scratch test scheme[33].*

Failure modes on scratch tests

There are different types of failure in the path drawn by the stylus, mainly categorized according to the substrate behaviour: brittle or ductile (**Figure 10**).

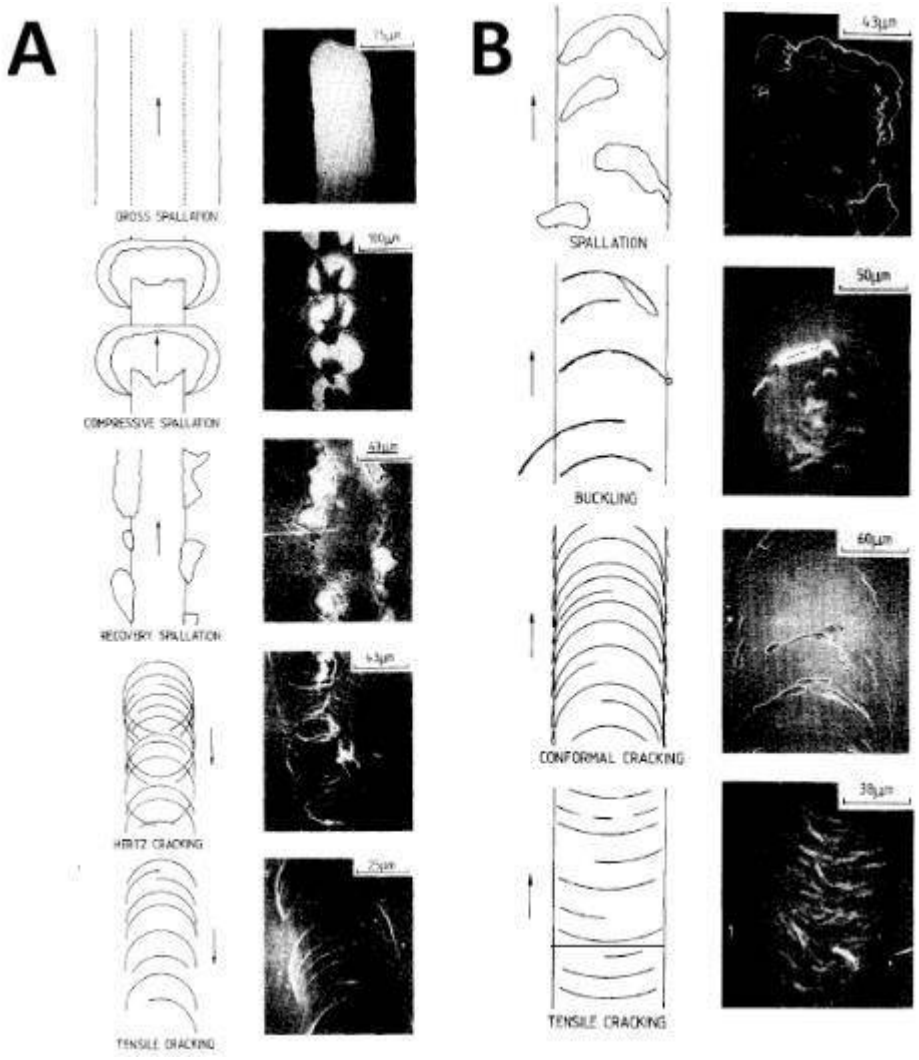

Figure 10. *Failure modes in scratch testing. A) Brittle behaviour. B) Ductile behaviour*[34].

For brittle substrates, large area spallation is one of the common failure modes, if there is poor adhesion from the coating, or if there are high levels of residual stress. As the diamond contacts the coating, a crack is formed at the interface between coating and substrate, that propagates considerably before stopping. The crack commonly begins in a coating flaw.

Another common failure mode is compressive spallation, where the coating is detached from the substrate in order to minimize the elastic energy stored by the large compressive stresses ahead of the stylus. This also implies poor adhesion, and leads to semicircular cracks that propagate outwards from the track drawn by the stylus. This leads to chipping at the trackside, if the crack propagates outside of the scratchline before the stylus passes over it. Once the stylus reaches the region, it will sometimes press the coating back to contact again the substrate, while other times it will cause a chip to be removed (if there is through-thickness cracking as well), which is known as recovery spallation. This failure mode becomes more common as coating thickness increases.

As very little plastic deformation occurs on brittle substrates, conformal cracking rarely occurs. However, sometimes hertz cracking can be seen for very brittle substrates, where hertzian ring cracks are observed along the stylus track. The tensile radial stresses at the edge of the diamond contact generate a ring crack, which propagates from the surface inwards, reaching the substrate. As the stylus advances, there are several cracks formed, which can intersect, causing a crack network along the edge of the track, and in those intersections, considerable chipping occurs, and delamination may occur. Cracks may also be the consequence of the response to the tensile stresses generated during the sliding, in which case they appear at the rear end of the diamond contact. As the load in this case is mostly supported on the front half of the intender, cracks form with less curvature than in the hertzian case.

For ductile substrates, failure shows similarities with brittle cases, but generally in lower cracked areas, smaller chipped or spalled regions, and thus, a larger number of failure events occur. Spallation and buckling are similar to the spallation mode in brittle substrates, but the failure presents a smaller area. Generally, spallation occurs where the adhesion is poor or, for thicker coatings, where the driving force to reduce stored elastic energy is larger.

The other two common failure modes for ductile substrates are cracking and tensile cracking. Partial ring cracks can occur ahead of the indenter, that then passes over and pushes into the track, while also as the coating is bent into the scratch track it can become cracked ahead of the stylus. These issues lead to through-thickness cracking at the front and sides of the indenter, which is known as conformal cracking. Cracking also occurs at the rear end of the contact between stylus and coating due to the tensile stresses generated by sliding, which leads to tensile cracking failure[34].

Angular cracks, also known as chevron cracks, are seen in some cases at the beginning of the scratch failure (**Figure 11**). They are formed due to a combination of moving action and bending action around the stylus at the edge of the groove. The angle of the cracks is due to a superimposition of the two tensile stresses. They normally occur in thin coatings[35]. Another early failure mode is known as parallel or lateral cracking, that occurs typically at low loads, but higher loads than angular cracking. These cracks are thought to nucleate near the plastic deformation zone below the contact due to residual tensile stress during unloading phase[36]. Figure 11 shows these two failures seen at low loads of a scratch test.

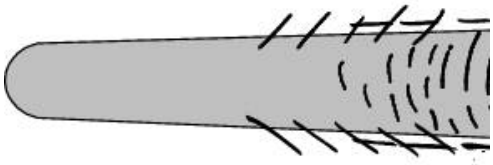

Figure 11. *Initial failure modes on scratch tests[37].*

2.3.3 Corrosion tests

2.3.3.1 Salt Spray Test

This is an accelerated corrosion testing technique that exposes samples to harsh environmental conditions to simulate the corrosive behaviour of them in longer times but less aggressive environments (**Figure 12**). The objective of this test is to provide information about the corrosion resistance on metals and coated metals.

Samples are placed in a closed chamber that follows ISO 9227 norm specifications, and exposed constantly to indirect spray of a salt water solution, at concentration and temperature also specified in the norm. Once the exposition is over, samples are analysed and compared to each other. Salt spray test is used to compare the corrosive resistance of different materials or coatings and determine coating adhesion and corrosion creep, among other features[38].

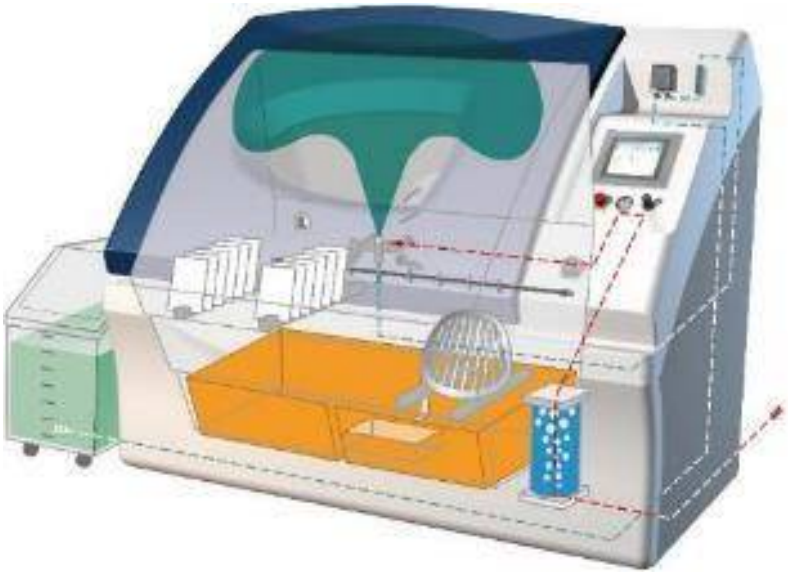

Figure 12. *Salt spray chamber[39].*

2.3.3.2 Immersion test

Immersion tests are used to measure the evolution of corrosion damage in a pre-set period of time on accelerated conditions. Samples are partially or fully immersed in seawater solution (3.5% NaCl) and removed after the required time lapse passes. Accelerated

conditions can be achieved by increasing pressure, salt concentration, temperature and/or solution acidity[40]. After the immersion test, samples are analysed and compared to each other in order to determine the effects of the exposition to the corrosive media, such as corrosion creep or, in the case of coated samples, coating adhesion to the substrate where it was deposited.

2.3.4 Microscopy techniques

2.3.4.1 Confocal Microscopy

This is an optical imaging technique that forms images using light from a discrete focal plane. A collimated light source is directed towards the object plane, from where it is reflected back through the objective lens. The point light source is scanned across the specimen surface, forming the complete image. The reflected light from each surface position is directed to a photomultiplier, via a detector pinhole, conjugated to the objective aperture in a way that only light from a discrete focal plane can reach the detector, while the rest of the light is discarded (**Figure 13**). The depth of the optical section depends of the pinhole diameter and the incident light wavelength. With a high precision motorized focusing stage, the objective is displaced along the vertical axis, what permits the production of a series of images regularly spaced along the axis. These images represent a volume of material of a three-dimensional distribution of intensities. This way, the images obtained can be processed in order to create different representations, such as 3D visualizations of the scanned material or a topographical representation of the surface with a coloured code, scaled similarly to a heat map, representing different depths[41].

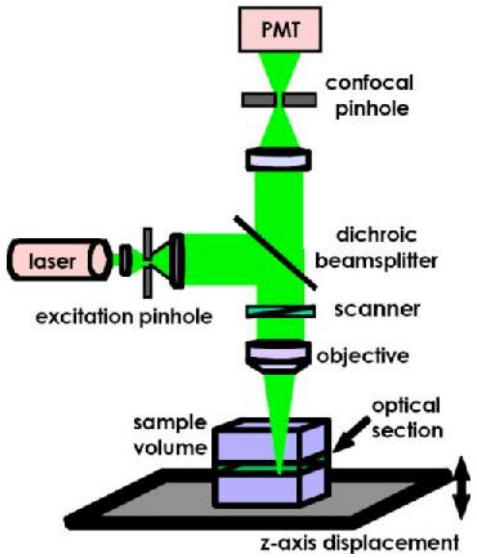

Figure 13. *Confocal microscopy technique[42].*

2.3.4.2 Scanning Electron Microscopy

This microscopy technique employs a focused electron beam that reacts with the sample in order to generate a topological image and relative composition. When the beam contacts the sample surface, part of the beam will remain unscattered, although most of it interacts with the sample and undergoes inelastic and elastic scattering. In the first case, the primary electrons direction is changed, but the overall energy is kept, unlike inelastic scattered electrons, that change direction and also lose part of their energy. Most of the beam energy ends up in the specimen as heat, but other effects occur as well, such as emitted secondary electrons, backscattered electrons and characteristic X-rays.

Secondary electrons are generated when an incident electron changes its path and loses part of its energy, that gets transferred to an atom in the sample (inelastic event), leaving the sample with a very small energy. When the scattered electrons are deflected in an angle of more than 90 degrees, they are called back scattered electrons. The production of backscattered electrons varies with the atomic number of the elements present in the sample: with higher atomic numbers, the region will appear brighter. X-rays emission is the result of the deenergization of an atom in the sample after a secondary electron is produced. The emission of depth of the different signals used in SEM is influenced by the electron beam energy, the specimen nature, composition and sample preparation. At higher voltage applied on the electron beam, larger interaction volume is achieved.

Imaging occurs by using the emission of secondary electrons and the backscattered electrons. Analytical X-rays provide qualitative and quantitative analysis of the specimens. Then, SEM can provide information on topography, morphology, composition and crystallographic nature of the analysed specimens[43].

2.3.4.3 Energy Dispersive X-ray Spectroscopy

This is an analytical non-destructive technique used for the elemental analysis or chemical characterization of a sample. To do this the SEM must be equipped with a EDX probe that emits X-rays to the sample. This electromagnetic radiation transfers part of its energy to the atoms of the sample. This energy can be used by the electrons of the atoms to “jump” to an energy shell with higher energy or be knocked-off the atom, leaving behind a hole positively-charged. These positive holes attract the negatively-charged electrons from higher-energy shells, the energy difference of this transition can be released in the form of an X-ray. This released energy depends on the atomic number of the element, which is a unique property of every element. In this way, X-rays are a “fingerprint” of each element and can be used to identify the type of elements that exist in a sample. The data that is generated by EDX

analysis consists of spectra with peaks corresponding to all the different elements that are present in the sample[44].

2.4 Materials selection methods

There are three main methods to select materials. These are: the cost per unit property method (CPUPM), the limits on properties method (LOPM) and the weighted property index method (WPIM).

Cost per unit property method: It is mainly used for an initial approach in applications where one property is the most critical requirement. The cost to supply that requirement is what needs to be studied in order to choose the most suitable material.

Limits on properties method: In this method, the performance requirements are separated in three groups: the lower limit, the upper limit and the target value properties. This approach is mainly used when screening a large number of materials in computer databases. After the screening, the materials still considered are those that their properties are above the lower limits, below the upper limits and within the target values of the particular requirements.

Weighted property index method: It is used when the design involves the optimization of several properties or conditions, where a weighting factor (w) is assigned to each material condition or property, according to the requirements. This is a subjective decision that is done with care to stop partiality or to get the intended response. The weighted property values are calculated to give a proportional weighted property index.

This method has the disadvantage of having to combine properties with dissimilar units. The best procedure is to stabilize these differences with a scaling factor, which is an easy method to bring all the properties within a numerical range: Each property is balanced so that the highest value does not exceed 100. This scaled value of a property (β) is given by:

$$\beta = \frac{\text{numerical value of property} \times 100}{\text{largest value on the list}}$$

Or, when the low value is best, such as cost, wear rate, corrosion loss, etc:

$$\beta = \frac{\text{lowest value on the list} \times 100}{\text{numerical value of property}}$$

Some properties are not articulated in numerical value, such as weldability. For these cases, the condition is analysed accordingly to the performance: For example, “Excellent” could be scaled to 100, “Good” to 75, “Fair” to 25, and “Poor” to 0.

After every material property is scaled, the weighted property index (γ) is calculated:

$$\gamma = \sum_{i=1}^{n} \beta_i \times w_i$$

Where n is the total number of properties considered[45].

The materials with the higher values of γ are the most suitable ones for the studied application, and are the ones that should be considered to implement.

3 Experimental Methodology

In this section, the different techniques used during the present project are listed. The different studied and analysed variables each condition has, as well as the experimental parameters used for each technique, are also explained.

3.1 Substrate materials

3.1.1 SAE 4140

SAE 4140 is a low alloy steel, with chromium and molybdenum as alloying agents, for strengthening. It presents good atmospheric corrosion and wear resistance, combined with good levels of strength and fatigue strength. Anyways, it does not show good corrosion resistance in aggressive environments, such as seawater, as well as it does not present good tribological properties, limiting its use in applications requiring any of these two aspects. It is used mainly in the oil & gas and space industries, and in a lower grade, in automotive, agricultural and defence industries, typically to conform shafts, gears, collars and other machinery components. Its elemental chemical composition is listed in Table 1[46] [47]. The hardness for the samples used on this project is 285 HV, according to a previous research[17].

Table 1. *SAE 4140 composition.*

Elemental Composition [%wt]						
C	Mn	P	S	Si	Cr	Mo
0.38 - 0.43	0.75 - 1	0.035	0.04	0.15 - 0.35	0.8 - 1.1	0.15 - 0.25

3.1.2 AISI 304

AISI 304 is an austenitic stainless steel, with a high percentage alloying agent added, such as chromium and nickel, which form a solid solution with iron due to atomic similarities, besides a passivated film formed due to the high percentage of chromium added. This grants to the steel great corrosion resistance in both atmospheric and aggressive environments, but just as for SAE 4140 steels, it does not show good tribological properties. It is used mainly where corrosion resistance is greatly needed, such as food, dairy and chemical processing industries, among others. Its elemental chemical composition is listed in Table 2[48] [47]. The hardness for the samples used on this project is 167 HV, according to a previous research[49].

Table 2. *AISI 304 composition*

Elemental Composition [%wt]						
C	Mn	P	S	Si	Cr	Ni
0.08	2	0.05	0.03	1	18-20	8-10.5

3.2 Substrate Surface Conditioning

SAE 4140 and AISI 304 circular steel samples of 4 cm in diameter and 1cm thick were prepared by Rübig GmbH. on their facilities to be used as substrate for this project. The steel samples were mirror polished in a Struers automatic polishing machine (**Figure 14**), TegraPol-35 model, in the University of Applied Science of Upper Austria (FHOÖ), which consisted in a sample holder with six sockets, a water sink, a series of plastic hoses for the different polishing suspensions and a rotating magnetic circular surface, where the polishing disks were attached. The process used tree different polishing disks: Piano (120µm), Allegro (9µm) and DAC (3µm). In the Allegro and DAC polishing stages an abrasive particles suspension was used and in the Piano polishing stage water was poured gently in the disk surface. The total time of the polishing pre-process took about 30 minutes per batch of six samples.

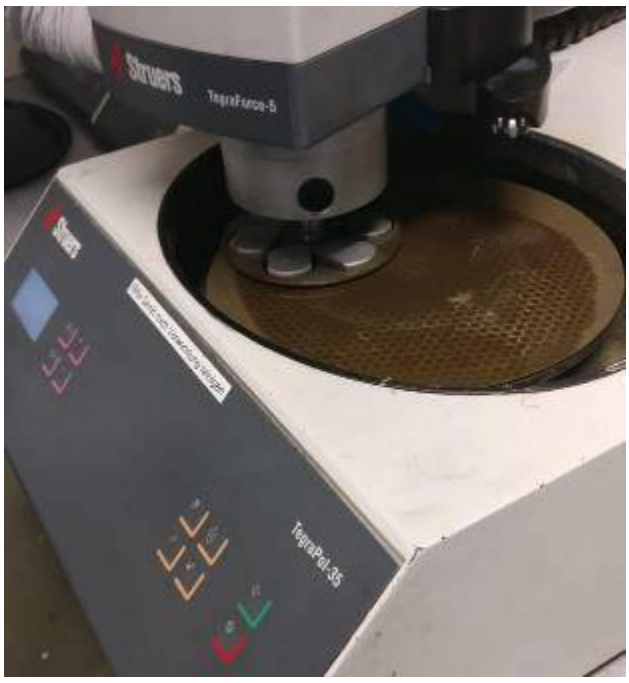

Figure 14. *Struers TegraPol-35 polishing machine with samples loaded in the holder.*

3.3 Plasma Nitriding

The plasma nitriding pre-treatment was done in two parts: All of the AISI 304 samples were nitrided by us in the same PACVD reactor used for the DLC deposition (**Figure 15**), and the SAE4140 samples were nitrided by the company Rübig in a reactor exclusively dedicated

to it. It was originally intended to do all the nitriding processes by us, but that would demand long periods of time with the PACVD reactor occupied for this process, which is why the second batch of nitrided samples was done by Rübig. Both took place at a temperature range between 395-400 °C for a total duration of 30 hours. The gas mixture utilized was a 12% nitrogen gas dissolved in hydrogen.

Figure 15. *Reactor loaded with polished AISI 304 samples before nitriding process starts.*

3.4 PACVD Reactor Conditioning

Before each process, the thermocouples and plates were sandblasted in order to remove the DLC coating from the previous batch. After this was finished, the samples, electrodes and bases were properly cleaned with acetone and ethanol before being situated in the PACVD Rübig reactor (type 40/60 – S), shown in **Figure 16**. The samples were placed vertically, with a minimum distance of 2 cm between them. In addition, four L-section panels were introduced to the chamber (two shorter and two larger ones) in order to have a larger effective area to distribute the reactor plasma current, and the thermocouples were placed, one in the base and the other one in the top of one of the panels. This distribution is shown in **Figure 17**. When everything was ready, the chamber lid was situated in position, the corresponding recipe was loaded in the software and the PACVD process started.

When the coating process was finished, the chamber lid was lifted, the samples were properly labelled with the batch number and position inside the chamber, and removed for further testing.

Figure 16. *Rübig PACVD reactor in FHÖO tribology lab.*

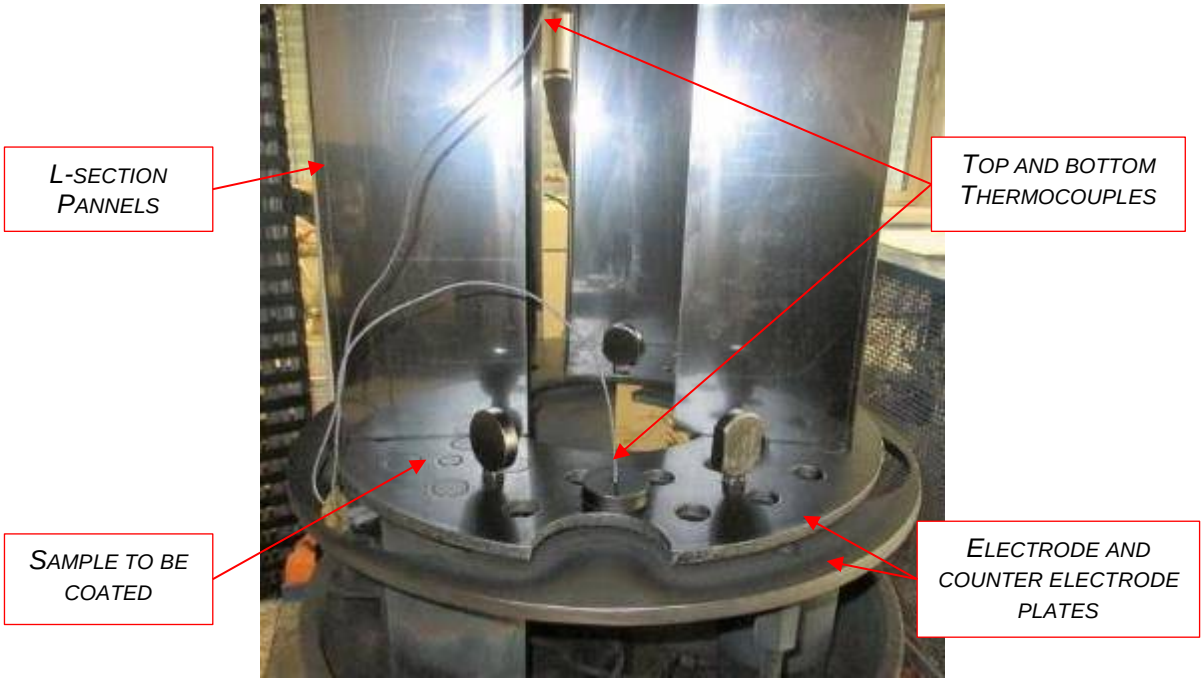

Figure 17. *Layout of a typical PACVD process in FHOÖ.*

3.5 Process Parameters

A test parameter layout was designed with several material properties and deposition process parameters to analyse their effect on coating properties. These conditions were binary, meaning that they were grouped in antagonistic pairs where one condition or the other was fulfilled, but not both at the same time. For example, for coating thickness the condition is either thick coating or thin coating. These parameters were the following:

- Coating thickness: By modifying the PACVD coating deposition step duration, thin and thick DLC layers were produced. This was expected to affect the formation possibility of passing through defects. Thin coated samples have a DLC coating around 3 microns thick, while thick ones have around 30 microns of coating applied

- Silicon interlayer: Since the interlayer may act as an additional barrier between the substrate and the corrosive medium, it was used to analyse its effect on corrosion resistance. This interlayer was either thick (300-500nm) or thin (less than 10nm). It is important to clarify that a silicon interlayer is needed to prevent instant coating delamination after the deposition process, according to the experience at the FHÖO surface laboratory. This is why there are no samples without interlayer, although the original plan was to contrast a thick interlayer with no interlayer at all. Hence, thin interlayer samples in this project are labelled as “no interlayer”.

- Silicon doped DLC: Silicon doping during the DLC deposition alters some of the coating properties (like hardness and electrical conductivity), this could affect the corrosion resistance of the sample so coatings with and without silicon doping were produced. The doping, in those samples where it is applied, is 0.5%wt of silicon.

- Metallic substrate: The DLC coatings were deposited on alloyed steel and stainless steel due to their difference in corrosion resistance.

- Nitriding pre-treatment: The last parameter is the existence of a surface pre-treatment on the metallic substrates, the nitriding process improves the surface hardness consequently enhancing the adherence with the DLC coating. Those samples that were not nitrided are labelled as polished, as although every sample was originally polished, only the non-nitrided ones keep the mirror polish condition.

The combination of these five parameters, with two states each, gives a total of 32 unique combinations that form the parameter matrix. Given the extended number of condition and variables tested, in order to facilitate identifying the parameters involved in the possible combinations, a nomenclature for naming each condition was developed, as can be seen in Table 3.

Table 3. *Parameter nomenclature.*

Parameter		**Nomenclature**
Material	AISI 304	**SS**
	SAE 4140	**AS**
Thickness	Thick	**TK**
	Thin	**TN**
Si Doped DLC	Si Doped	**Si**
	Not Si Doped	**NSi**
Si Interlayer	Thick IL	**IL**
	Thin IL	**NIL**
Pre-treatment	Polished	**P**
	Nitrided	**N**

For a better understanding of this labelling, two examples are shown. An AISI 304, polished (not nitrided), with thick Si interlayer, with a thick and silicon-doped coating is labelled as SS-P-IL-TK-Si, while a SAE 4140, nitrided, with thin Si interlayer, with a thin and non-doped is labelled as AS-N-NIL-TN-NSi.

For every unique combination of conditions, 8 samples were needed in order to complete the analysis:

- 3 for salt spray testing
- 3 for immersion testing
- 2 for mechanical testing

Thus, every process was run with at least 10 samples, in order to have spare samples for any unexpected situation.

3.6 Microscopical and Chemical Characterization

3.6.1 Raman spectroscopy

A Renishaw inVia Raman microscope with a 514 nm wavelength laser beam was used to run Raman spectroscopy in selected coated samples in order to characterize their molecular structure. According to the mechanical and corrosion tests results that will be addressed further on, the interlayer thickness and coating thickness variables were fixed in their “thick” value (TK and IL). This means that the only variables possibly affecting the resulting Raman spectra are the type of metallic substrate, its pre-treatment and the coating’s silicon content.

By performing a deconvolution of the Raman spectrum, it is possible to extract molecular bonding parameters of the DLC coating, such as sp^3 fraction or hydrogen content. In order to do so, and with the aid of OriginPro software, the first step is to subtract the baseline, as seen in Figure 18, in order to remove undesired data of the spectrum, due to

background noise or instrument fluctuation. Then, a double gaussian approximate function is fitted for each coated sample using the theoretical D (1350cm^{-1}) and G (1585cm^{-1}) peaks position obtained from bibliography as seed value. As a result, the deconvoluted D and G bands are obtained (Figure 19).

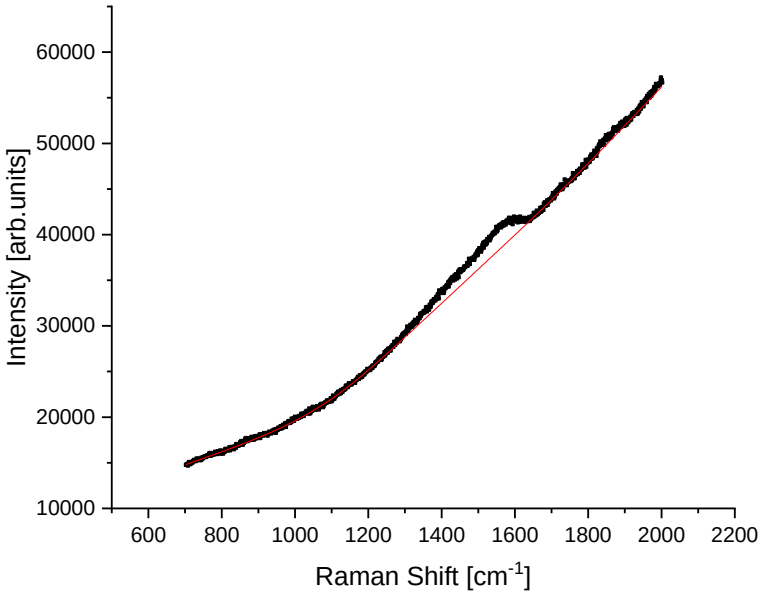

Figure 18. *Raman spectrum with its approximate baseline.*

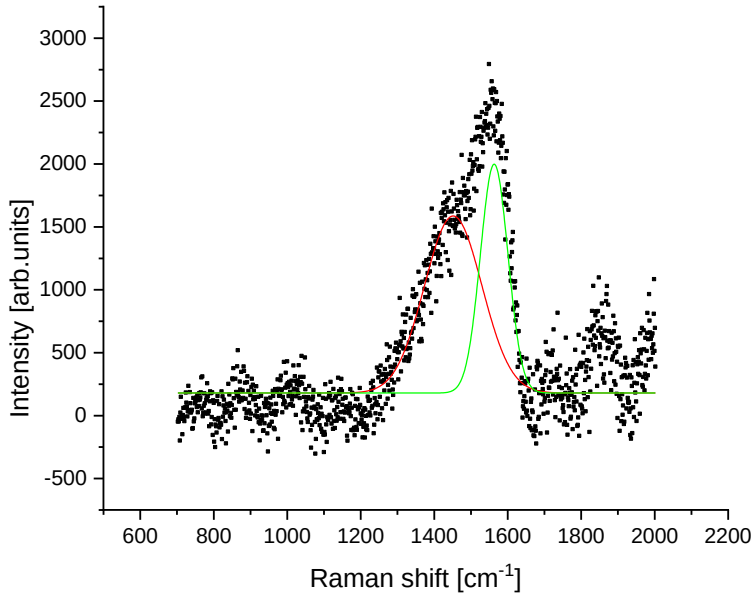

Figure 19. *Raman spectra with the respective deconvolution.*

Raman was done for 8 different combinations of variables, thrice per sample, consisting in a total of 24 tests.

3.6.2 Optical/stereo microscopes

An Olympus GX51 optical microscope (30x-1000x) was used, as well as a MOTIC SMZ-168 stereo microscope (7.5x-30x). All microscope pictures used in this project were obtained with those two devices. The image processing software used was PicEdCora, which features the possibility to add reference tools for measurements, such as length bars or diameter of circles. With this method, macroscopic defects can be analysed at a lower magnification, as well as microscopic features, invisible to the naked eye.

3.6.3 SEM/EDX

A Tescan Vega2 SEM (50x-10000x) with an Oxford AztecEnergy EDX was used for this project. First of all, points of interest were marked with arrows made with marker pens, in order to help to find them in greater augments when using the microscope. If the electrical conductivity of the sample was too low due to the insulating properties of its coating, those samples were then gold sputtered in order to gain conductivity, a feature needed for the SEM to work properly. A copper strip was attached as well, to increase conductivity even further, and then the sample was placed inside the sample holder. Coating and corrosion damage related defects were analysed at high magnifications in combination with the EDS compositional analysis, which allowed to determine if the observed defect was pre-existent or corrosion damage related.

3.6.4 Confocal Microscope

A Leica confocal microscope was used in order to obtain the 3-D topographic mapping of defects, corroded areas, pin on disk's wear track, etc. In order to do so, a mapping area had to be defined, as well as the starting point of the mapping, with the aid of this equipement's xyz coordinate system and its dedicated Leica software. Small areas of about $1mm^2$, like in **Figure 20**, take about 30 min to realize a full scan, while bigger areas of about 10mmx8mm can take up to three hours to complete.

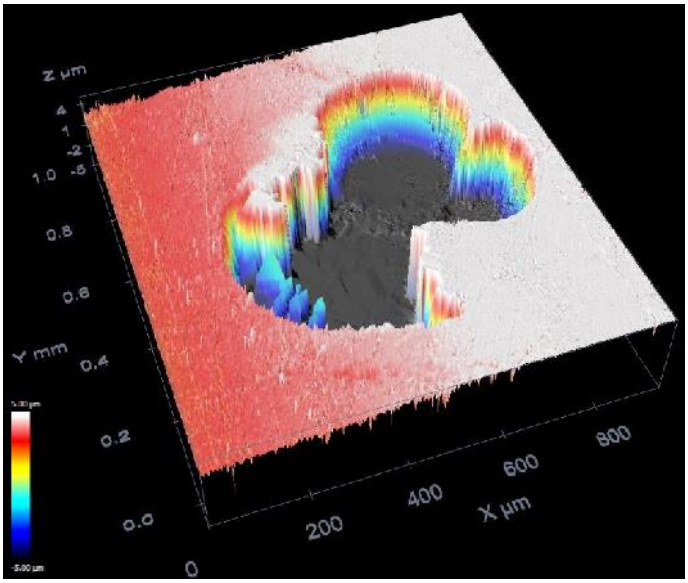

Figure 20. *1mm^2 confocal mapping of a DLC defect after exposure to a corrosive media.*

With the intention to quantify corrosion superficial damage, the precise mapping of the centre of the DLC coated samples, before and after the exposure to the corrosive media, was sought. To achieve this, a sample holder with a micrometric reference point was manufactured. The coated samples were glued to a triangular ABS base that fitted perfectly on a triangular counterpart (**Figure 21**). In this counterpart a SAE 4140 semicircle with five nanoindentation pyramidal marks was glued. These marks served as reference in order to locate the measured centre of the coated sample. Since this experiment's precision was uncertain large areas of 10.2mm x 7.64mm were mapped, the process took 2.5 hours per coated sample.

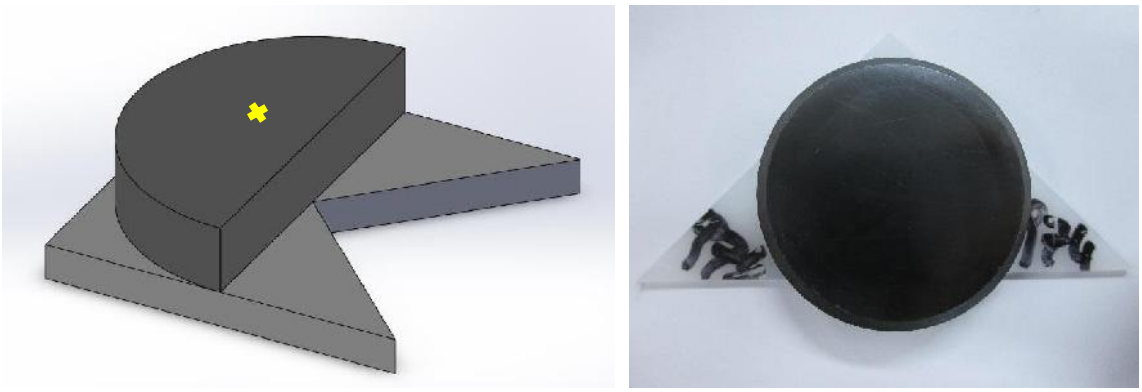

Figure 21. *Confocal sample holder and a corrosion test sample, glued to a triangular ABS base. The approximate location of the nanometric reference point is indicated with a yellow cross.*

3.7 Mechanical tests

3.7.1 Calotesting (Coating Thickness Measurement)

A handmade calotesting device is used for this test. The sample is fixed by four screws behind a cylindrical rod. A steel sphere is then situated between the sample and the rod. The device is turned on, and the rod starts to rotate, which transmits its movement to the sphere. A few drops of a diamond abrasive suspension are poured in the spot where the sphere and the sample are in contact. This suspension abrades the coating, leaving a circular hole in the sample. Then the sample is cleansed with ethanol, and the coating thickness can be determined with a microscope. Two different kinds of diamond suspension were used: an 8nm particle size one for the thick DLC samples and a 3nm particle size one for the thin DLC samples.

Sample results are obtained with the aid of a computer program called PicEdCora, a microscope imaging software that features the possibility to do measures digitally, add reference bars and other useful tools such as diameter measurements or stitch images together, among others. After the correct lens is placed, the reference bar is attached in the software, and by measuring the diameter of the inner and outer circles produced by the ball abrasion, DLC thickness is automatically calculated. In order to get statistical results, this process is repeated twice per sample, on three different samples per batch, resulting in a total of 192 tests. **Figure 22** shows a thick and a thin coated sample observed in the microscope after calotesting was performed.

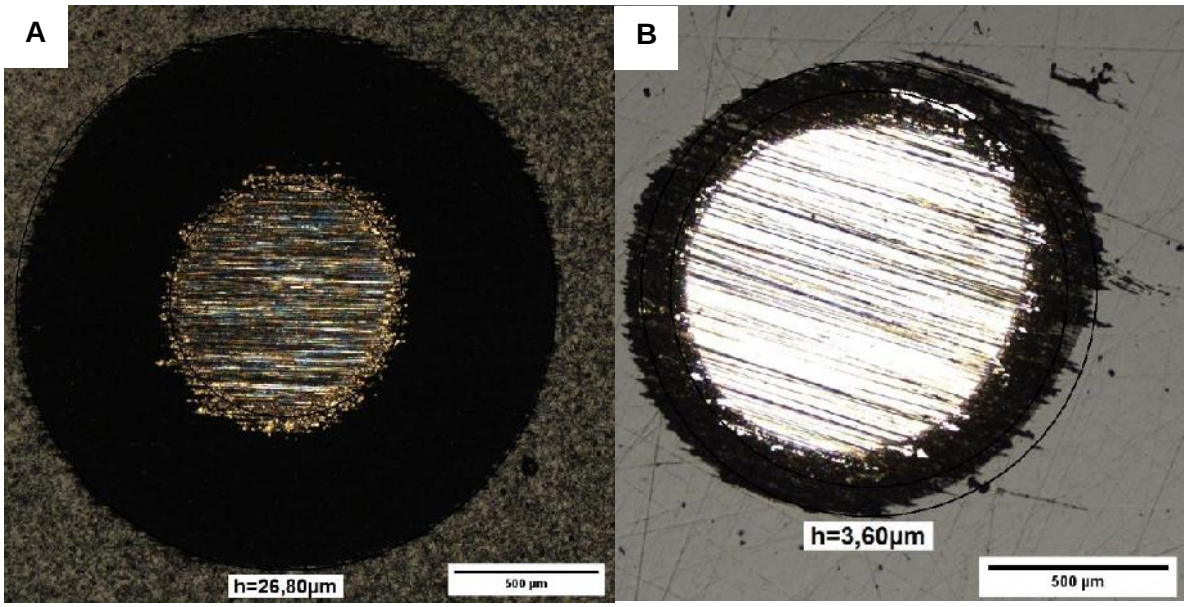

Figure 22. *Calotesting samples analysed in the microscope. A) Thick coated sample. B) Thin coated sample.*

3.7.2 Scratch test

A Revetest Xpress Scratch Tester is used for this test (**Figure 23**). The sample is situated in the moving platform of the device, where it is fixed. A fixed diamond tip is lowered in order to contact the surface of the sample. When everything is in position, the process starts. The sample moves in a straight line for 1 cm, while the tip applies load downwards, progressively in a constant ramp. Depending on the coating thickness, this load increases from 1 to 51 Newton for the thin coatings, and from 1 to 101 Newton for the thick coatings. The software detects the LC1 and LC2 of each process, but anyways the LC1 and LC2 results are double checked in a microscope, in order to get a more precise value.

Figure 23. *Revetest scratch test device.*

Sample results are also obtained with the aid of PicEdCora software. Firstly, a full picture of the scratch line is prepared by stitching three consecutive pictures together. Once this is done and the reference scale is properly attached, a lens with a bigger zoom is used in the microscope in order to identify where LC1 and LC2 critical loads are placed: LC1 is the load where damage can be first seen, and LC2 is the load where the substrate is firstly revealed due to coating failure. Once these loads are found, the areas containing them are located in the full picture obtained at a lower zoom, by identifying features such as coating failures or small imperfections such as scratches or inclusions found in the surroundings of the critical loads. In order to get statistical results, this process is repeated thrice per sample, on three different samples per batch, for a total of 288 scratches made.

In figure **Figure 24** an example of a scratch test on a thick coated sample is shown. The distance measurements util the LC1 and LC2 critical loads are reached allowed to estimate both of their values, in Newtons.

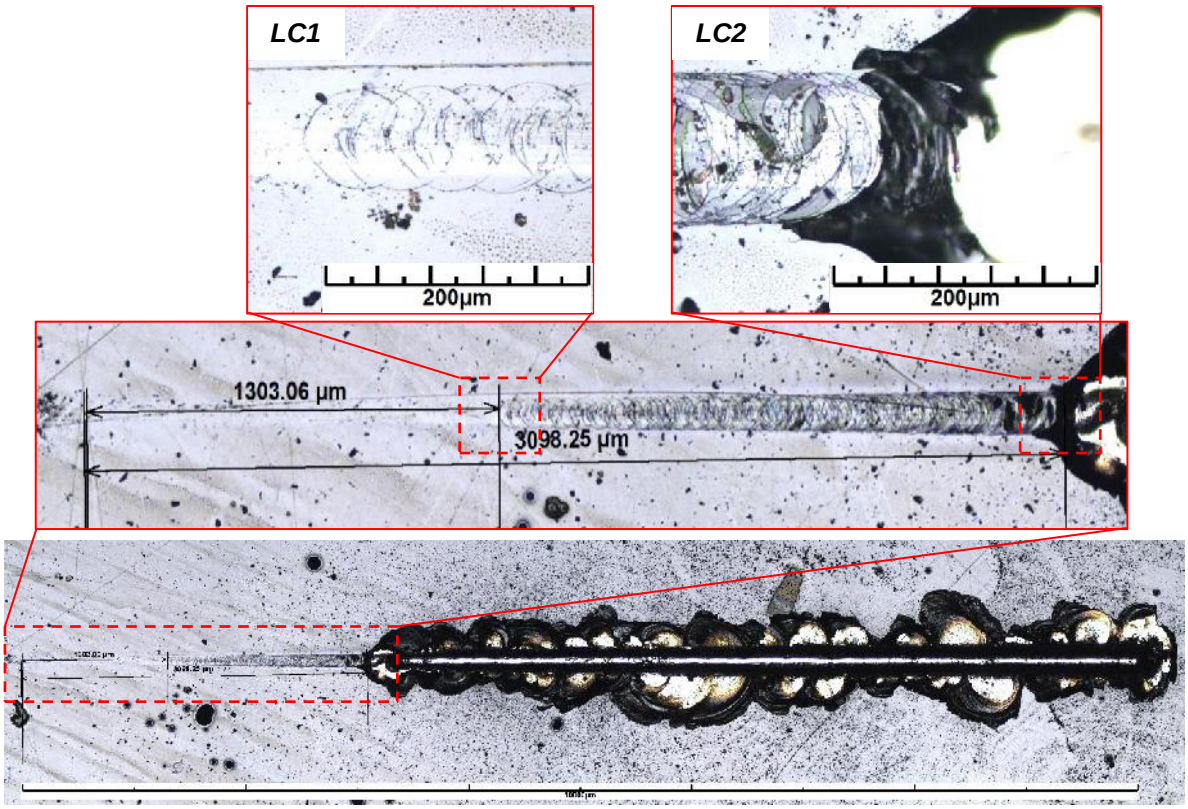

Figure 24. *Scratch of a thick coated sample.*

Since the LC1 is not always easy to identify, a more trustworthy result is used to compare the adhesion between the samples, such as the first complete stripping of the coating to uncover the substrate (LC2 value).

Additionally, while observing the development of scratch tests on the different samples, it was found that the LC1 had different failure modes between the samples. Hence, these were analysed according to the variables each coated sample had, in order to understand which properties affected the changes in coating failure mode.

3.7.3 Nanoindentation

Four samples were introduced in a holder to analyze simultaneously, and fixed to hold position, taking care that each sample is at the same horizontal level. The holder was then introduced into a MTS Nanoindenter XP machine (shown in **Figure 25**). According to the FHOÖ laboratory member's experience, the software was configured to use a maximum fixed indentation force value of 10 mN for thin coated samples, and 30 mN for thick ones. These values translate in different penetration depth: approximately 300 nm for thin coatings and 800

nm for thick coatings. Each sample hardness was measured by a nine-points indentation grid, for dispersion. The process was then let overnight to finish, as the high sensitivity of the machine would be compromised by daily situations, such as street traffic causing vibrations.

Figure 25. *MTS Nano indenter.*

After the dedicated software of the nanoindenter calculated the hardness of the tested samples, results were saved in a Microsoft Excel sheet, where hardness was exposed in Vickers units. This process was repeated 3 times per sample, for a total of 96 tests, plus repetitions in multiple samples where the results were suspicious of being incorrect.

3.7.4 Roughness evaluation

In one sample per combination of variables, coated samples were scanned in order to extract some surface information such as arithmetical mean height (a roughness unit known as Ra and defined as the average of the absolute value of height in a straight line) and superficial arithmetical mean height (a roughness unit known as Sa and defined as the superficial extension of Ra). The scan was made in four quadrants and stitched together. As the scan was performed with 200x resolution, each of the four scans performed for each sample lasted about two and a half hours.

In order to compare results, the confocal microscope files were firstly processed in Gwyddion software where, besides obtaining roughness values, some data corrections can be made as well, such as levelling the surface (which was done in every file as the first step), or change the colour spectrum for a better observation. Sa values obtained this way were reported for each sample.

3.8 Pin on disk

A Tribotechnic Pin-on-disk device is used for this test (**Figure 26**). The sample is fixed in the rotating surface of the device, and a small 100Cr6 ball is situated in a holder, above the sample. The process is done either in a moist atmosphere, provided by wet sponges, or a dry one, in which silica spheres are situated inside the lid. The system is then let to stabilize for the time needed to acquire the atmosphere humidity conditions required. After this is done, the software is configured for the required diameter at which the ball will be in contact with the sample, and also the linear distance used (2 km in our process), which is converted in number of revolutions (22738 for the radius of 14mm used).

Figure 26. *Pin on disk device*

When the process is over, the steel ball is observed in an optical microscope and analysed in PicEdCora software. Its wear forms a plain circle, and this can be compared between each process by obtaining the circle diameter, while the friction coefficient is determined by the software for every cycle, and the maximum, minimum and mean coefficients are obtained. This process is done thrice per DLC system, both on wet and dry environment, and once per sample. Additionally, it is done in uncoated samples of each substrate. **Figure 27** shows an example of a worn sphere after performing the test.

The test variables regard only the variation in DLC compositions, meaning that the analysed condition is just the doping of Silicon on the DLC. Additionally, atmosphere variation as dry (less than 25% air humidity) and humid (more than 80% air humidity) are analysed. The

test was done thrice per condition, for a total of 12 runs, plus extra runs for uncoated samples, in both humid and dry atmospheres.

Figure 27. *Steel sphere wear during tribo test.*

Finally, a representative sample per condition was scanned in confocal microscope, and wear track depth was analysed. In the topographic profile obtained from the confocal microscope, three roughness profile lines crossing the wear track were drawn and the median height of the track was compared with the median height outside the track using Gwyddion software to extract this data.

3.9 Corrosion tests

3.9.1 Salt Spray

Three samples of each batch were painted with waterproof paint in the lateral surface, to avoid corrosion damage caused by border effects, and then introduced inside an Erichsen Salt Spray chamber, adding as well uncoated samples of both metal substrates, both nitrided and non nitrided. Every sample was placed in a plastic holder, and properly labelled. The test was then prepared according to ISO 9227 standards. The 5%wt saline solution was prepared and introduced to the recipient at the back of the chamber. Then the process was configured to last 300h in a 35ºC atmosphere. Every 100 hours the coated sample with biggest degree of damage of each batch was removed, in order to obtain results for 100h, 200h and 300h of exposition. The surface of each sample was analysed with a microscope for a better observation of the corrosion damage, and those samples removed after 300 hours of explosion were analysed in SEM-EDS microscope as well. Additionally, confocal scans were performed as well for discontinuities in the sample's surfaces.

3.9.2 Immersion test

A handmade immersion testing device (**Figure 28**) was built by a fellow colleague specifically for this project, in which 16 samples could be tested at the same time. Samples are placed in the corresponding sample holders, where needleless syringes with an O-ring attached to each one of them are placed on top of each sample. The syringe-sample systems are fixed through a series of screws and washers, as seen in **Figure 29**. The same volume of a 3.5%wt saline solution is poured inside each syringe to produce the sample immersion, and after that a plastic pipe is attached, that is connected to a steel hollow tube on the other end. The steel tube is connected at the same time to a bubbling system consisting in a syphon containing tap water and connected to compressed air on its other connection, in order to ensure a constant and uniform bubbling on the solution in each syringe.

After 50 hours of exposition, the process is over. The syringes are detached from the plastic tubes and attached to an empty syringe in order to remove the remaining solution. The samples were later examined in a microscope for a better observation of the corrosion damage. **Figure 30** shows a DLC coated sample after the test was performed, where the mark produced by the O-ring attached to the syringe can be easily appreciated.

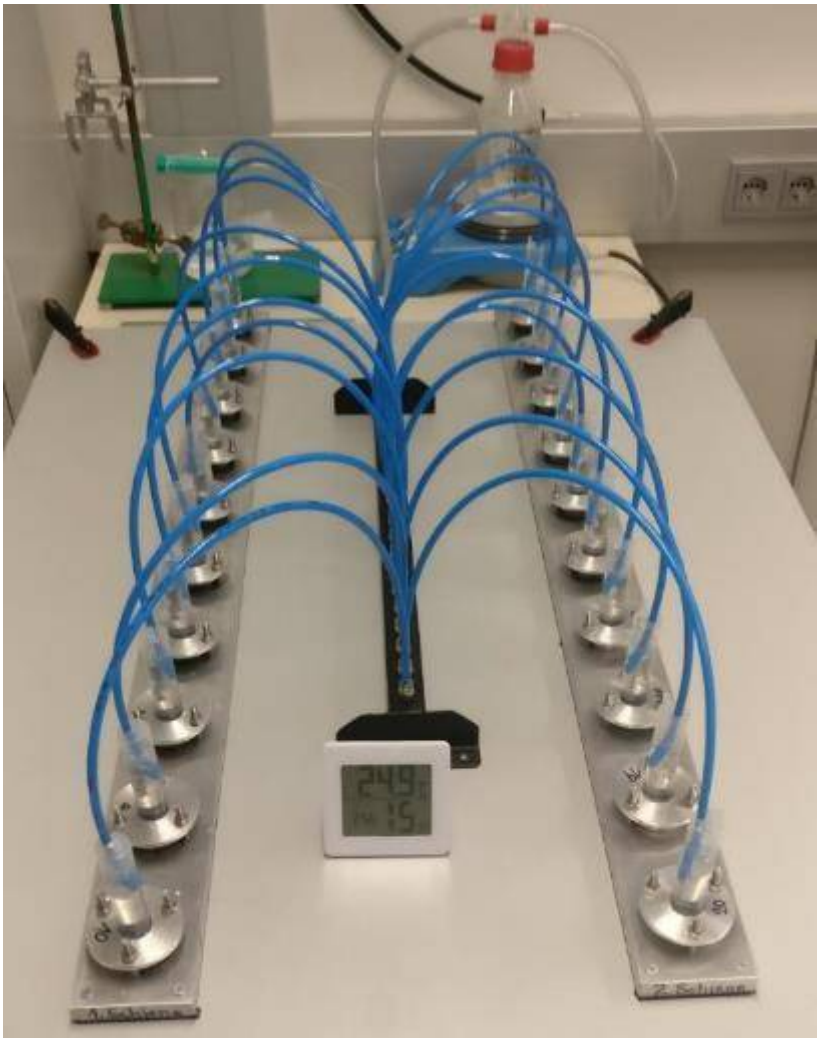

Figure 28. *Immersion test device.*

Figure 29. *Immersion device fixed to position.*

Figure 30. *DLC coated sample after immersion test was performed.*

In one of the three immersion tests performed, coated samples were scanned before and after the immersion in the confocal microscope test in order to visualize surface changes due to corrosion. Besides using Gwyddion software to level the sample surface and change the colour spectrum, additional information was extracted with an imaging software called ImageJ, like quantifying superficial changes in a coated sample by estimating areas with pre-defined topographic height thresholds, before and after the immersion. As each scan was done by dividing the studied surface in four different files, the total area estimation is obtained by a sum of the areas on the four files corresponding to each coated sample. The damage provoked by the exposure to the test is obtained as a percentage regarded to the initial mapped area before the immersion test.

Information can be obtained not only by extracting quantitative information from the confocal scanning files, but also by observing the spectrum in every scan. These spectra show different altitudes in the surface of the sample as colour gradients, meaning that when the colour of a certain region changes, it has a different altitude. This way, different defects such as pits, protuberances or delaminations can be easily identified. For instance, **Figure 31** shows a full map consisting of four separate scans of a sample with a partial corrosion-induced delamination.

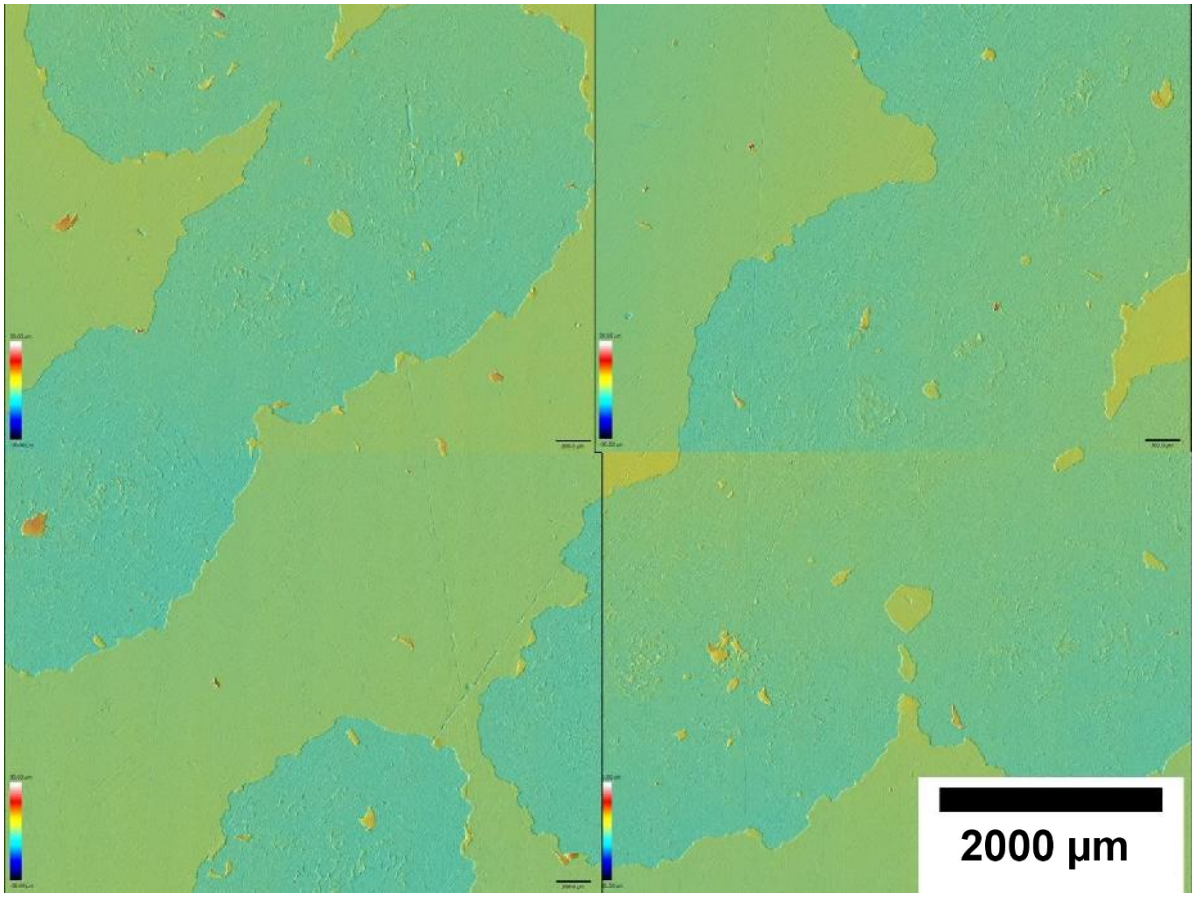

Figure 31. *Confocal scan of sample with partial delamination after immersion test.*

It is important to clarify that the scan was done in a given area before and after the immersion test, making it impossible to know if corrosion attack would appear in that region. Hence, it can only be confirmed if there is corrosion, but it cannot be said there is not when there is no evidence, as the scan is only done in a region on the centre of the sample - there could be corroded areas outside the scanned region but inside the tested area.

3.9.3 Weighted property index method

In order to determine the set of variables that result in the best corrosion-related behaviour, from a qualitative point of view, the weighted property index method is used (WPIM)[45]. To do so, the different damage morphologies were given a relative weight from 0 to 100, related to the degree of damage observed for each sample on the immersion and salt spray tests. In **Table 4**, the relative weight for each damage morphology is summarized. Since bibliography material regarding these kinds of damage was not found, a name for each morphology is proposed according to our criteria. As an example, on Figure 32 a picture of each damage morphology is shown.

The individual relative weight for each test run is added and multiplied by the test type corresponding weight factor, in this case the weigh factor was chosen as 0.1 for both salt spray and immersion tests. In order to clarify the procedure an example is presented in **Table 5**.

Table 4. *Damage morphologies relative weight.*

N°	Damage Morphology	Corrosion Resistance	Weighted Property
1	*No Damage*	Excellent	100
2	*Punctual Concentric Cracking Point*	Very Good	80
3	*Lonely Pit*	Very Good	80
4	*Isolated Pits (< 5 pits)*	Good	50
5	*Multiple Pits (> 5 pits)*	Poor	30
6	*Spray Delamination*	Very Poor	10
7	*Multiple Concentric Cracking Points*	Very Poor	10
8	*Nitriding Edge Effect Zone Wave Delamination*	Very Good	80
9	*Nitriding Edge Effect Zone Spray Delamination*	Very Good	80

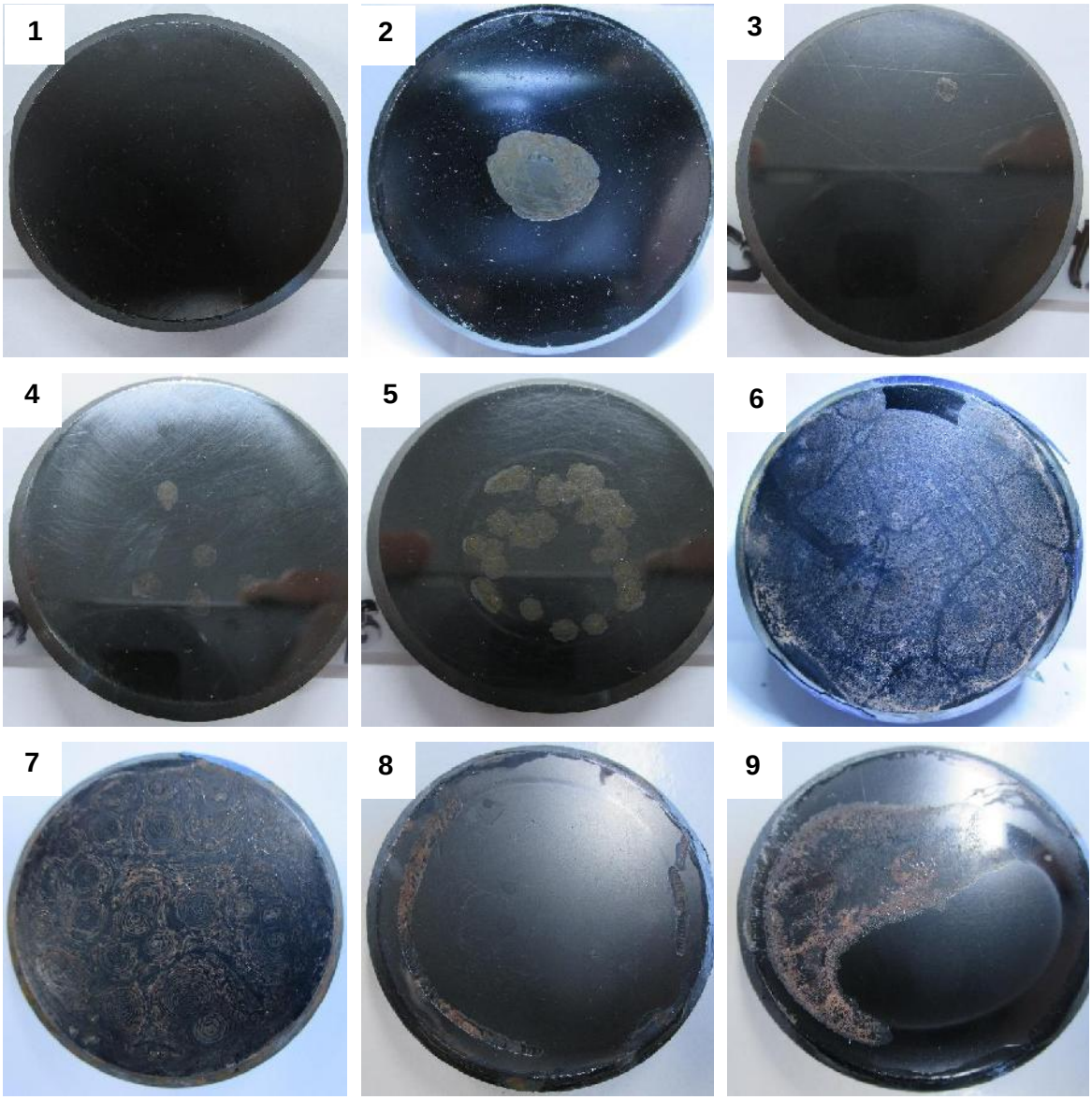

Figure 32. *Examples of each morphology considered for WPIM.*

Table 5. *Example of total WPI calculation for different damage morphologies during immersion and salt spray tests.*

Sample	Salt Spray			WPI	Immersion			WPI	Total WPI	Ranking
	100h	200h	300h		1st	2nd	3rd			
AS-TK-Si-NIL-P	1 100	1 100	3 80	28	1 100	1 100	1 100	30	58	1°
AS-TN-Si-IL-N	1 100	4 50	4 50	20	1 100	1 100	1 100	30	50	2°
AS-TN-NSi-IL-P	5 30	5 30	5 30	9	3 50	5 30	4 50	13	22	3°

4 Results and Discussion

4.1 DLC Characterization

In this section, chemical and mechanical characterization results are presented and briefly discussed.

4.1.1 Raman Spectroscopy

The only variable that affected the Raman spectra shape was the coating's silicon doping. **Figure 33** displays the two types of obtained spectra, before and after the D and G bands deconvolution was made. It can be observed that there is an increase of the linear fitted background's slope by silicon doping of the DLC. This effect is due to the photoluminescence background increase of the Raman spectra under the D and G peak spectral region that takes place with hydrogen content increase. The ratio between the slope of the linear fitted background under the peaks (m) and the intensity of the G peak (I(G)) can be used to estimate the bonded hydrogen content in the DLC coating with the following equation: $H[at.\%] = 21.7 + 16.6\ \log\left\{\frac{m}{I(G)}\,[\mu m]\right\}$[60]. In this case the mean hydrogen content was 57±1% for NSi coatings and 27±1% for Si coatings.

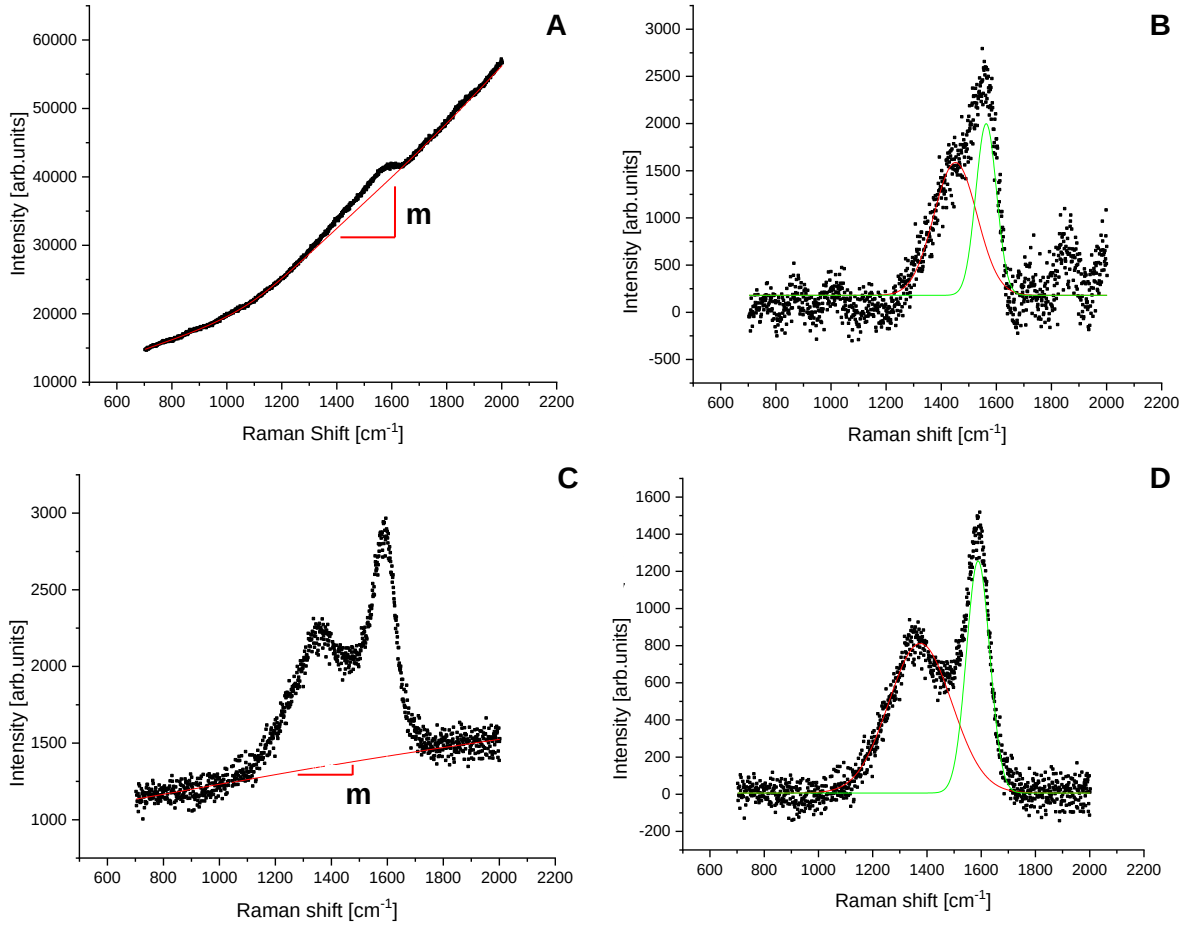

Figure 33. *Raman spectra of Si/NSi DLC coated samples. A) AS-P-IL-TK-Si coated sample before baseline subtraction. B) AS-P-IL-TK-Si coated sample after baseline subtraction and D and G peak deconvolution. C) AS-P-IL-TK-NSi coated sample before baseline subtraction. D) AS-P-IL-TK-NSi coated sample after baseline subtraction and D and G peak deconvolution.*

In hydrogen-free carbons and a-C:H's with H<20%at, the structural disorder, measured as FWHM(G), and the topological disorder, measured as Displacement(G), both increase as disorder increases. This disorder increase is usually linked to higher sp^3 content, density, and mechanical properties. By further increasing the amount of hydrogen over 25%at, the overall sp^3 content can still increase, but most of the sp^3 bonds are hydrogen terminated, meaning there is not necessarily a raise in C-C sp^3 content. This results in structural disorder (bond angle and length distortion) decreasing with hydrogen content, while topological disorder (size and shape of sp^2 clusters) continues to increase, meaning that FWHM(G) and Displacement(G) will have opposite trends[50].

The silicon doped coatings displayed a FWHM(G) decrease and a Disp(G) increase when compared with the non-silicon doped ones (**Figure 34**). This result is consistent with what was expected for DLC coatings with high hydrogen content. Additionally, in **Figure 35** the I(D)/I(G) ratio of the different analysed coated samples can be seen. Taking these values into account as well as the position of the peak corresponding to the G band and the three-

stage model proposed by Ferrari et al[51], the sp^3 bonds fraction can be estimated in approximately 10% for Si coatings and 15% for NSi coatings.

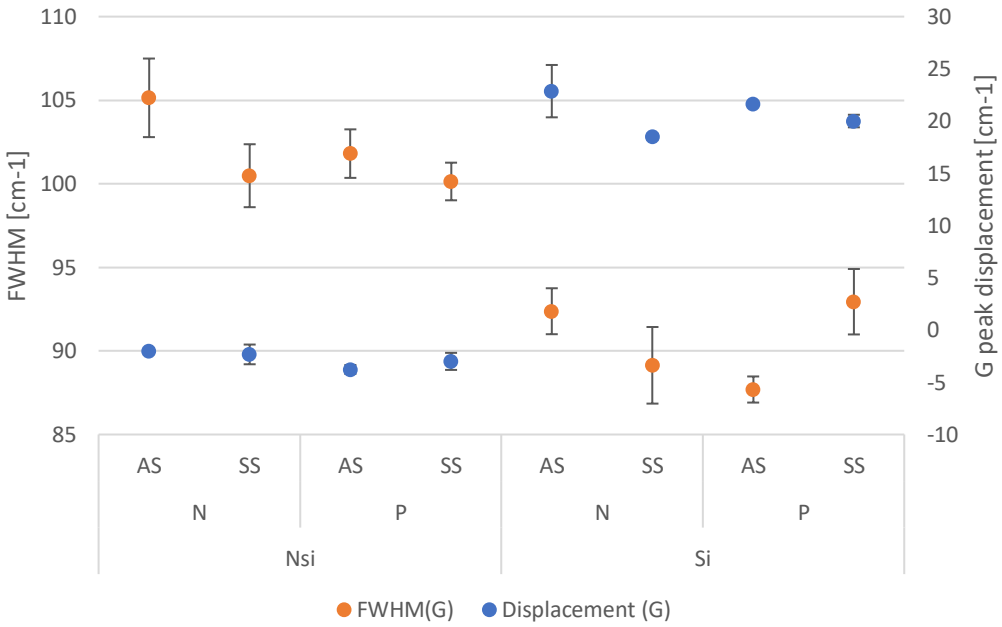

Figure 34. *FWHM(G) and Disp(G) as function of the type of substrate, its pre-treatment and the coating's silicon doping.*

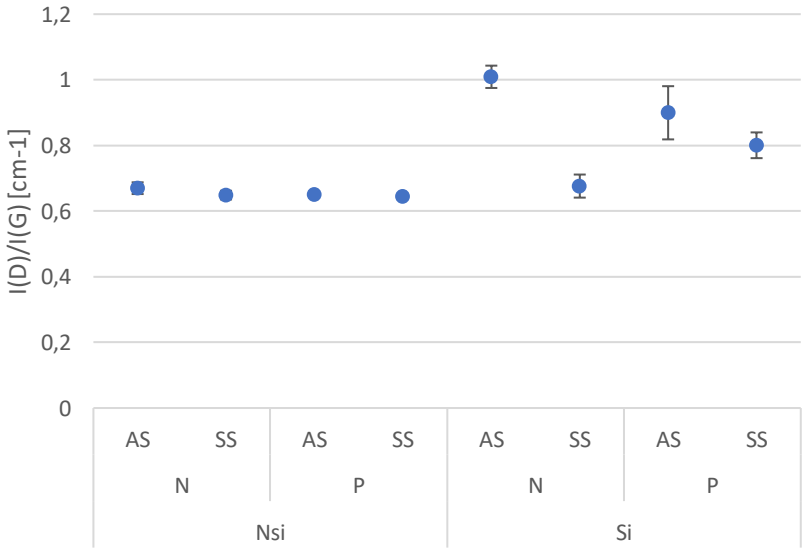

Figure 35. *I(D)/I(G) ratio as function of the type of substrate, its pre-treatment and the coating's silicon doping.*

4.1.2 Roughness

Roughness results extracted from the confocal microscopy files are exposed and the effect of the different examined variables is discussed. **Figure 36** shows the roughness values

for each coating. It should be mentioned that the AS-TK-Si-NIL-N sample had an unusually large value of roughness, presumably due to an incorrect surface conditioning of the substrate.

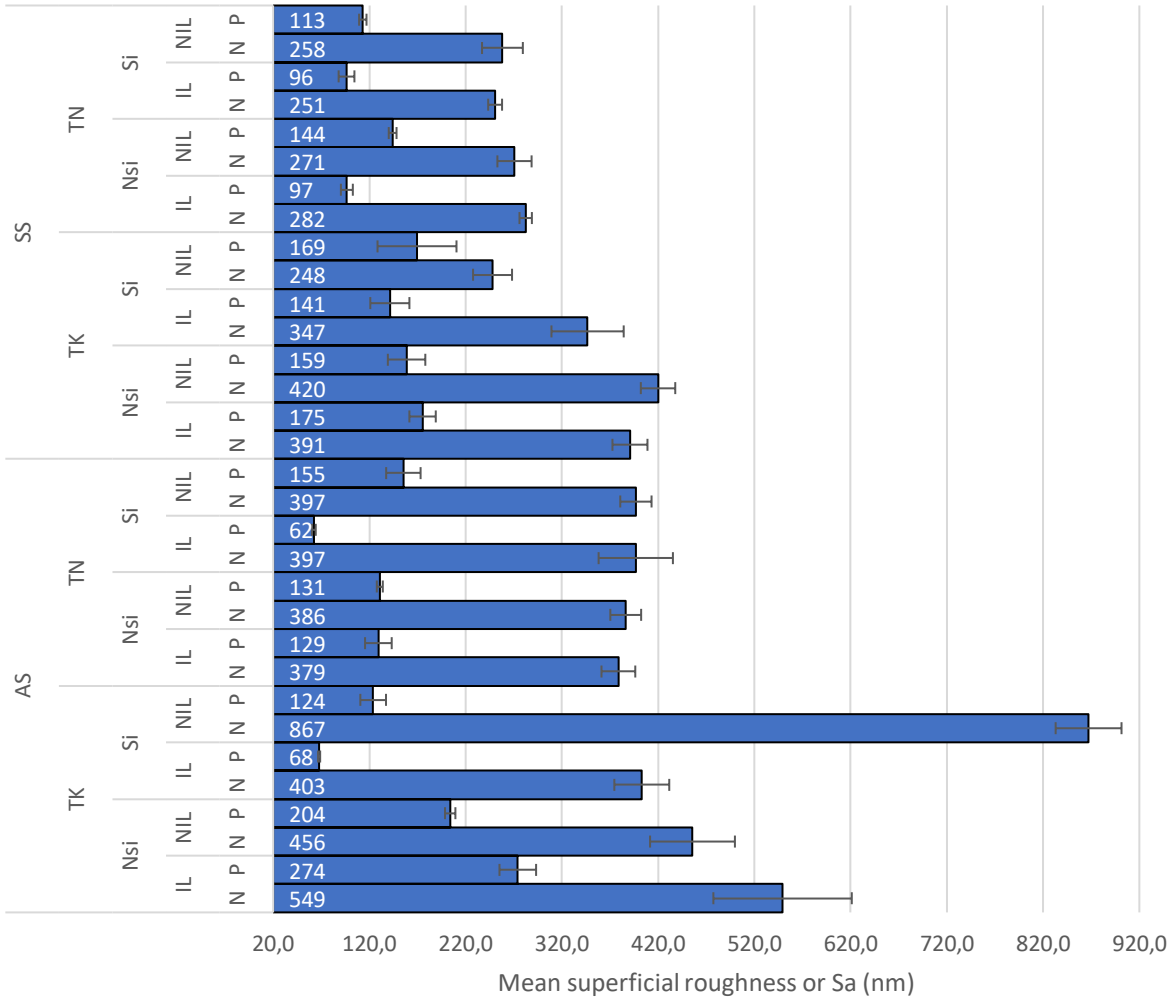

Figure 36. *Roughness results for every parameter tested.*

Silicon doping, silicon interlayer and substrate do not seem to affect roughness values. Firstly, regarding the doping, this means that the silicon doping may not interfere in the coating surface finish. On the other hand, the interlayer copies the surface of the substrate, and likewise, the coating copies the surface of the interlayer. Thus, the DLC surface is similar to the substrate surface. On the side of the metallic substrate, every sample was thoroughly polished by the same processes in the same machine, so there should not be remarkable differences in the substrate roughness. As the coating copies the substrate roughness, and both substrates should present a similar roughness, this condition should not affect the system roughness.

Except on a few samples, thick coated samples tend to have a higher roughness than thin ones (**Figure 37**). It was found in other researches[52] [53] that roughness initially increases,

as the growth rate of the films is higher in the peaks than in the valleys, but this effect changes as the film gets thicker, as the lateral growth in the valleys lead to its filling up. This is not in concordance with the results obtained in the current investigation, but it is important to note that the coating thicknesses in both studies cited are lower than the thin coated samples in this project. Thus, a different possible explanation to this behaviour was reached. As DLC deposition time increases, DLC thickness increases as well due to the constant flow of precursor gases. Due to the DLC amorphous nature, defects in the coating appear, and are likely to appear more on thick DLCs than thin ones, as they have higher coating volume[54]. This may cause irregularities in the surface that translate in a higher roughness on thick samples.

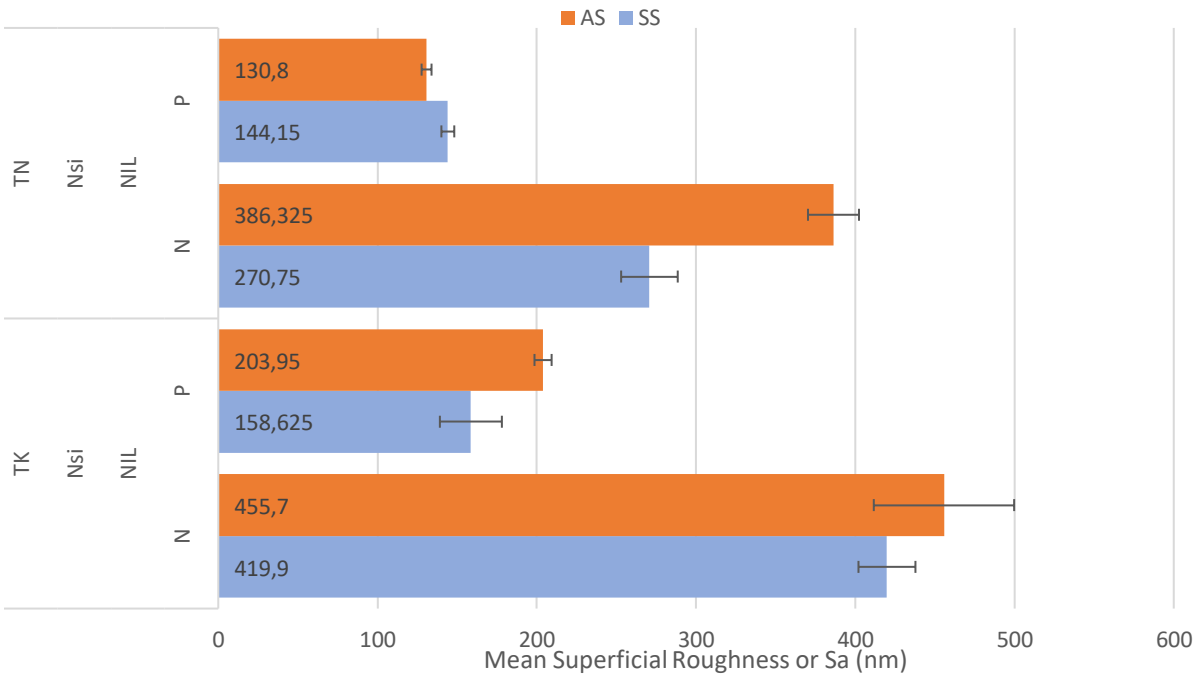

Figure 37. *Effect of coating thickness in roughness.*

Nitrided samples have in every case a higher roughness than the non nitrided ones, as it can be seen in **Figure 38**. This behaviour may be a consequence of a different lattice expansion of the grains in the polycrystalline steel with the inward nitrogen diffusion from the differential swelling of the grains, and the volume difference between the nitrides inside the diffusion zone and the matrix. While the formation of nitrides in SS substrates was intended to be avoided with a low nitriding temperature, the AS substrates were nitrided at higher temperatures, and the formation of iron nitrides along the grain boundaries is to be expected[13].

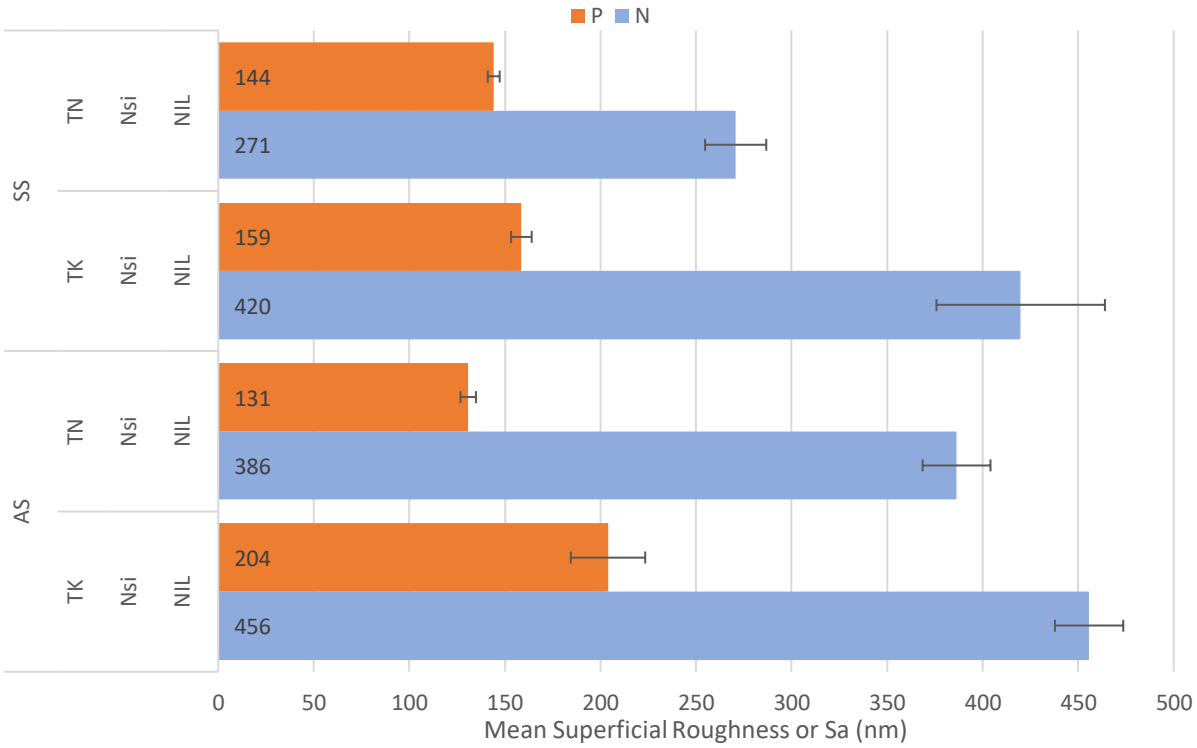

Figure 38. *Effect of nitriding pre-treatment on roughness.*

4.1.3 Coating thickness

Figure 39 shows the coating thickness values obtained from the Calogrinding test, for the thick and thin coated samples. The effect of the different examined parameters is explained.

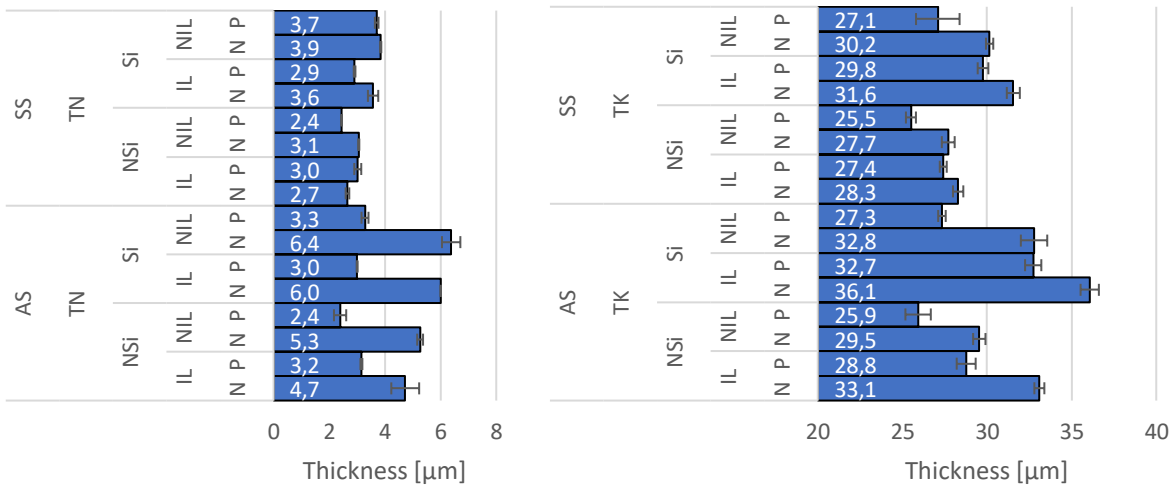

Figure 39. *Coating thickness results for every parameter tested. Left: on thin coated samples. Right: on thick coated samples.*

Regarding the silicon interlayer, since the NIL samples have at least a thin silicon interlayer, and no difference in coating thickness behaviour can be seen between NIL and IL samples, it could be said that the interlayer thickness does not have an appreciable effect on the coating thickness.

As seen on **Figure 40**, the nitriding pre-treatment had an increasing effect on the thickness of the AS samples, while SS achieved similar thickness values between P and N samples. More work needs to be done in order to identify the nature of this phenomenon, for example, a FIB (Focused Ion Beam) cut could be performed in order to measure the coating thickness of the alloyed steel samples, to evaluate if some kind of error was introduced with the Calogrinding thickness measuring technique.

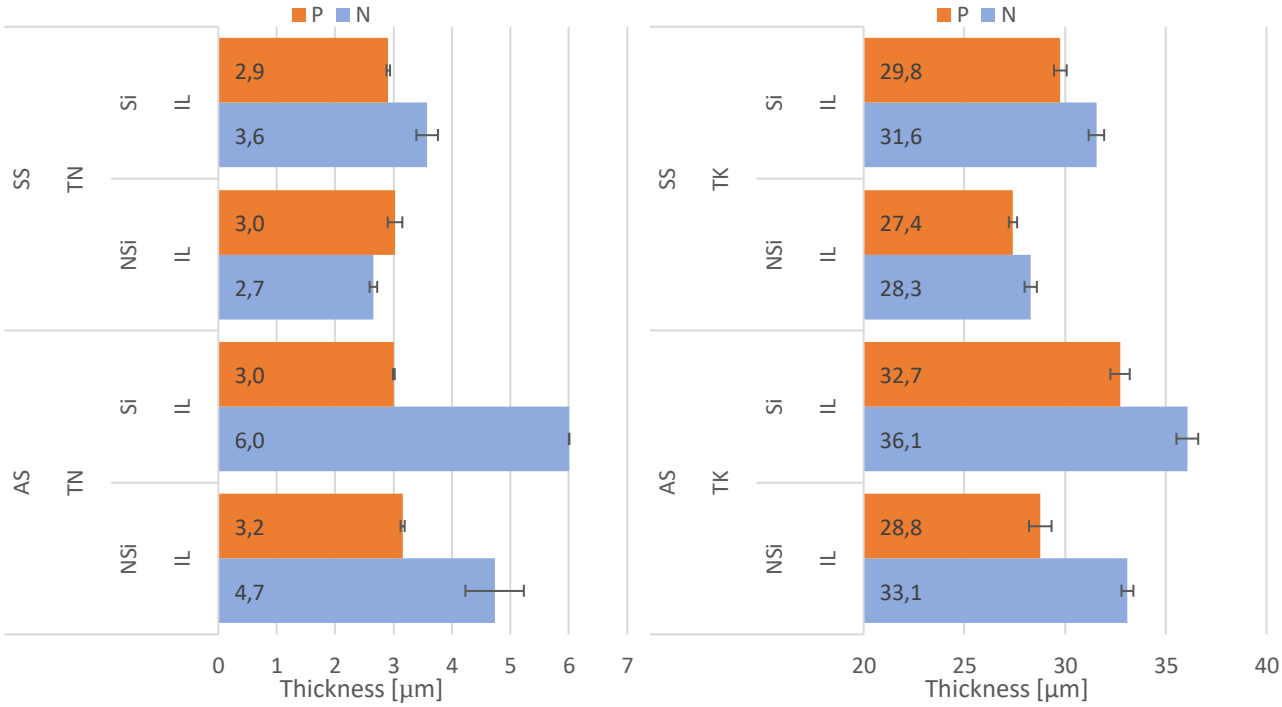

Figure 40. *Effect of nitriding pre-treatment on coating thickness. Left: on thin coated samples. Right: on thick coated samples.*

4.1.4 Hardness

Hardness results from the nano indentation test are shown in **Figure 41** and the possible effect of the different variables is discussed.

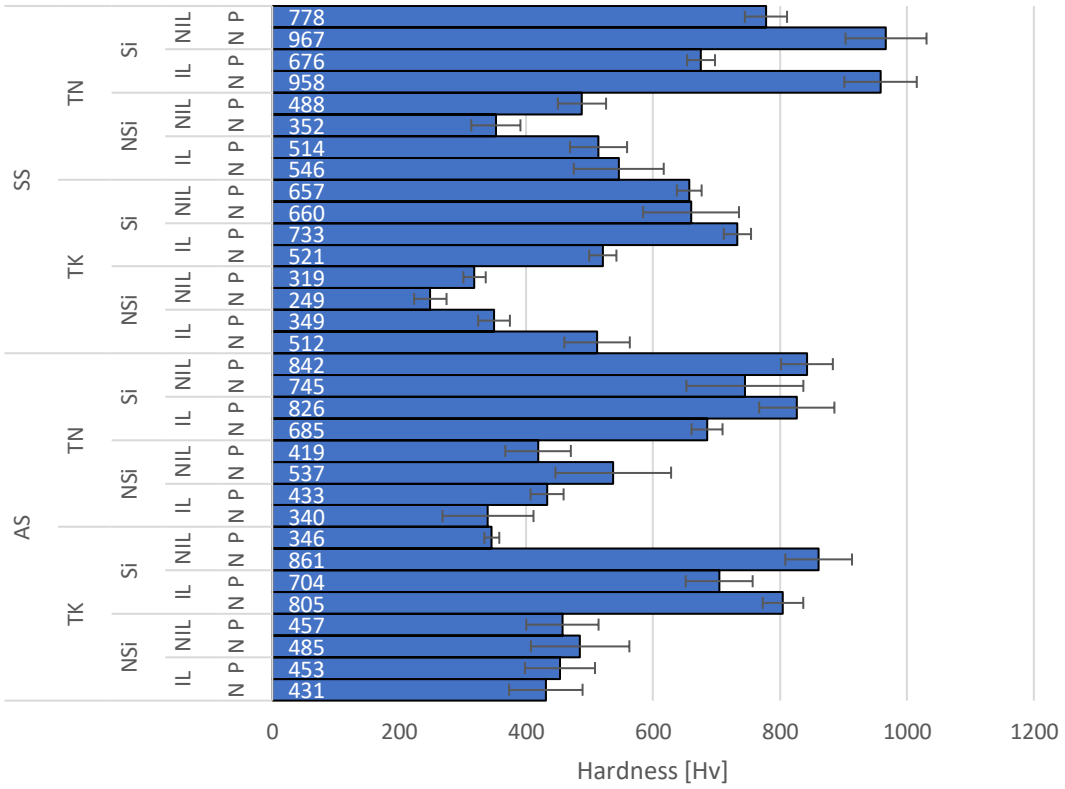

Figure 41. *Hardness results for every parameter tested.*

The indenter's maximum penetration depth ranges between 200 - 400 nm and 800-1000 nm for thin and thick films, respectively. This means that the observed hardness reflects the actual hardness of the DLC itself with slight-to-none effect of the substrate material, its pre-treatment, the coating thickness or the silicon interlayer thickness. Consequently, hardness results do not show any significant behaviour pattern regarding these variables.

The effect on the coating hardness by adding Si to the DLC chemistry can be observed for both metal substrates (**Figure 42**). It can be seen that in all but two cases the hardness of the coating increases by 300-500 HV with a 0.5% Si doping.

The effects of the DLC silicon doping on the coating mechanical properties, like hardness, residual stress and elastic modulus are contradictory in most literature reports. Some researchers have found that increasing silicon atomic concentration results in a decrease of hardness and residual stress[6] [7] [55], while others have found a dependence between PECVD deposition parameters, like TMS (Silicon precursor gas) flow rate and pulse voltage, with hardness and friction coefficient[56]. Lee et al.[57] observed that the mechanical properties of Si-DLC coatings increased significantly when the silicon concentration was less than 5%at. For higher concentrations, the mechanical properties showed a saturated behaviour.

Since the silicon content in the present work is 0.5%at and resulted in a hardness increase, the adopted structural model in Lee et al's. paper contributes to analyse the observed behaviour. This DLC structural model, proposed by Robertson and O'Relly, suggested that sp^2 clusters are connected by sp^3 bonds and that the hardness and residual stress are proportional to the degree of three-dimensional inter-links of the sp^2 clusters. Since silicon atoms can have only sp^3 hybridized bonds its addition to the DLC amorphous network of C-H bonds might increase the three-dimensional inter-links. Since this increase in the network interlinks affects the distortion of atomic bonds angles and/or lengths, an increase of the residual stress and short-range order could be expected in amorphous materials. Lee et al. analysed the FTIR spectra of the DLC allowing to characterize the different changes in the DLC bonding with increasing Si% content. The results showed that the silicon atoms would firstly replace sp^1 triple bonded carbon, which plays the role of network termination. This replacement of network terminations with sp^3 hybridized silicon bonds would increase the three-dimensional inter-links in the atomic bond network resulting in the increase of the mechanical properties.

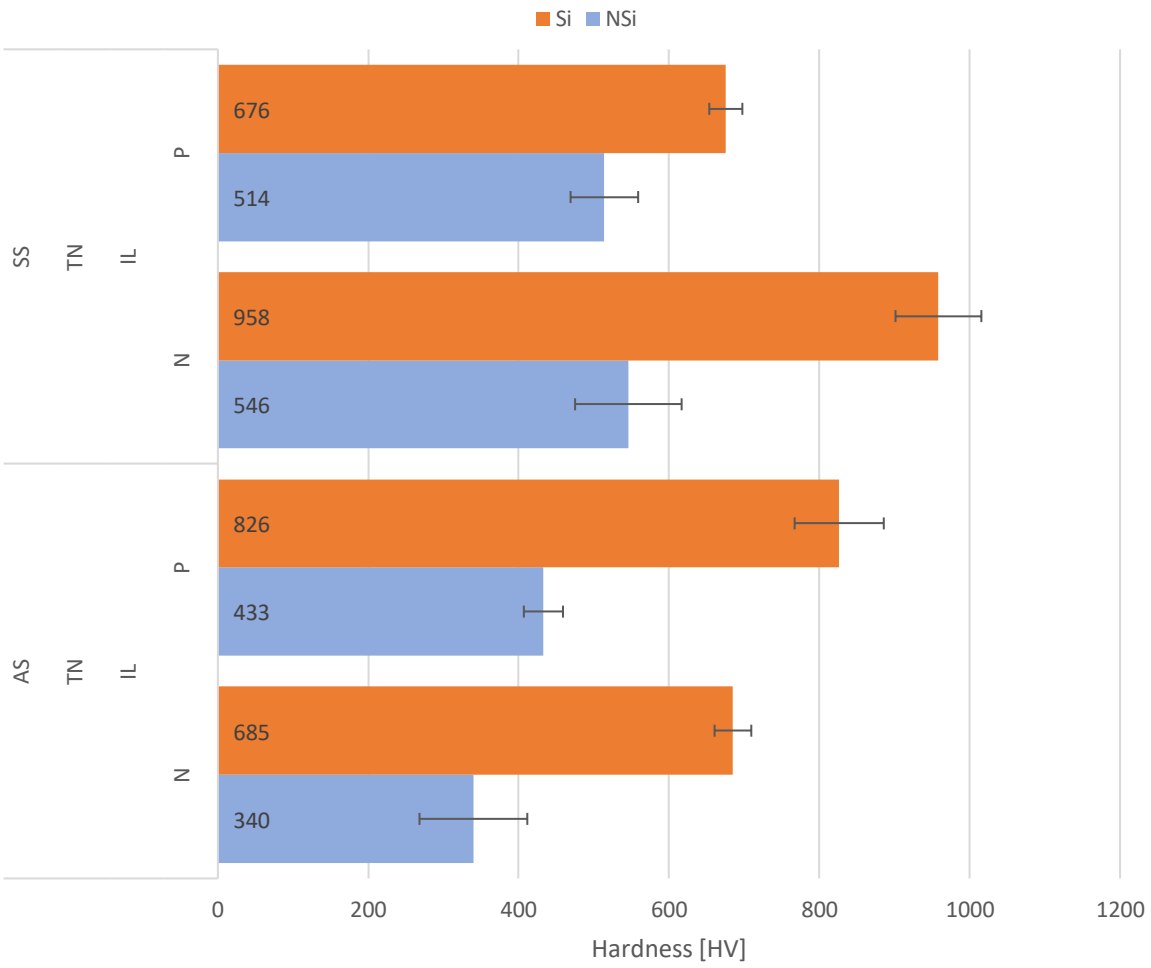

Figure 42. *Effect of silicon doping in hardness.*

4.1.5 Scratch test

The LC1 (coating cracking critical load) values were not as precise and easily determined as LC2 (coating total delamination critical load) values, and since they are both used to represent adherence properties, LC2 will be taken as a measure of the DLC's adherence resistance since it represents the load at which the coating fully delaminates. The scratch test results are presented in **Figure 43**.

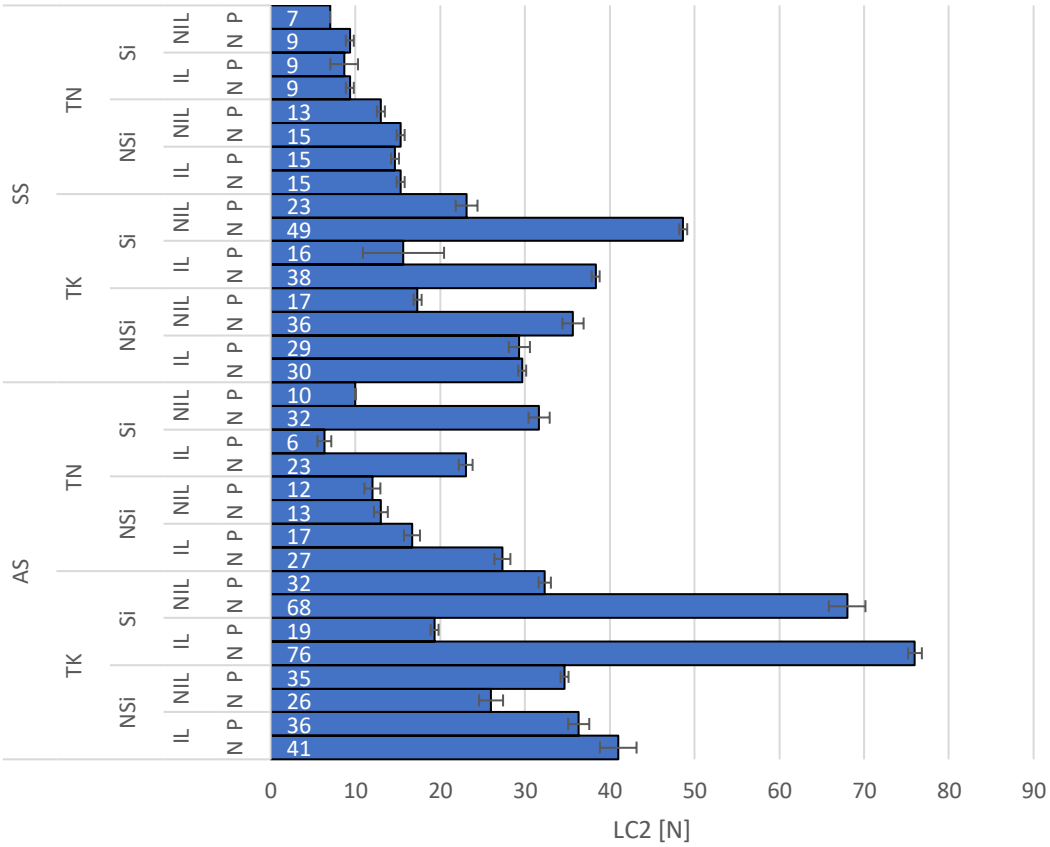

Figure 43. *Adhesion results for every parameter tested.*

Contrary to the improvement in DLC-substrate adhesion that was expected, the DLC silicon doping does not have a clear effect on LC2 values, as also noted by another investigation[58]. This may be a consequence of the presence of a silicon interlayer in every sample: As the interlayer already provides a better adhesion for the coating, the expected effect of improving the adhesion by the silicon doping is already fulfilled, hence, the adhesion is already high and no additional improvement is seen.

It is a fact that the use of silicon-containing interlayers in industrial processes is a well-known approach for improving DLC adhesion on steels[11]. Thus, since a difference in adhesion is not observed between the samples regardless of the silicon interlayer thickness, it could be

concluded that a thicker silicon interlayer does not enhance the adhesion between the coating and the substrate.

Regarding the DLC coating thickness, in every case the thick coating samples LC2 values increased for both metallic substrates (**Figure 44**). Thick DLC coatings were expected to show an increased load-bearing capacity, and hence a higher load would be needed in order to produce delamination, resulting in better adhesion. This may happen because thicker coatings distribute the resulting stress more homogeneously during loading in a way that nearly no stress appears at the interface [17]. It may also be influenced by a difference in the load ramp between thin-coated samples and thick-coated ones, which could have had an effect in the critical load behaviour and make the results not comparable. As in every case LC2 is higher in every thick coated sample, this was disregarded, but still, the different load ramp may imply a difference in the strain rates of the coatings, an effect that exceeds the investigation for this project. To confirm this, thick coated samples should be submitted to the same load ramp as thin coated ones, and check if the LC2 values are consistent.

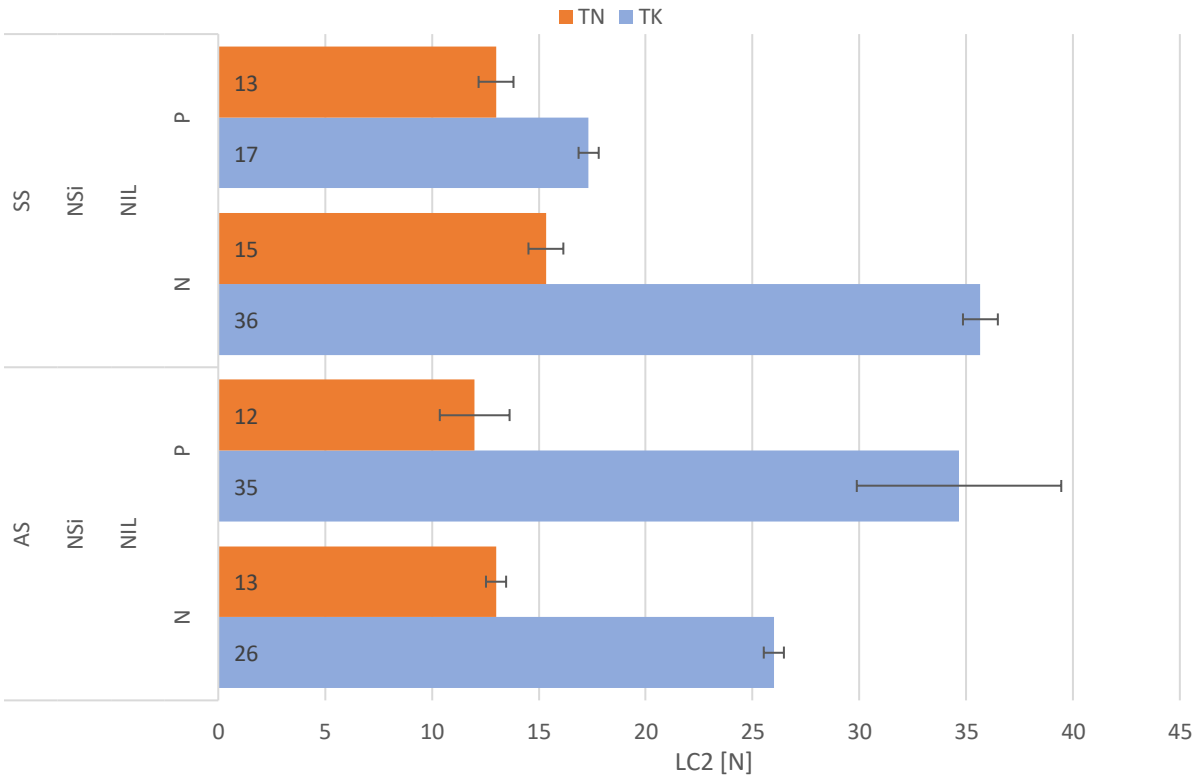

Figure 44. *Effect of coating thickness in LC2.*

As it can be seen in **Figure 45**, the nitriding pre-treatment of almost all the samples resulted in an increase of the LC2 value. This was expected, as the nitriding process should improve the DLC-substrate adhesion. In the plasma nitrided samples, the nitrided layer provides a graded interface between the DLC coating and the metallic substrate. This layer's

enhanced mechanical properties and higher roughness improve the load bearing capacity of the surface layer, resulting in a better adhesion and causing stress reduction in the interface[10].

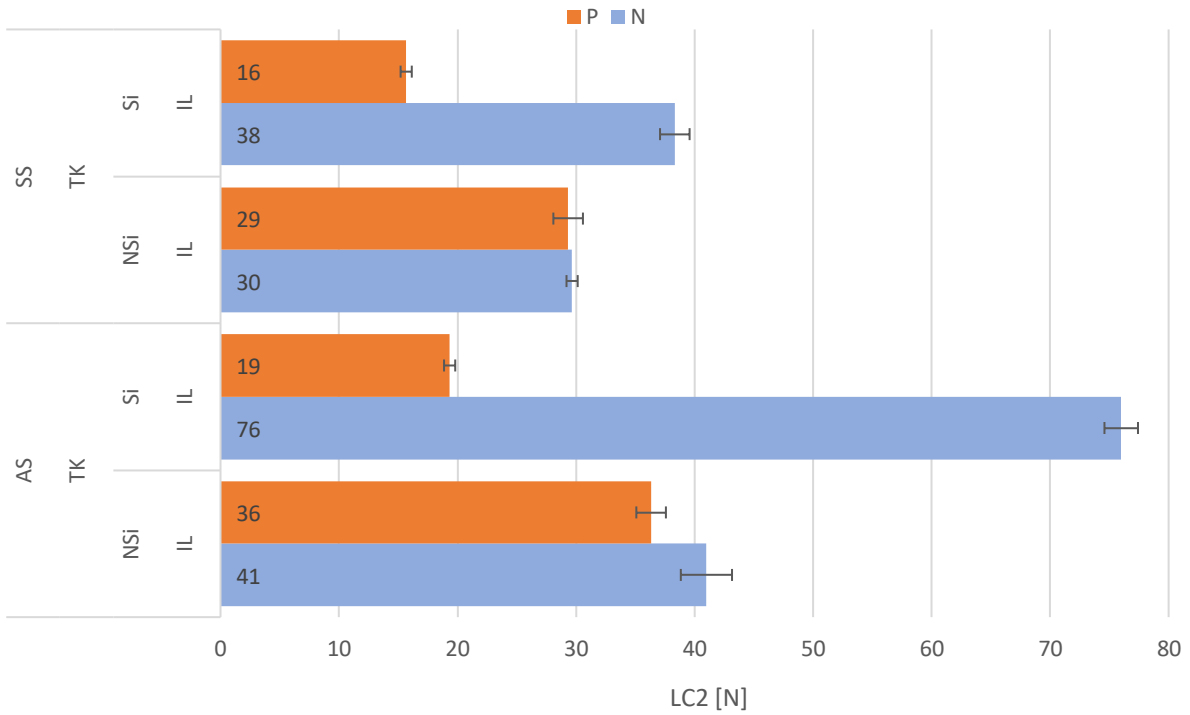

Figure 45. *Effect of nitriding pre-treatment in LC2.*

Figure 46 shows that in almost every case the LC2 value resulted higher for the alloyed steel coated samples. The non-nitrided coated samples displayed similar adherence values in most cases for both substrate materials, while nitrided alloyed steel coated samples had increased adherence compared to nitrided stainless steel coated samples. This change in the alloyed steel coated samples behaviour could be related to their roughness after the nitriding was performed.

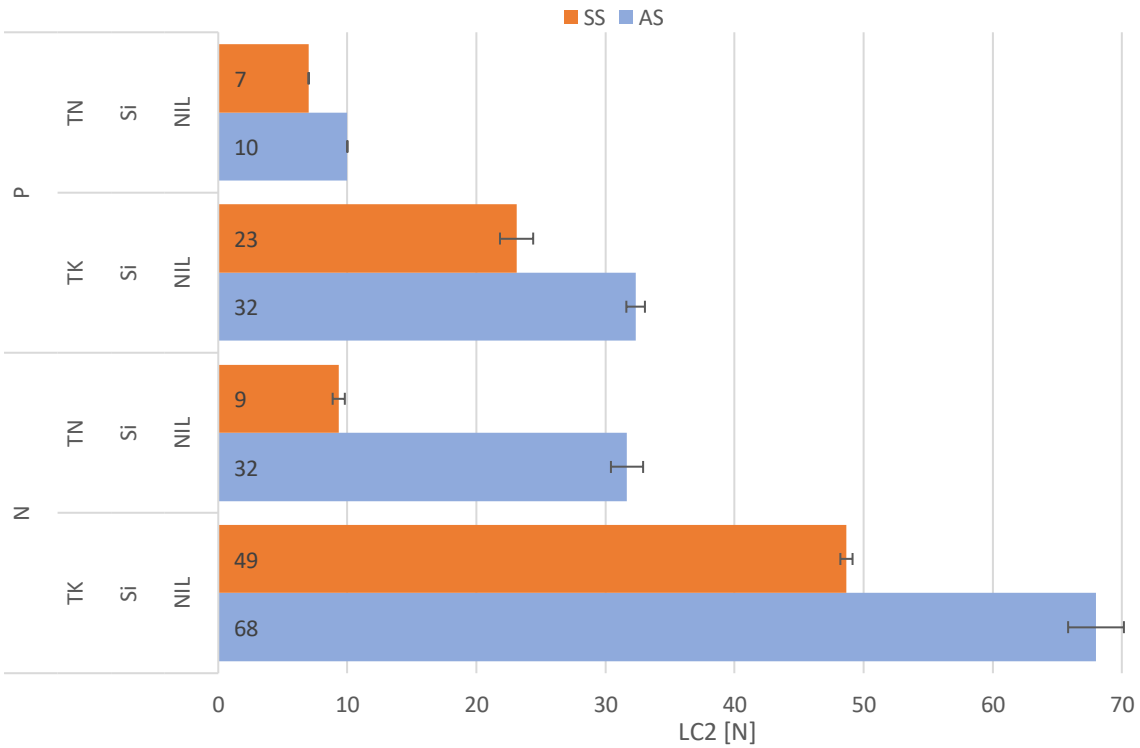

Figure 46. *Effect of substrate material in LC2.*

Coating Failure modes

By observing the microscope images of the scratches on the coatings, their failure mode type is discussed.

The different coating fracture observed behaviours are related to the substrate-coating hardness difference, if this difference is relatively small a certain degree of plastic deformation is achieved, and the harder material, the DLC coating in our case, develops ductile failure modes. When the substrate-coating hardness difference is high, a harder coating material will not be able to achieve the same degree of deformation as a softer substrate, thus developing brittle failure modes. Additionally, the coating thickness also affects the failure mode behaviour. Thicker coatings distribute applied external loads more homogeneously, lowering the substrate-coating interphase stress. Hence, hard thick coatings fail only related to their own deformation limitations, developing brittle failure modes.

The softer non-silicon doped coatings developed ductile failure modes regardless of their thickness, such as conformal cracking (**Figure 47-A1** and **B1**). While thick silicon doped coatings failed by brittle failure modes, such as Hertzian cracking (**Figure 47-A2**). Thin silicon doped coatings failed by brittle failures as well, such as compressive spallation (**Figure 47-B2**). It can be seen that the coating thickness had a bigger impact on the failure behavior for harder silicon doped coatings.

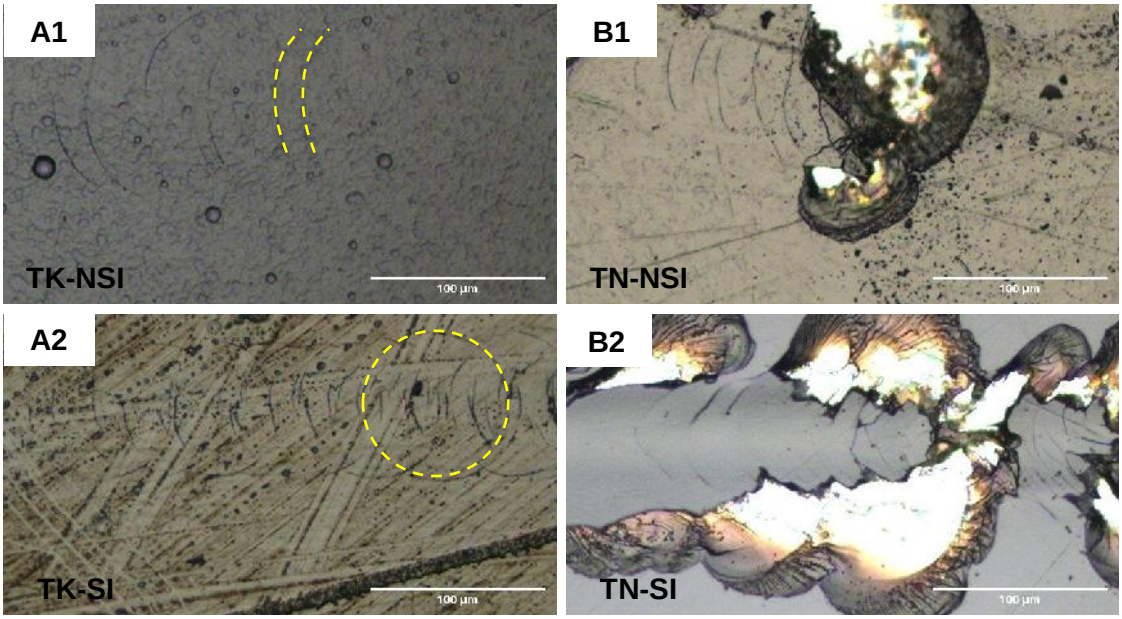

Figure 47. *Silicon doping effect on the coating failure mode, optical microscope images of the scratch track path. A1) AS-P-IL-TK-NSi coating. A2) AS-P-IL-TK-Si. B1) AS-P-IL-TN-NSi. B2) AS-P-IL-TN-Si.*

In stainless steel coated samples, the failure type changes from a ductile behaviour (such as parallel cracking in **Figure 48-A1**) to a brittle one (Hertz cracking on **Figure 48-A2**) by performing a plasma nitriding pre-treatment. An analogous result is seen for the low alloy steel substrate, where the failure mode changes from ductile (conformal cracking in **Figure 48-B1**) to brittle (gross spallation in **Figure 48-B2**) by hardening the substrate. The plasma nitriding pre-treatment results in a hardness increase of the substrate, which limits its degree of deformation under an applied external load. In the nitrided and coated samples the coating is not allowed to deform as much as with the non-nitrided one, thus failing in a brittle manner.

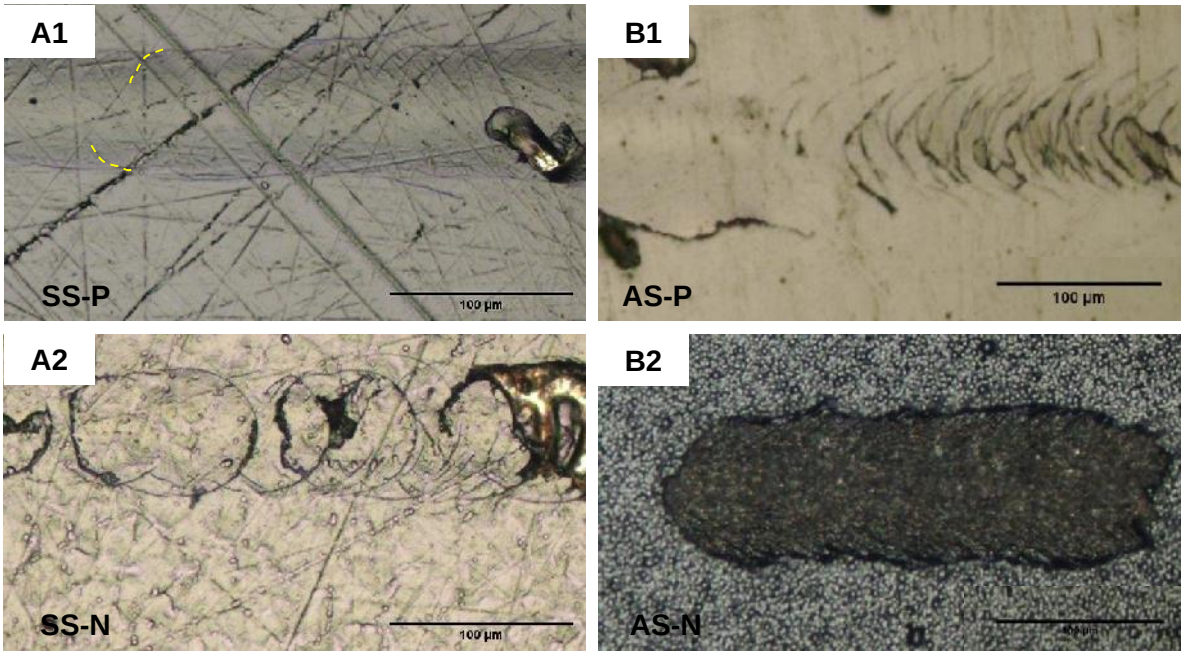

Figure 48. *Pre-treatment effect on the coating failure mode, optical microscope images of the scratch track path. A1) SS-Si-NIL-TN-P. A2) SS-Si-NIL-TN-N. B1) AS-Si-NIL-TN-P. B2) AS-NSi-NIL-TN-N.*

4.1.6 Pin on Disk

In this section, results of pin-on-disk test are shown. Two different measures were taken and shown on different graphs: friction coefficients (**Figure 49**) and steel ball wear radius (**Figure 50**). Results for uncoated samples are added for comparison. Humid SAE4140 uncoated sample was not tested due to lack of time during the experimental period of the project. Regarding coated samples, interlayer thickness, metallic substrate and coating thickness do not affect the results of this test, as mentioned in **section 3.8**. Thus, AISI304 and SAE4140 samples were used indistinctively. The same criteria was used with thick and thin coatings and thick and thin interlayers.

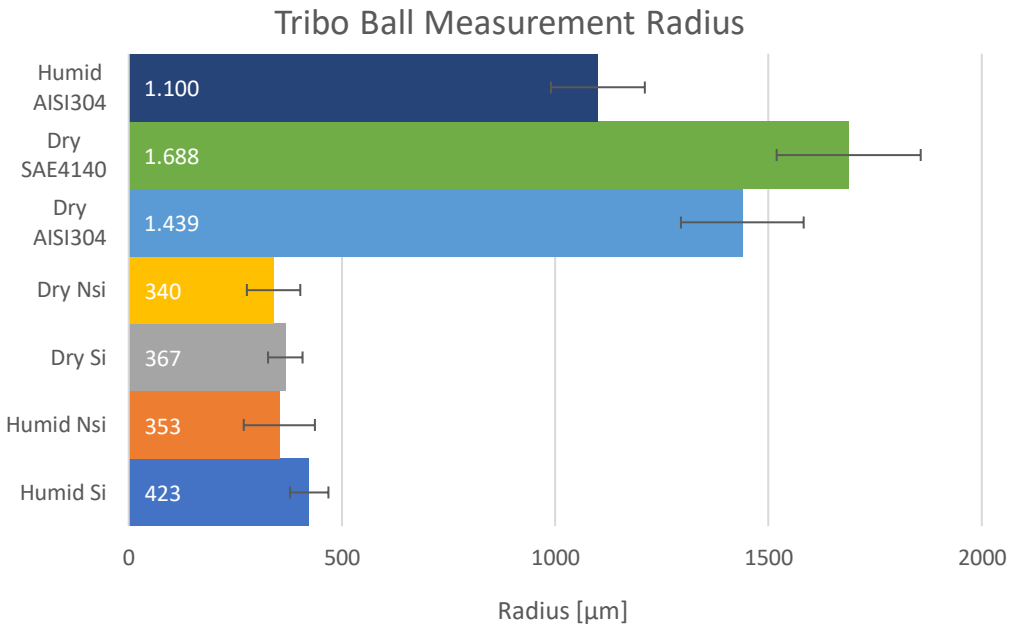

Figure 49. *Tribo results for grooved ball radius.*

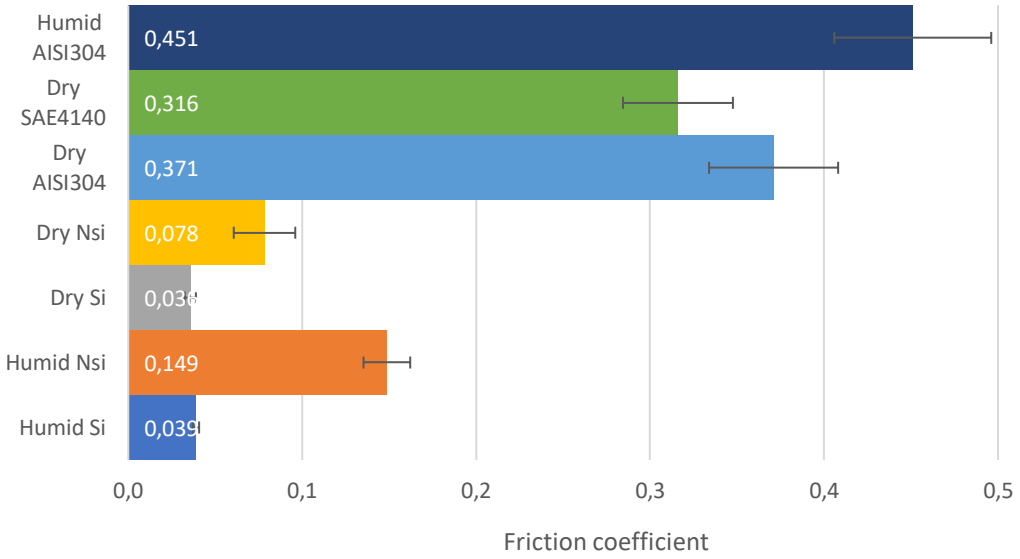

Figure 50. *Tribo results for friction coefficient.*

It is clearly seen the difference between coated and uncoated samples: both friction coefficient and ball wear are dramatically reduced when DLC coating is applied, proving this coating greatly enhances tribological properties on these steels. This feature is greatly desired, and it is in many applications the main reason for the use of DLC coatings.

Silicon doping increases the ball wear, while it decreases the friction coefficient. Friction coefficient results were as expected[7], showing lower value on silicon-doped samples, where this difference is much higher in a humid environment. This may be the result of silicon-rich oxide debris formation, which acts as a barrier between the steel ball and the coating, making the ball slide and thus, lowering the friction coefficient. When enough water is present, as in a humid environment, this effect is complemented by water lubrication effect: superficial SiOH groups absorb water molecules, reducing shear strength between the coating and the ball. Non-doped DLCs do not have silicon to form SiOH components, so the friction coefficients are not reduced by these effects. They are sensitive to oxidizing agents such as vapour during friction, provoking a rise in its friction coefficient[59]. Humid samples result in a slightly higher wear of the ball. Regarding friction coefficient, humid and without silicon display a much higher friction coefficient than the others. Ball wear results show a higher wear on humid samples, probably due to an oxidizing effect during friction on the ball by the environmental vapour.

Figure 51 shows an example of the method used for determining the track depth: three lines crossing horizontally the track (marked as 1, 2 and 3) are seen, as well as the corresponding profile graph for line 1 as an example, where the depth of the wear track can be appreciated. The region of the line taken as part of the track is highlighted in blue, while the region taken as outside the track is highlighted in green, both in the line and in its profile

graph. Results are shown in **Table 6** as an average of the values on the three lines for each sample, where there is no data for uncoated samples and for the non-doped coated sample that was tested in humid, as the confocal scans were unsuccessful, resulting in a blurry image where the wear track is undetectable (it was intended to repeat these scans, but it was not possible due to the limited time spent in FHÖO). It can be seen that the track depth is similar in both silicon-doped samples, while the depth of the non-doped sample on dry conditions is lower.

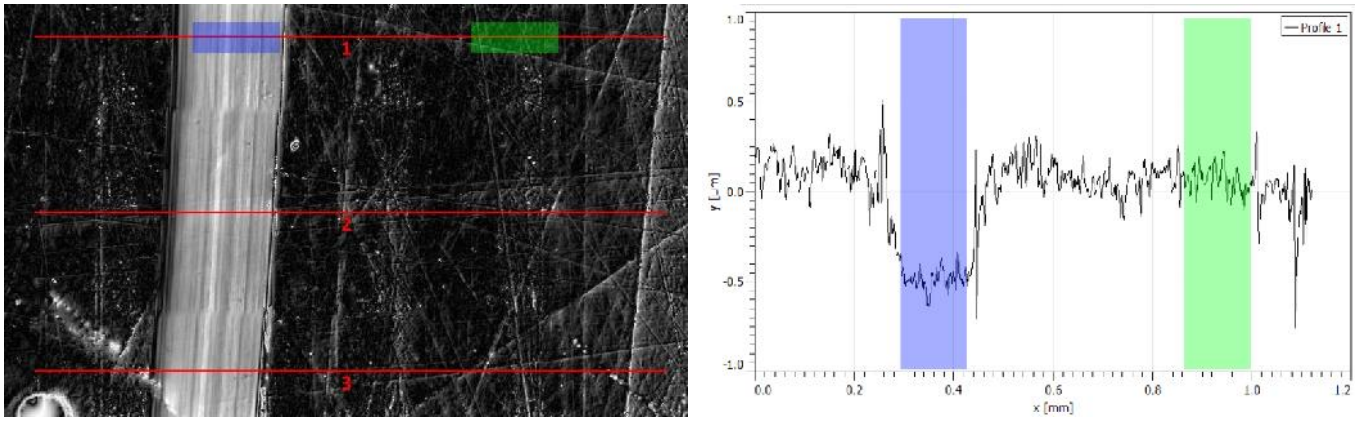

Figure 51. *Wear track on Confocal Microscope, lines used for test and Linear profile example.*

Table 6. *Wear track depth of pin on disc tested samples.*

Conditions	Wear track relative depth [µm]
Humid Si	0.46 ± 0.08
Dry Si	0.6 ± 0.05
Dry NSi	0.18 ± 0.05

4.2 Corrosion Tests

The analysis exposed in this section is qualitative in nature. The correct procedure to evaluate the corrosion behaviour is to first characterize the sample's surface before the exposure to the corrosive environment, and after the testing, a corrosion product removal or cross section of the sample is due in order to analyse the type of damage characteristics. Most of these evaluations were scheduled to be made in Argentina, and in the end it was not possible for them to take place because of the COVID-19 2020 lockdown.

The SS uncoated samples exhibited better corrosion resistance than AS uncoated samples after both salt spray and immersion tests, as expected. The SS uncoated samples with no pretreatment showed no signs of corrosion damage for both tests, while the nitrided ones exhibited preferential corrosion damage on the plasma nitriding edge effect zones for

both tests (**Figure 52**). This behaviour could imply that the plasma nitriding edge effect is worsening the already good SS corrosion resistance.

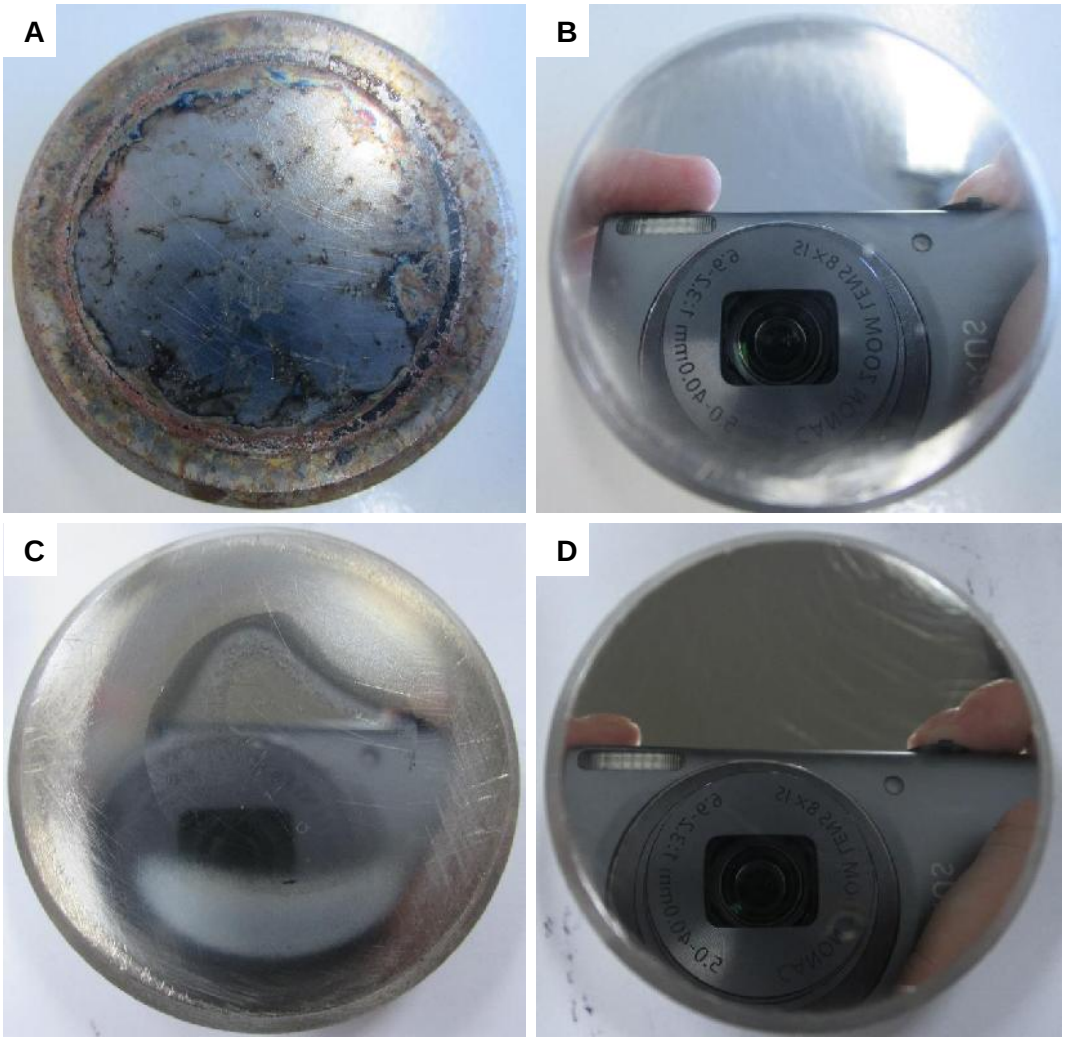

Figure 52. *SS uncoated samples after corrosion tests. A) SS-N after 300-hour salt spray test, showing preferential attack on the ring-shaped plasma nitriding edge defect. B) SS-P after 300-hour salt spray test, showing no appreciable damage. C) SS-N after 50-hour immersion test, showing light damage on the central nitriding defect. D) SS-P after 50-hour immersion test, showing no appreciable damage.*

In the case of the alloyed steel uncoated samples, both with and without the plasma nitriding pre-treatment, they suffered uniform corrosion of the exposed area in a similar degree (**Figure 53**).

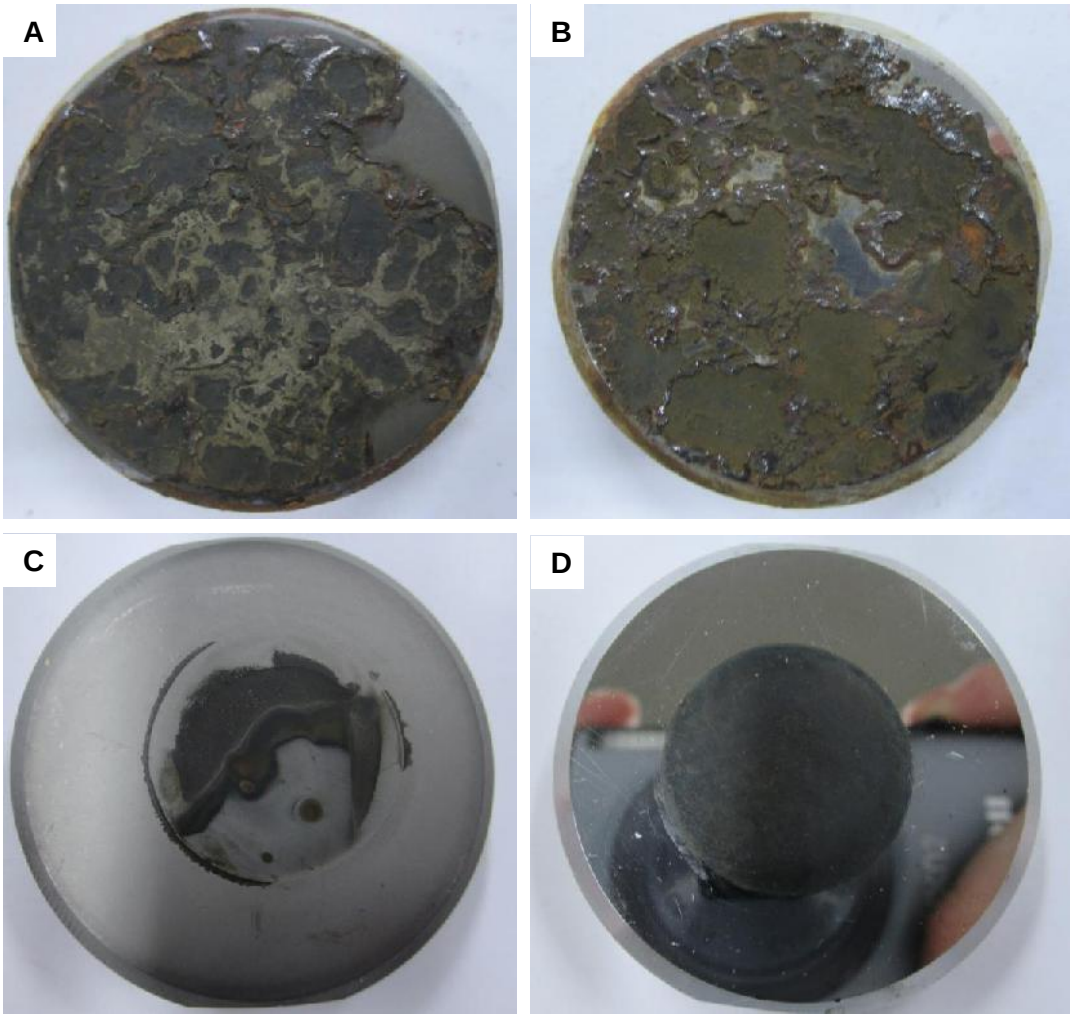

Figure 53. *AS uncoated samples after corrosion tests, all of them showing uniform corrosion damage. A) AS-N after 300-hour salt spray test B) AS-P after 300-hour salt spray test C) AS-N after 50-hour immersion test. D) AS-P after 50-hour immersion test.*

The behaviour of the DLC coated samples was analysed for both, immersion and salt spray tests, separately.

4.2.1 Immersion Test

After the immersion tests were performed, the changes observed on the coated samples were documented and analysed in order to determine the effect that each variable could have on their corrosion behaviour.

The thick and silicon doped coatings showed no superficial damage after the test for both substrates, independently of the pre-treatment used and the silicon interlayer thickness (**Figure 54**). Since both substrates exhibited different corrosion damage morphologies, the remaining set of conditions are analysed separately.

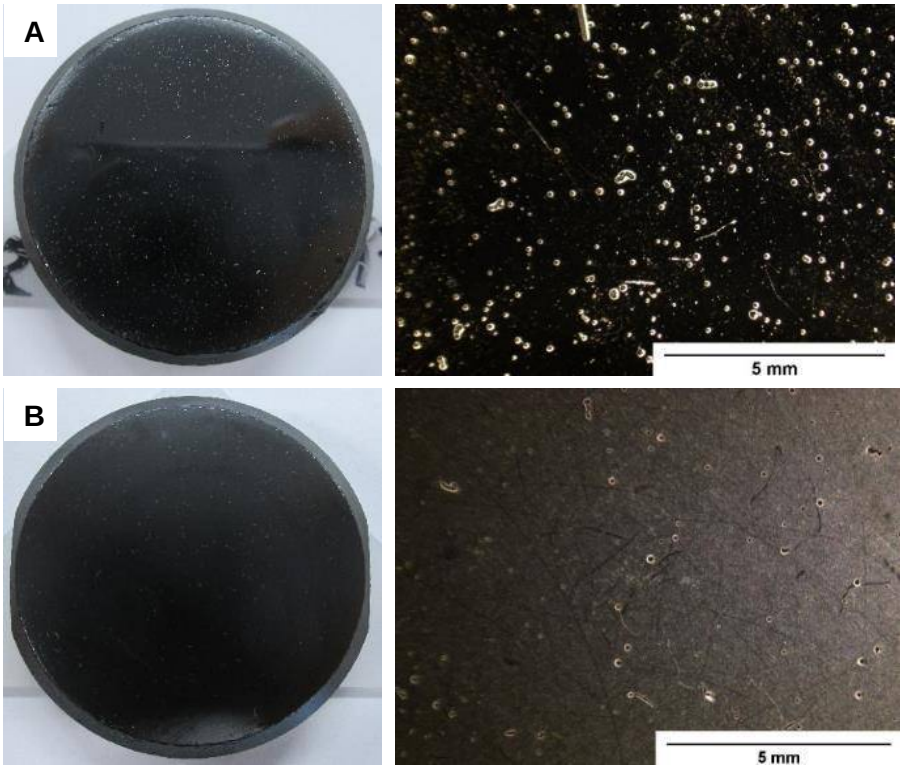

Figure 54. *Samples that showed no damage after the 50-hour immersion test. A) SS-TK-Si-NIL-N. B) AS-TK-Si-NIL-N.*

4.2.1.1 AS Samples

For the nitrided substrates, only the thin and not silicon doped coatings showed corrosion damage, regardless of the silicon interlayer thickness, identified by the reddish corrosion products formed on the surface (**Figure 55**). At a higher magnification, using SEM, it was possible to observe that multiple pits developed on the surface of several samples, presenting a circular morphology with sharp edges (**Figure 56**). EDS spectrum showed elevated concentrations of oxygen inside the pit, probably due to the presence of iron and chromium oxides (**Figure 57**).

Figure 55. *Reddish corrosion products on the AS-TN-NSi-NIL-N sample's surface after the 50-hour immersion test.*

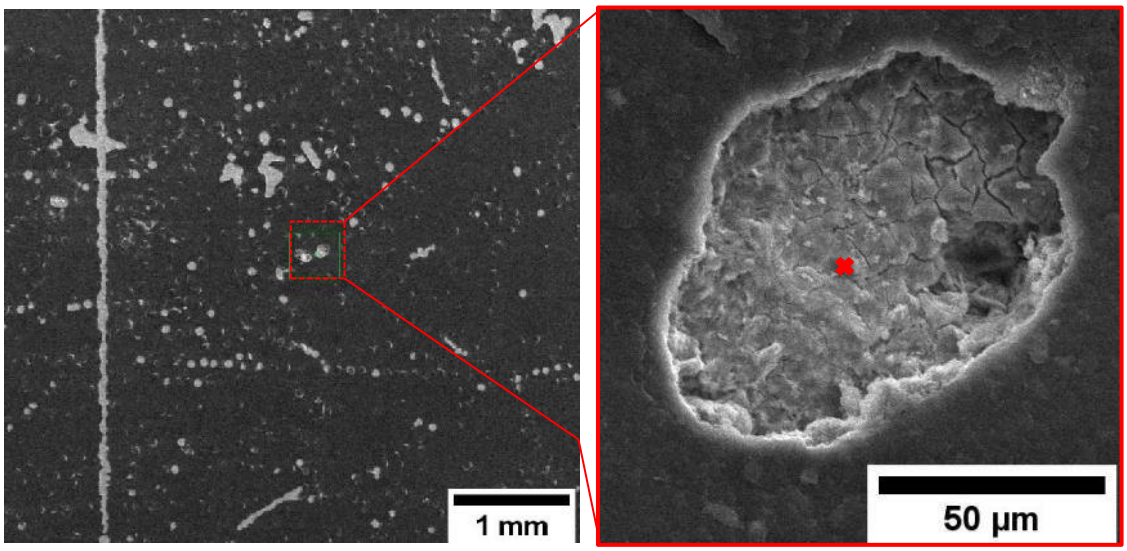

Figure 56. *SEM images of the AS-TN-NSi-NIL-N sample pitting. A reference point is indicated with a red cross.*

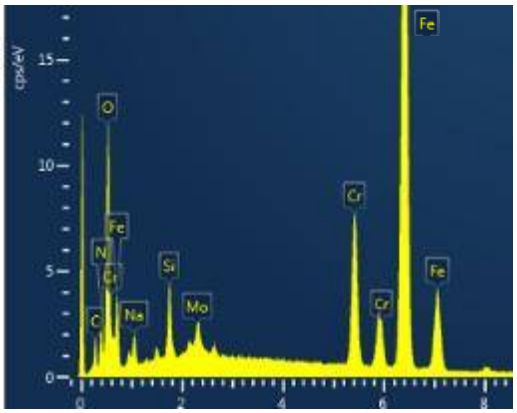

Figure 57. *EDS spectrum of the corrosion products inside a pit on the sample AS-NIL-TN-NSi-N. Reference point* ***Figure 56****.*

On the other hand, all non-nitrided and coated samples, except thick and silicon-doped ones, displayed multiple or isolated pitting (**Figure 58**). The pit's morphology results similar to

what was observed for the AS-N-TN-NSi-IL/NIL samples: circular shape with sharp edges and elevated oxygen concentrations inside it (**Figure 59** and **Figure 60**).

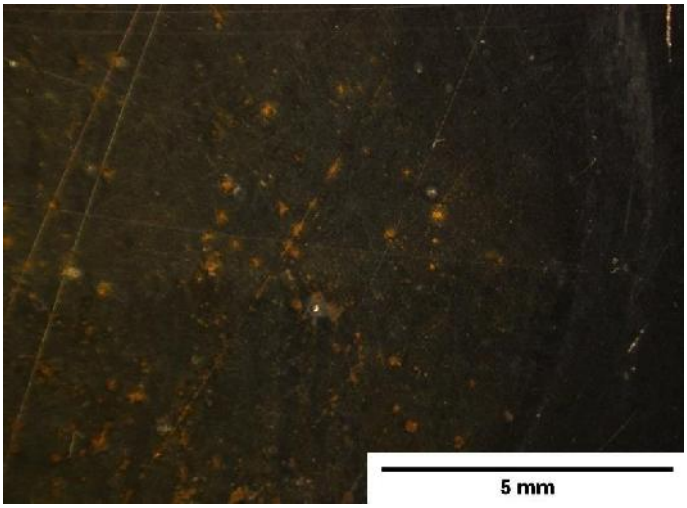

Figure 58. *Reddish corrosion products on the AS-TN-NSi-IL-P sample's surface after the 50-hour immersion test.*

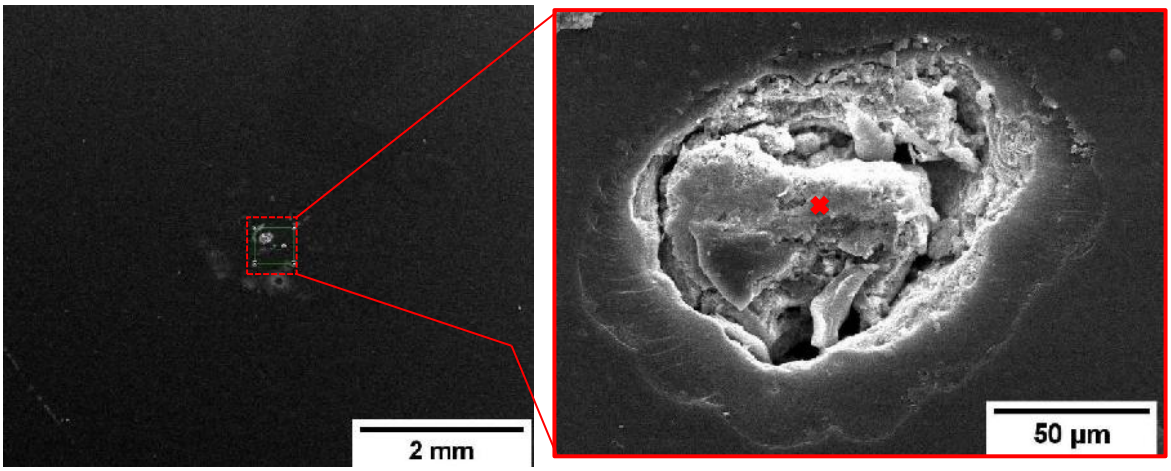

Figure 59. *SEM images of the AS-TN-NSi-IL-P sample's pitting. A reference point is indicated with a red cross.*

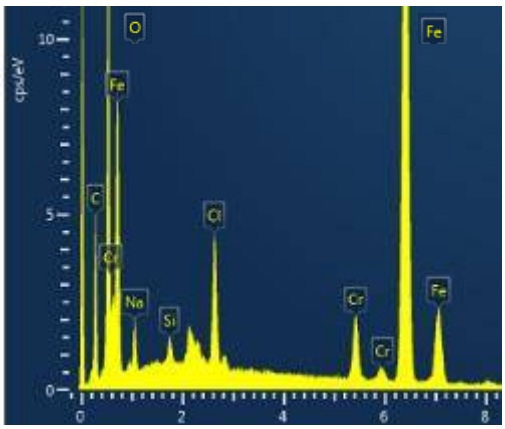

Figure 60. *EDS spectrum of the corrosion products inside a pit on the sample AS-TK-NSi-IL-P. Reference point* ***Figure 59****.*

No signs of degradation of the DLC coating were observed on any sample. This could mean that the 8 DLC systems are chemically inert when exposed to the corrosive media.

The observed pitting on the samples present similar characteristics and could be related to pre-existing passing-through defects on the film that connect the corrosive media with the substrate. During the deposition process dust particles and silicon or carbon agglomerates can be deposited on the surface of the sample (**Figure 61** and **Figure 62**). When the vacuum is removed and the PACVD reactor is opened, these particles are removed and passing-through defects are formed (**Figure 63**).

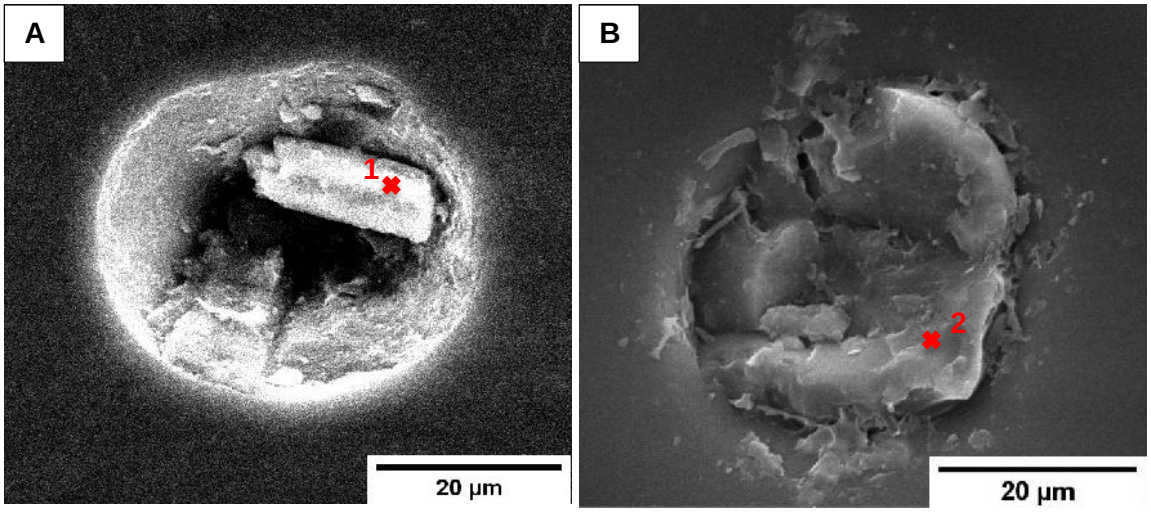

Figure 61. *SEM images of silicon clusters embedded in the DLC coating. A) AS-TK-Si-IL-P. B) AS-TK-NSi-NIL-P. Reference points 1 and 2 are indicated with a red cross.*

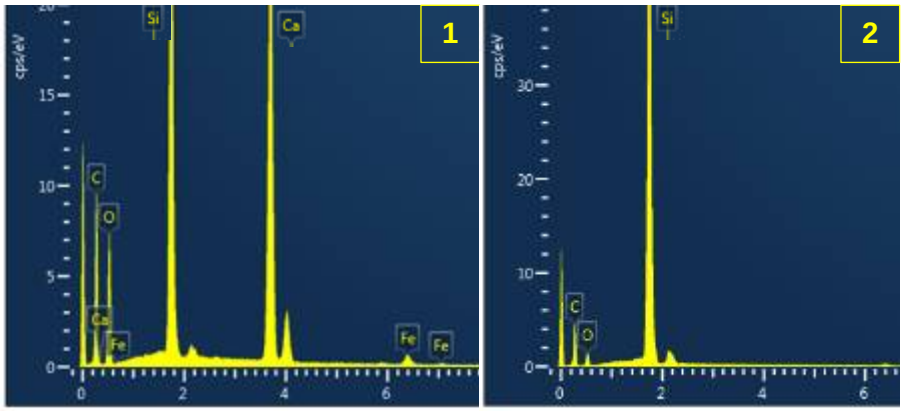

Figure 62. *EDS spectrum of silicon clusters embedded in the DLC coating. Reference point 1 and 2,* ***Figure 64****.*

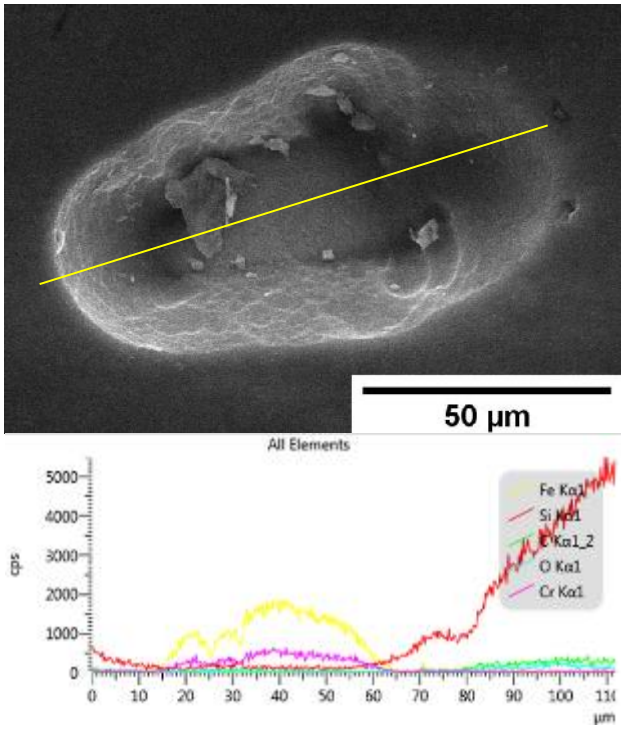

Figure 63. *EDS linescan spectrum in a passing-through defect on the sample SS-TK-Si-NIL-N.*

The nitrided and coated samples showed increased corrosion resistance to the corrosive media and no effect of the silicon interlayer could be observed.

4.2.1.2 SS Samples

The nitrided samples showed no sign of DLC failure or corrosion products formation on their surface. It is worth noting that the nitriding edge effect on the samples, which suffers preferential corrosion damage and is analysed further on, was not exposed to the corrosive media during the immersion tests, since this inhomogeneity in the nitrided layer develops close to the sample edges in most of them.

On the other hand, the non nitrided samples displayed either multiple or isolated localized corrosion points in almost all cases. The thin and non-silicon doped samples suffered multiple DLC concentric cracking points while the thin and silicon doped samples exhibited the same failure mechanism but in isolated points, independently of the silicon interlayer thickness (**Figure 64**). The thick and not silicon doped samples only failed next to the O-ring, independently of the silicon interlayer thickness.

The damage mechanism morphology shows a concentric pattern that could reflect the corrosion advance over time (**Figure 65**). The centre of the defect seems to have more deposits, which could mean that it might have been exposed longer to the corrosive media. Elevated concentration of oxygen could be related to the formation of iron and chromium oxides (**Figure 66**). This defect also observed in the 3-D topographical representation done

by confocal scan seen in Figure 67, where a rather homogeneous surface can be appreciated along the defect.

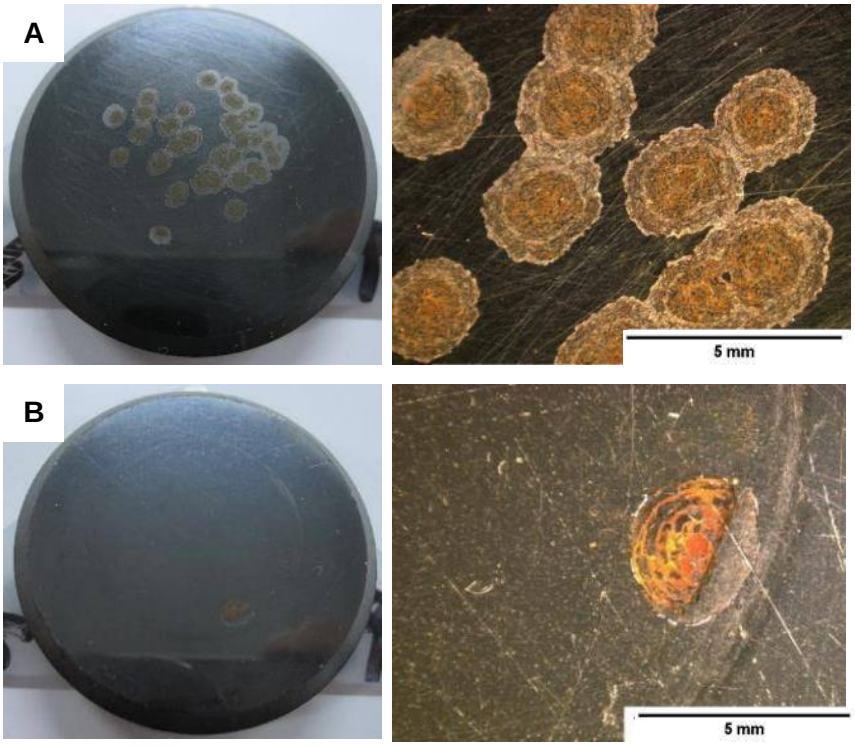

Figure 64.*A) multiple localized corrosion sites on SS-TN-NSi-NILi-P sample. B) Isolated localized corrosion site on SS-TN-Si-NIL--P sample.*

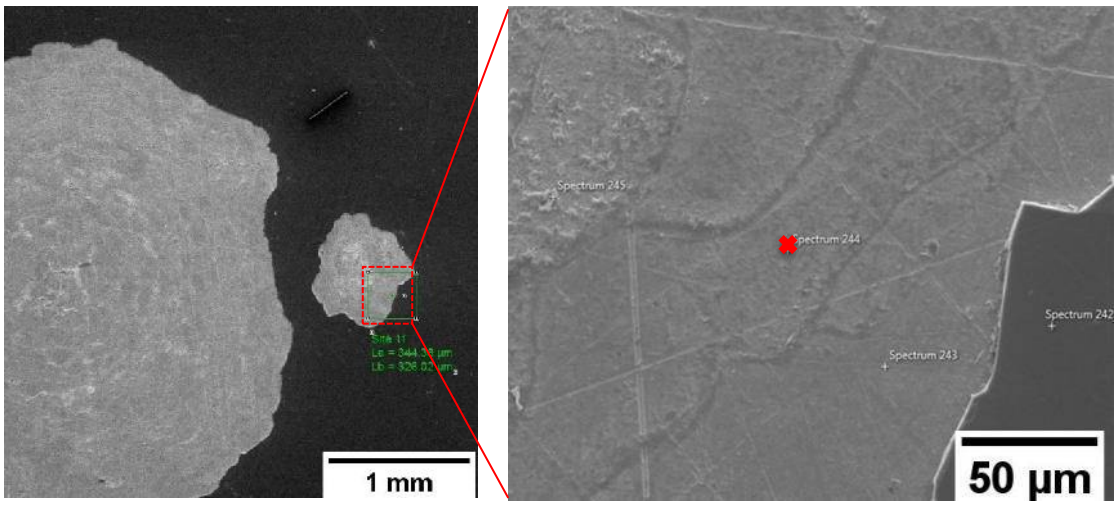

Figure 65. *SEM images of the SS-TN-NSI-NIL-P sample's localized corrosion site. A reference point is indicated with a red cross.*

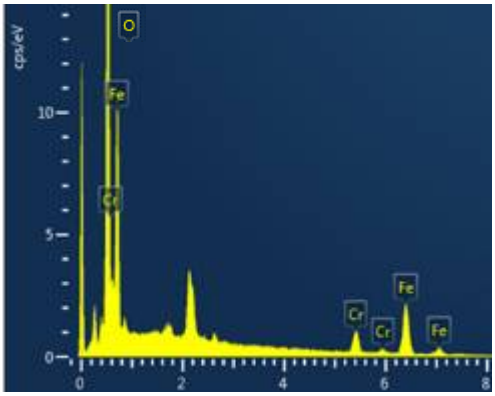

Figure 66. *EDS spectra of the corroded metallic substrate on the sample SS-TN-NSI-NIL-P. Reference point* ***Figure 65****.*

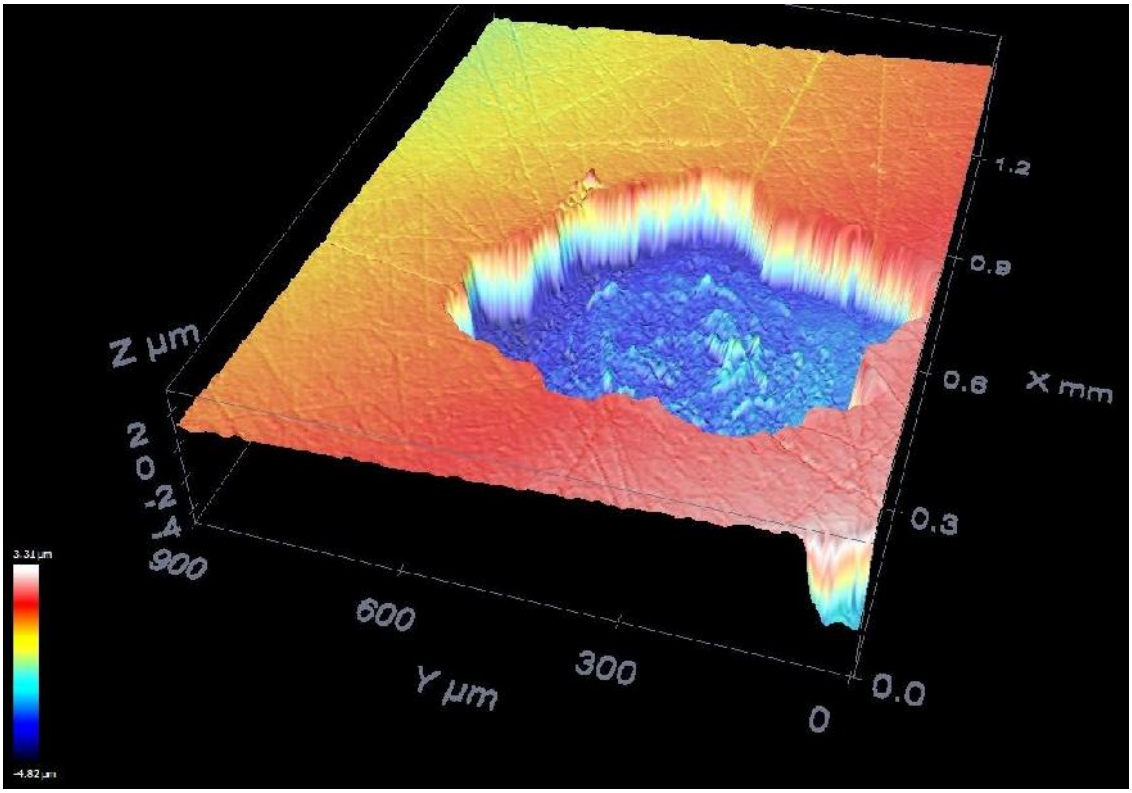

Figure 67. *3-D confocal mapping of corrosion defect on SS-TN-NSi-NIL-P.*

As in the alloyed steel samples, the silicon interlayer thickness variable does not seem to have an appreciable effect on the samples' behaviour during the immersion test.

4.2.1.3 Confocal microscope analysis

The manufacture of a plastic sample holder, with a nanometric reference point, allowed to use the confocal microscope´s coordinates system in order to map the centre area of the samples. This surface mapping was performed on the coated samples before and after one of the 50-hour immersion test, which allowed the approximate quantification of area damage by image analysis software. As an example, **Figure 68** shows a full 4-quadrant confocal scan

before and after the immersion test, where the damage provoked by the corrosive media can be appreciated. In the same figure, a close-up of a determined region is seen as well, that verifies this is the same region on the sample, as the same superficial scratch can be appreciated in both scans. The rainbow-like effect seen on the scan done before the test is due to a lack of levelling of the sample glued to the sample holder. This can be corrected with the confocal microscope´s dedicated software, although it was not possible to do so before the stay in Austria reached its end.

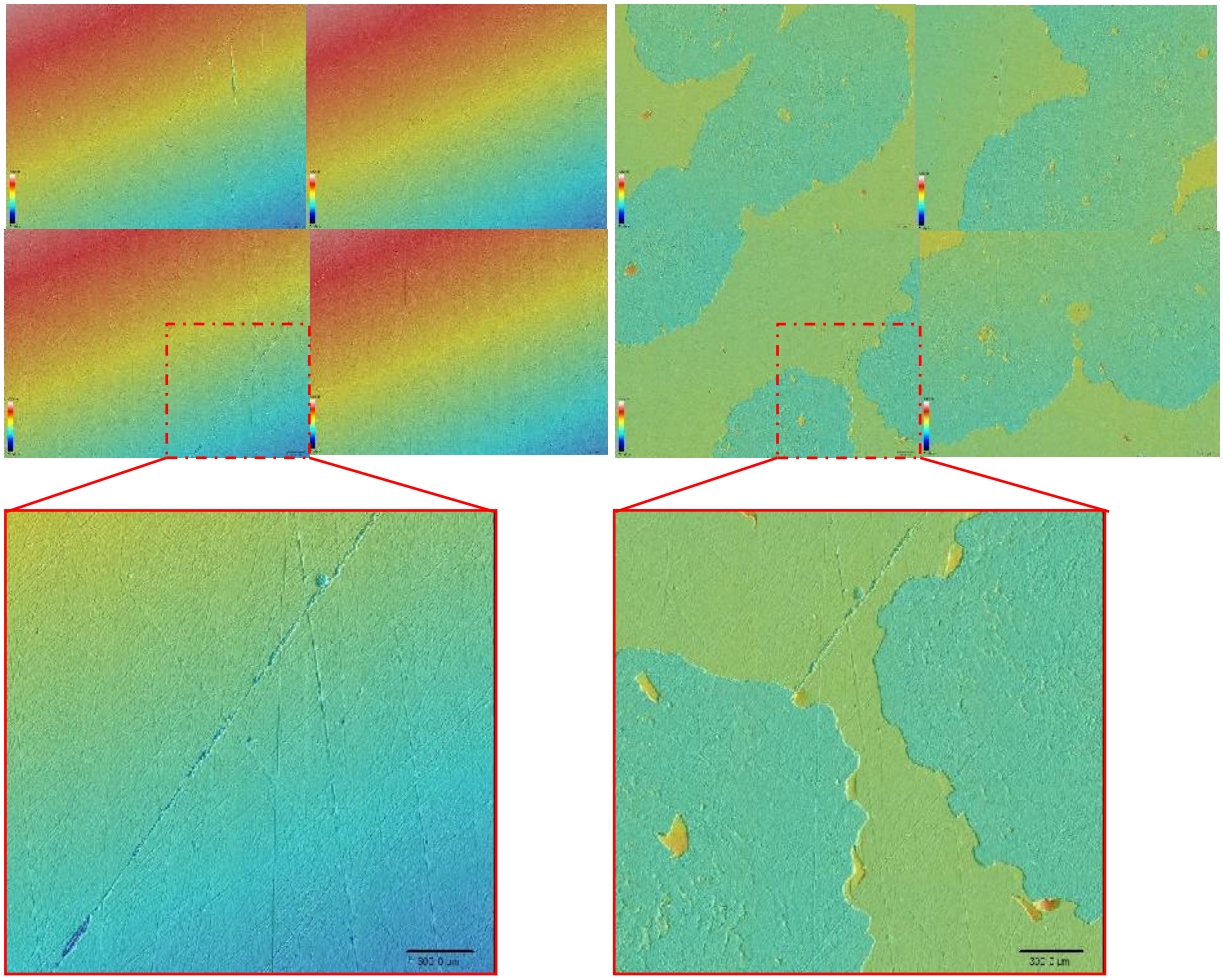

Figure 68. *Four-quadrant confocal scan before and after the immersion test on SS-TN-NSi-NIL-P. Close-up images on bottom-left quadrant added for better appreciation.*

Only three stainless steel and one alloyed steel coated samples showed measurable surface damage in the mapped area, as can be seen in **Table 7**. The measured area damage percentage resulted consistent with what was observed macroscopically on each of the mentioned samples. Changes of less than ±1% were disregarded as they were considered process imperfections, such as poor surface cleaning or small fixation misalignments.

Table 7. *Calculated area damage after the immersion test on confocal microscope mapped samples.*

Sample	Area Damage [%]
SS-TN-SI-NIL-P	9,80
SS-TN-NSI-IL-P	42,20
SS-TN-NSI-NIL-P	61,32
AS-TN-NSI-NIL-N	7,88

On the stainless steel, non nitrided, thin, non-silicon doped and either thin or thick silicon interlayer samples that showed the largest % area damage, multiple localized corrosion points were observed, resulting in a nearly complete film delamination on each of the concentric delamination points (**Figure 69** and **Figure 70**).

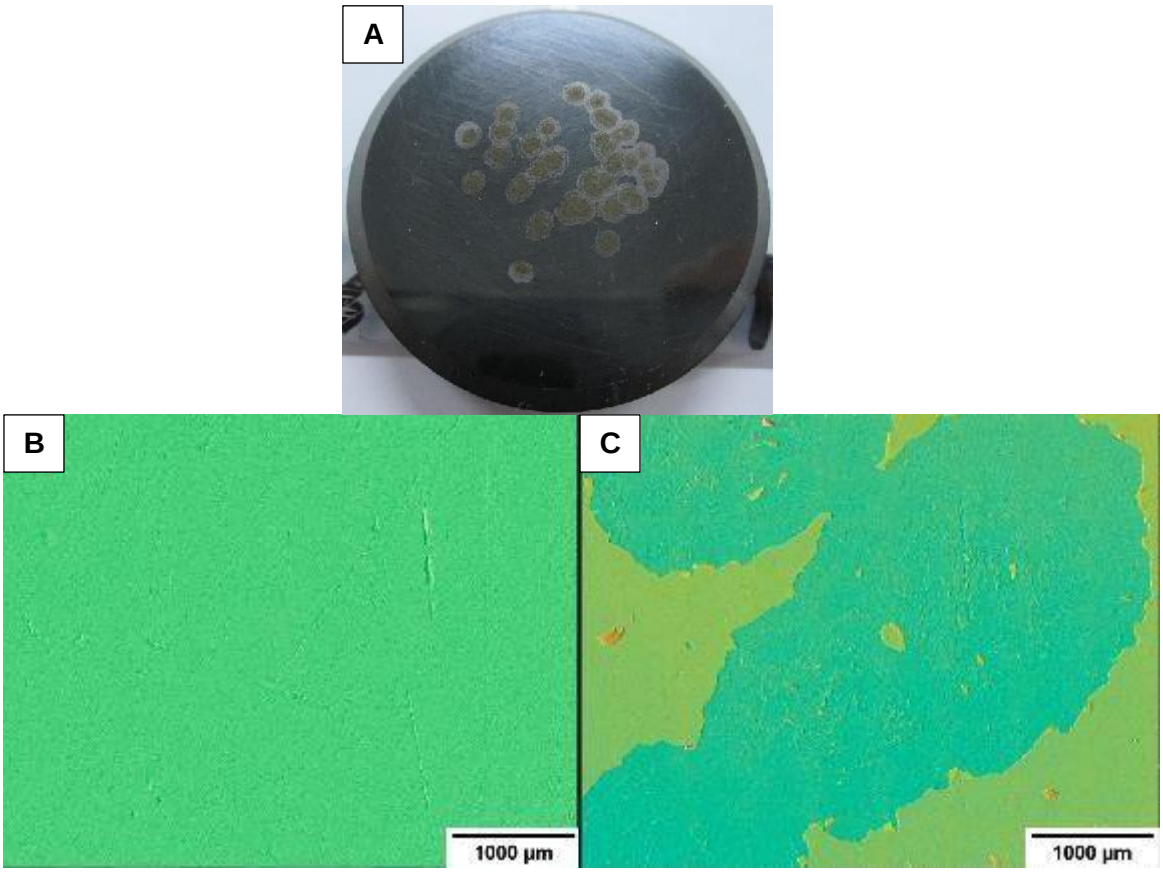

Figure 69. *SS-TN-NSi-NIL-P. A) Photographic shot after immersion. B) Confocal scanning before immersion. C) Confocal scanning after immersion.*

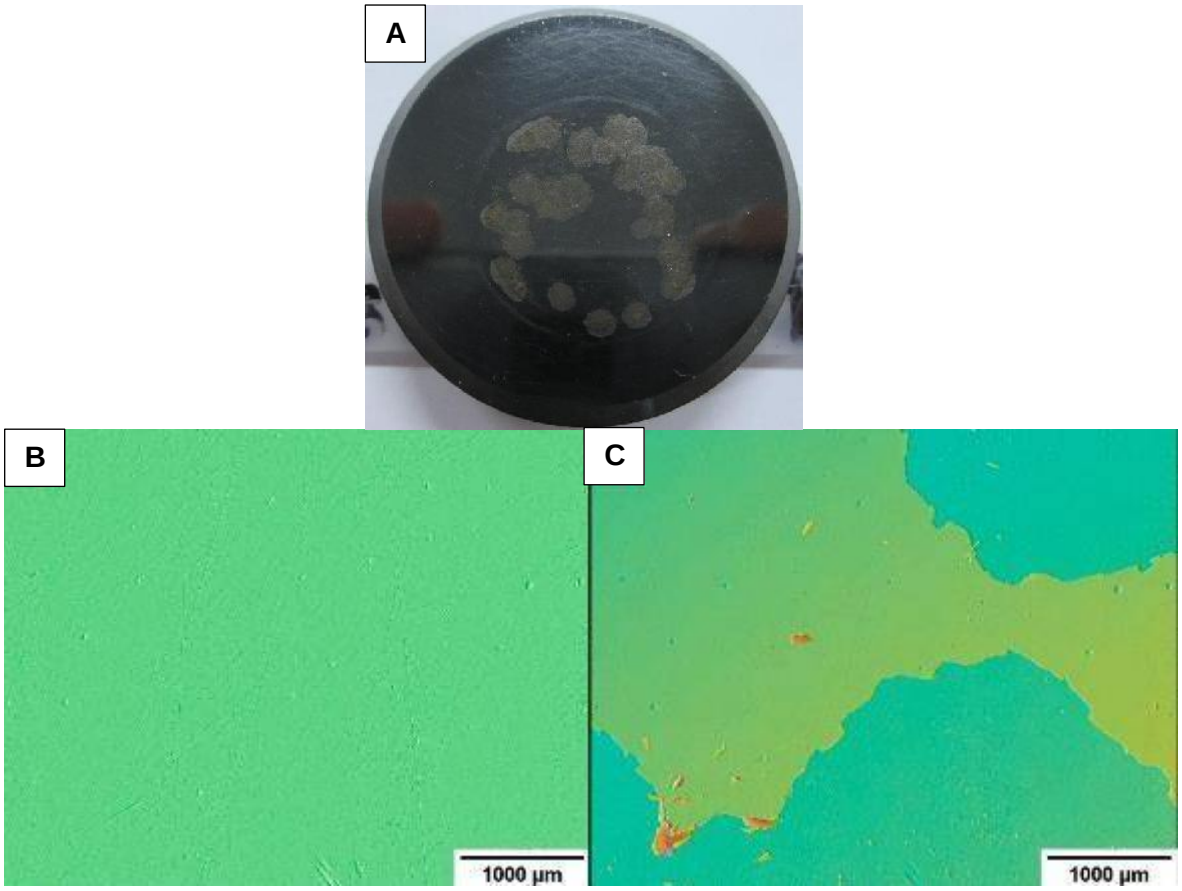

***Figure 70**. SS-TN-NSi-IL-P A) Photographic shot after immersion. B) Confocal scanning before immersion. C) Confocal scanning after immersion.*

The stainless steel, non nitrided, thin, silicon doped, with thin silicon interlayer sample suffered a similar type of damage as the other two SS samples shown in this section, but fewer concentric delamination points developed (**Figure 71**).

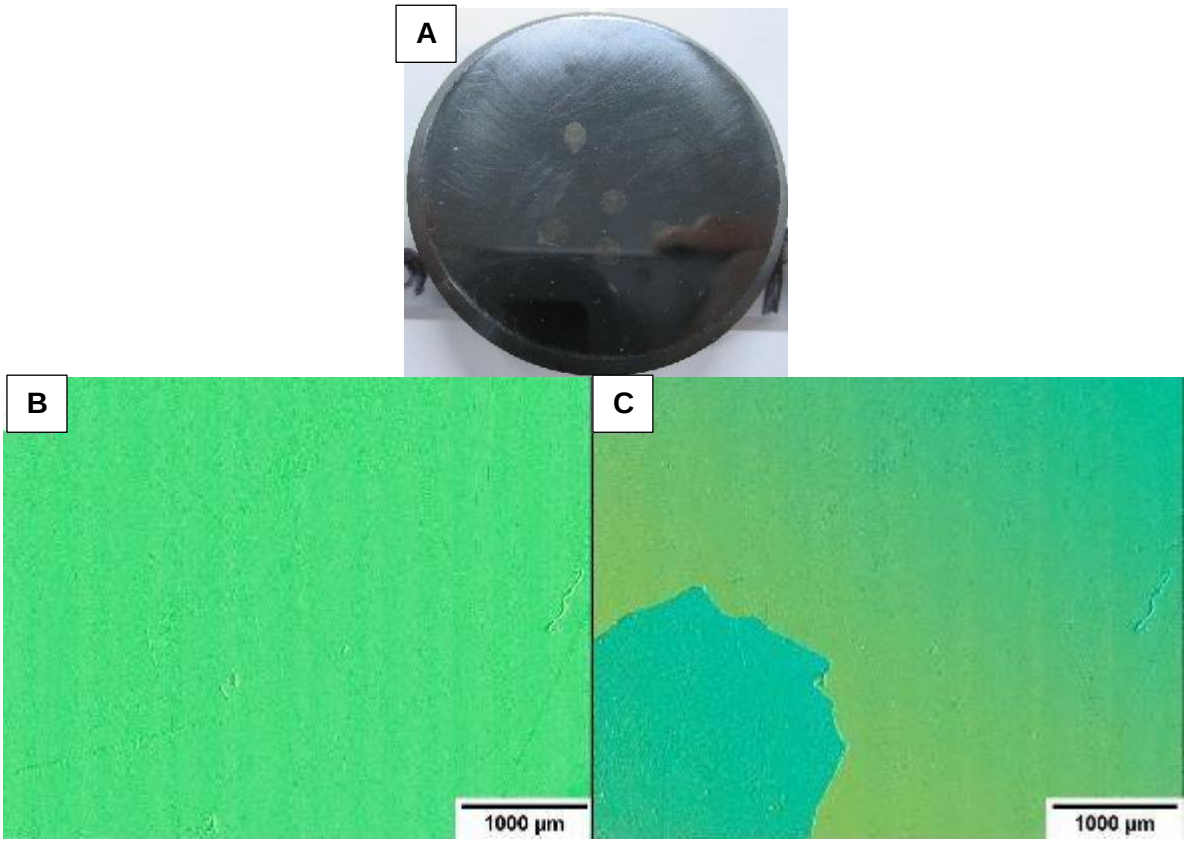

***Figure 71**. SS-TN-Si-NIL-P. A) Photographic shot after immersion. B) Confocal scanning before immersion. C) Confocal scanning after immersion.*

On the alloyed steel, nitrided, thin, not silicon doped and with thin silicon interlayer sample no film delamination was detected, the % area change was related to corrosion products surrounding multiple pitting on the DLC coating (**Figure 72**).

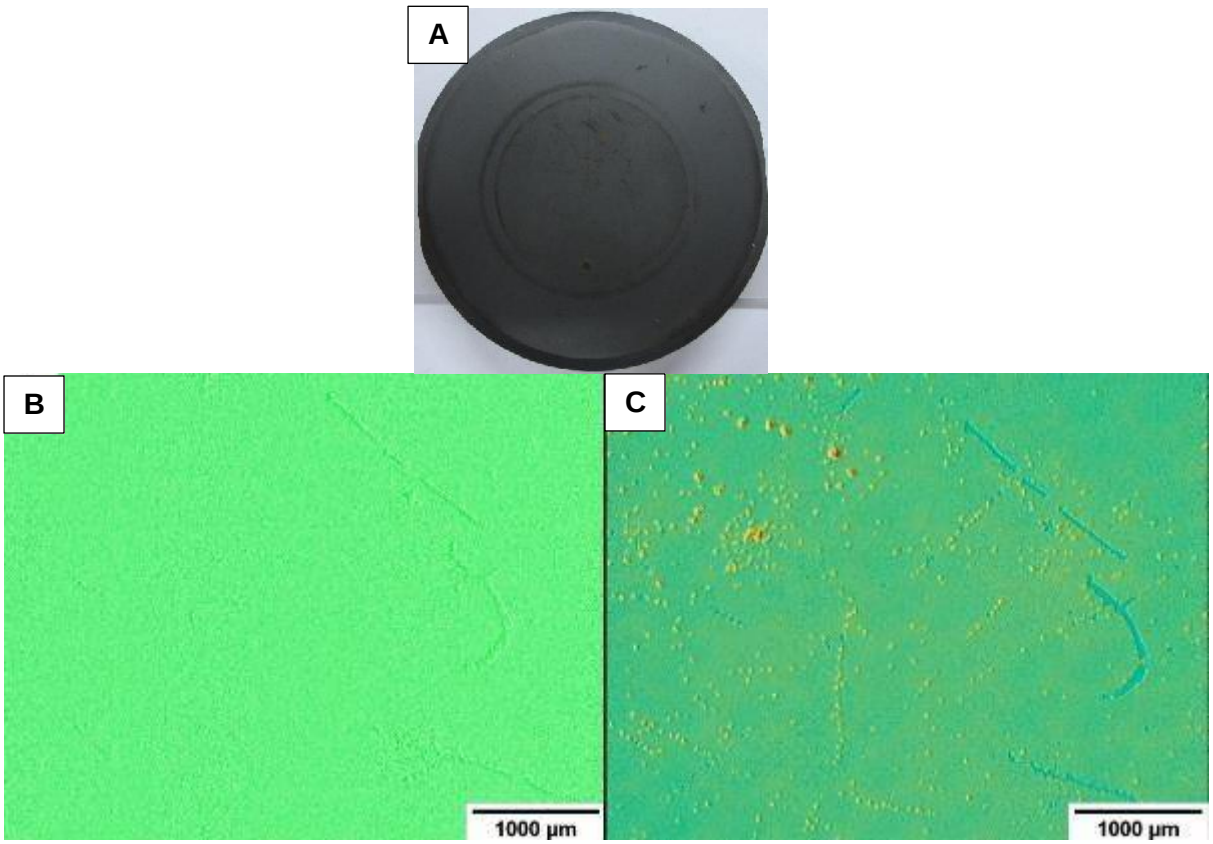

***Figure 72**. AS-TN-NSi-NIL-N. A) Photographic shot after immersion. B) Confocal scanning before immersion. C) Confocal scanning after immersion.*

4.2.2 Salt Spray Test

As it was observed in the case of the immersion test results, the silicon doped and thick DLC samples showed no corrosion damage, or at least one of the three tested samples presented isolated pits, independently of the pre-treatment and the thickness of the interlayer, for both substrates.

Since both substrates exhibited different corrosion damage mechanisms, they are analysed separately.

4.2.2.1 AS Samples

The nitrided and thick coated samples showed the best behaviour after the salt spray test. In the silicon doped samples, no damage was observed, except for an isolated pit on only one sample (**Figure 73 A**). On the other hand, the non-silicon doped coating samples suffered multiple pitting damage, identified mainly by oxide formation and optical microscopy (**Figure 73 B**). The interlayer thickness does not show an effect on the samples' behaviour.

The pit morphology is circular with sharp edges (**Figure 74**). Multiple cracks can be seen on the pits' edges, which are probably associated to its lateral growth. By means of EDS,

elevated oxygen content was detected, indicating the possible presence of iron and chromium oxides (**Figure 75**).

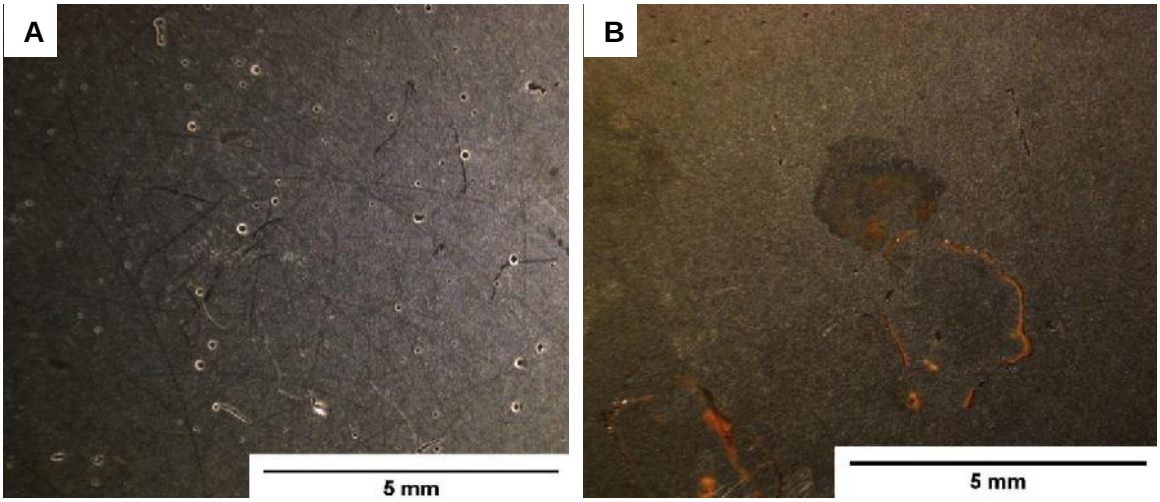

Figure 73. *A) AS-TK-Si-NIL-N sample showing no damage after the salt spray test. B) AS-TK-NSi-IL-N sample showing pits with oxides surrounding them.*

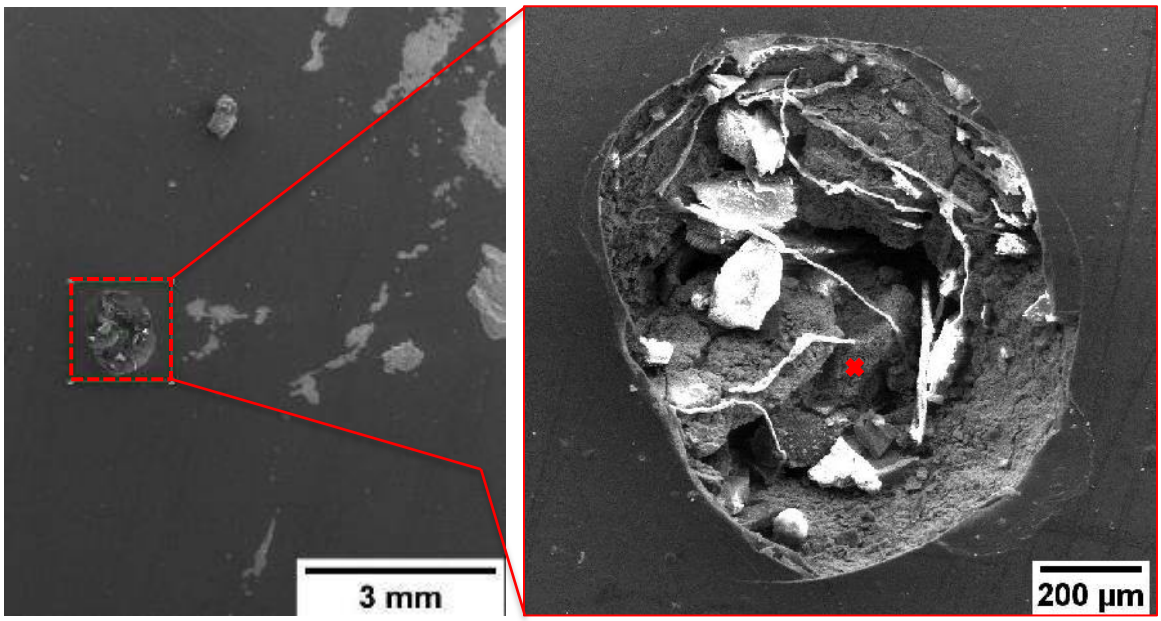

Figure 74. *SEM image showing the pit morphology in a AS-TK-NSi-NIL-N sample. A reference point is indicated with a red cross.*

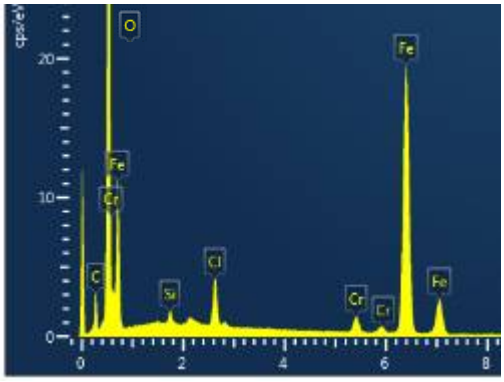

Figure 75. *EDS spectrum of the oxides inside a pit on the AS-TK-NSi-NIL-N sample. Reference point* ***Figure 74****.*

The nitrided substrate with thin and non-silicon doped coatings displayed a bigger pitting density than the silicon doped ones. The silicon doped coatings presented isolated pits in some samples, while non silicon doped ones suffered multiple pitting homogeneously distributed with a high degree of DLC damage (**Figure 76**). The samples with a thicker interlayer seem to have less DLC damage than the thin interlayer ones (**Figure 77**).

Similar to what was observed on thick coating samples, the pits on nitrided and thin coating samples have a circular morphology with sharp edges and a concentric crack (**Figure 78**). By means of EDS, an elevated concentration of oxygen was detected, possibly related to the formation of iron and chromium oxides inside the pit (**Figure 79**).

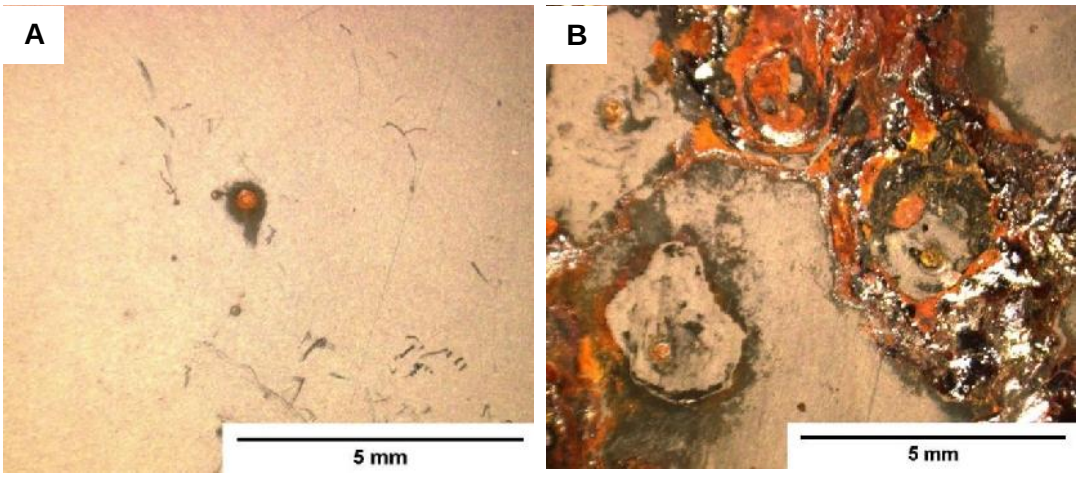

Figure 76. *A) AS-N-IL-TN-Si sample showing isolated pits. B) AS-TN-NSi-NIL-N sample showing multiple pits and reddish oxides.*

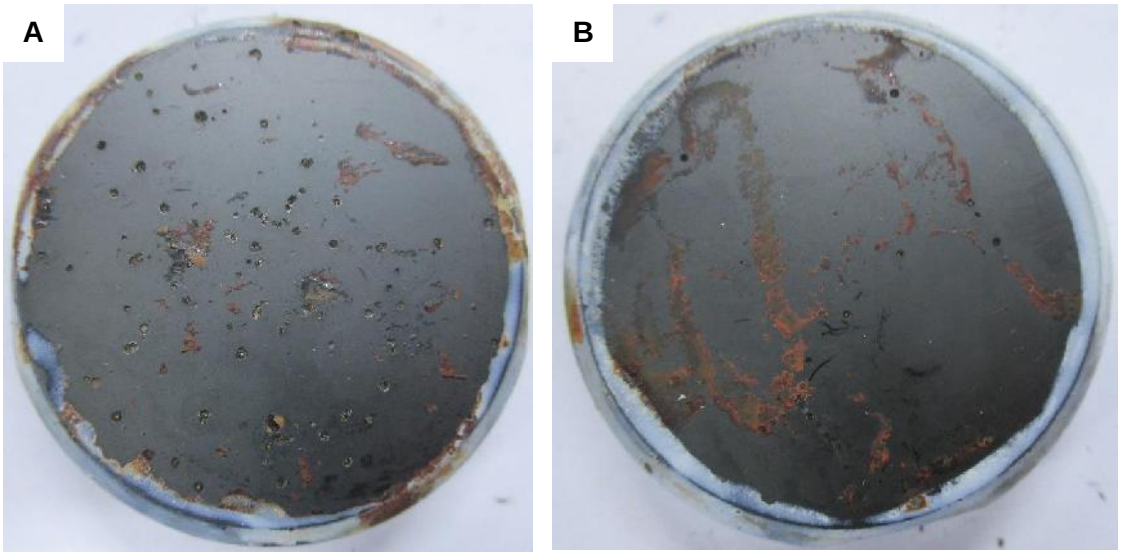

Figure 77. *A) AS-TN-NSi-NIL-N 300-hour sample. B) AS-TN-NSi-IL-N 300-hour sample.*

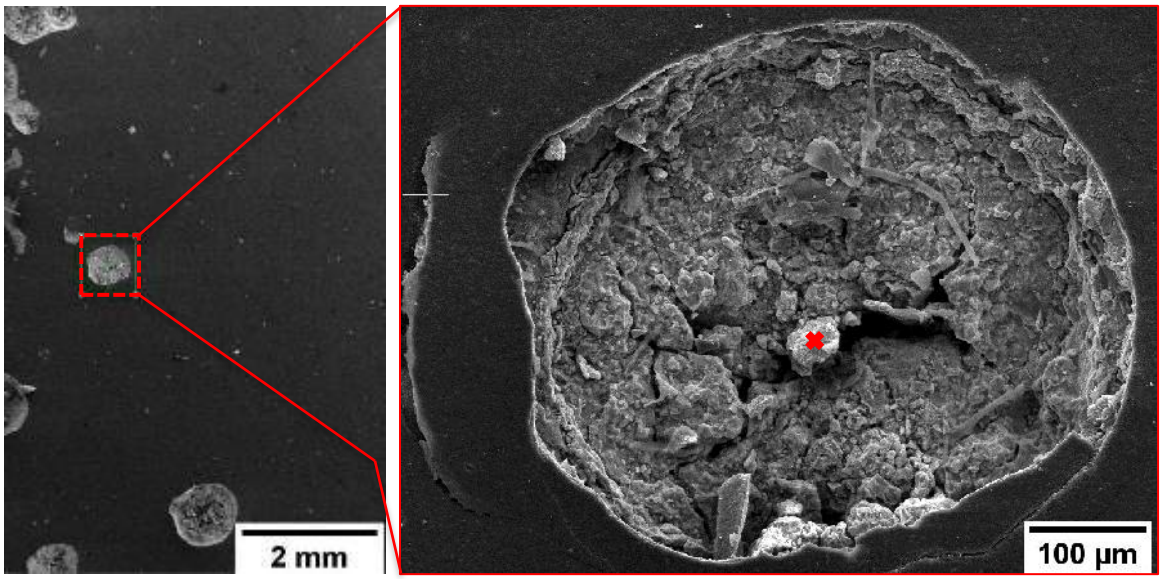

Figure 78. *SEM image showing the pit morphology in a AS-TN-NSi-IL-N sample. A reference point is indicated with a red cross.*

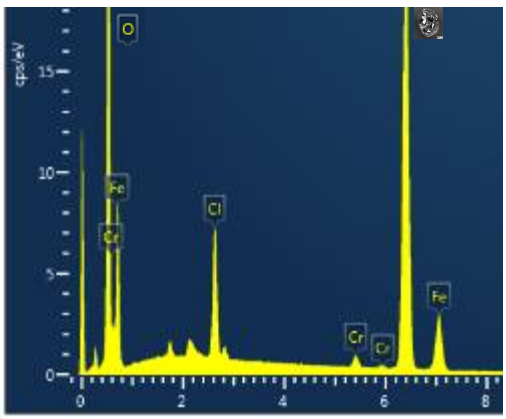

Figure 79. *EDS spectrum of the oxides inside a pit on the AS-TN-NSi-IL-N sample. Reference point* ***Figure 78****.*

The polished samples displayed a similar behavior to the nitrided ones. The thick and silicon doped coated samples suffered no damage, except for punctual isolated pits in two samples, while the non-silicon doped ones displayed multiple pitting (**Figure 80**). The thin coating samples suffered multiple pitting, being the non-silicon doped ones the most affected (**Figure 81**). No effect of the thickness of the silicon interlayer was observed.

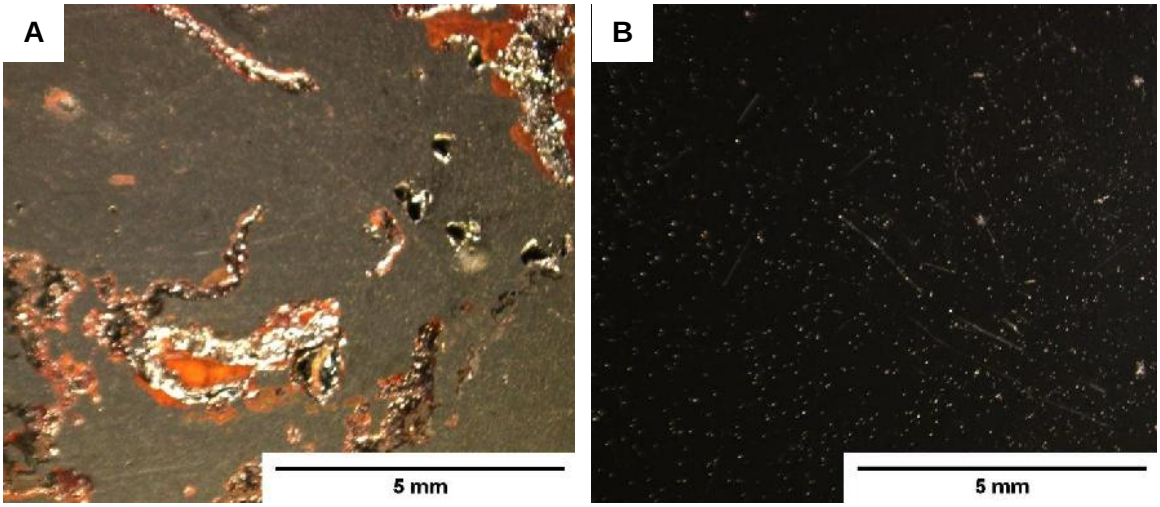

Figure 80. *A) AS-TK-NSi-NIL-P sample. B) AS-TK-Si-NIL-P sample.*

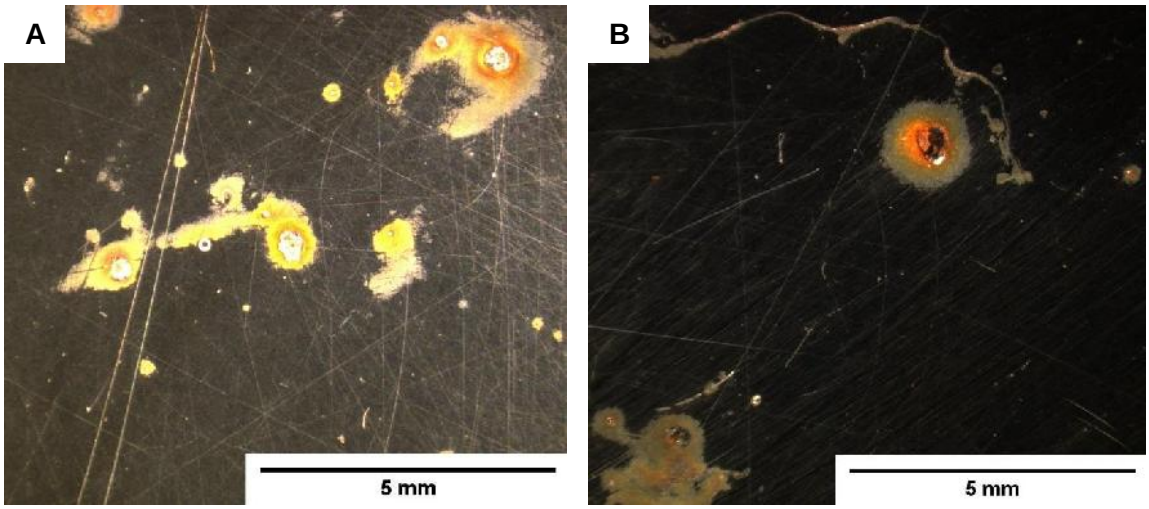

Figure 81. *A) AS-TN-NSi-IL-P sample. B) AS-TN-Si-NIL-P sample.*

In **Figure 82**, a SEM image of a pit can be seen exhibiting a concentric DLC cracking around it. This behaviour could be related to a lateral growth mechanism of the pit. By means of EDS, elevated oxygen, sodium, chlorine, and iron concentrations were detected, possibly related to the presence of iron oxides and sodium chloride (**Figure 83**).

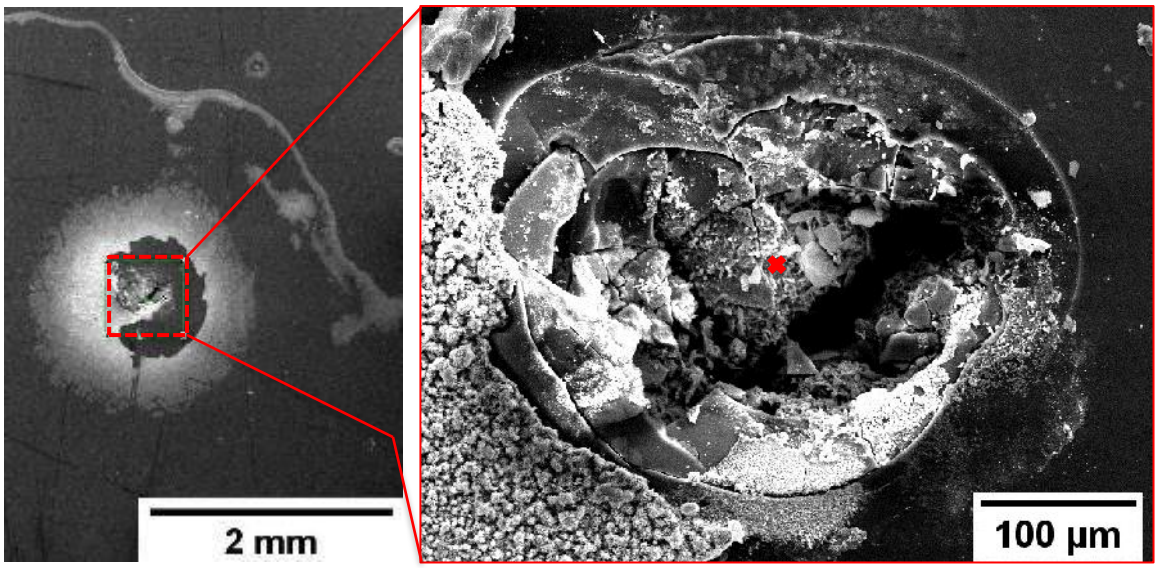

Figure 82. *SEM image showing the pit morphology in a AS-TN-Si-NIL-P sample. A reference point is indicated with a red cross.*

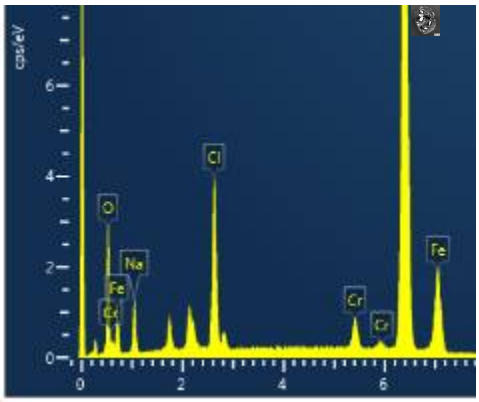

Figure 83. *EDS spectrum of the oxides inside a pit on the AS-TN-Si-NIL-P sample. Reference point* ***Figure 82****.*

4.2.2.2 SS Samples

On the nitrided stainless steel samples the nitriding edge effect played a major role on the observed behaviour, since most of them only suffered damage on this nitriding inhomogeneity.

The nitrided and thick coating samples showed the best corrosion resistance. The silicon doped coating samples did not suffer damage even on the edge effect zones, while the non-silicon doped ones exhibited a directional cracking following the edge effect pattern (**Figure 84**). No effect of the silicon interlayer thickness was observed on the corrosive behaviour.

The corroded area exhibits a directional wave-like pattern along the edge effect zone (**Figure 85**). By means of EDS line scan analysis, it was determined that these waves have elevated concentrations of oxygen, probably related to the deposition of iron and chromium

oxides (**Figure 86**). The light grey areas are mostly composed of iron, chromium and nickel with no traces of oxygen, indicating the absence of corrosion products on the base metal.

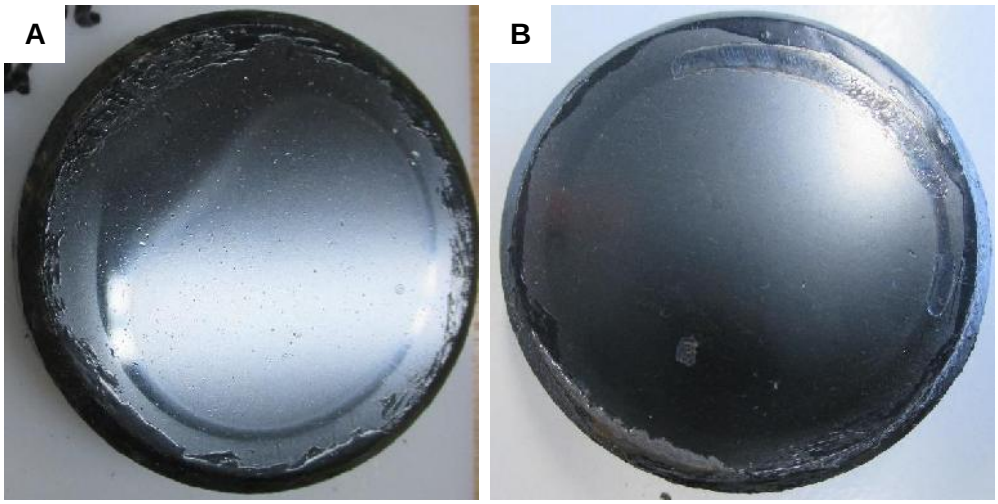

Figure 84. *A) SS-TK-Si-NIL-N 200-hour sample showing no damage after the salt spray test. B) SS-TK-NSi-IL-N 100-hour sample showing damage on the edge effect zone after the salt spray test.*

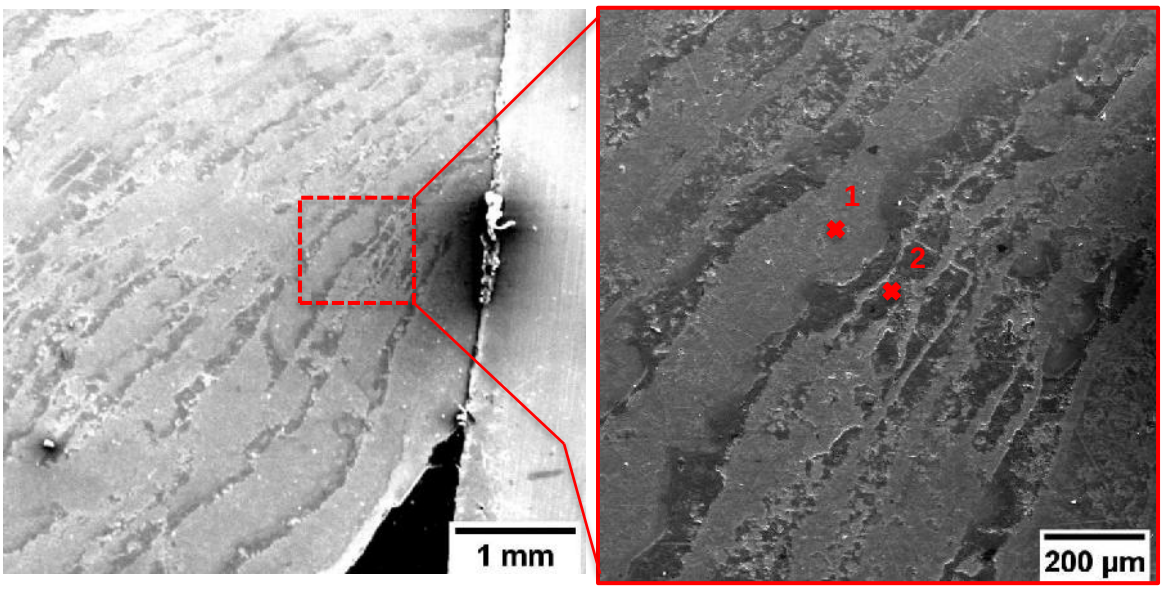

Figure 85. *SEM image showing the damage morphology in a SS-TK-NSi-IL-N sample. A reference point is indicated with a red cross.*

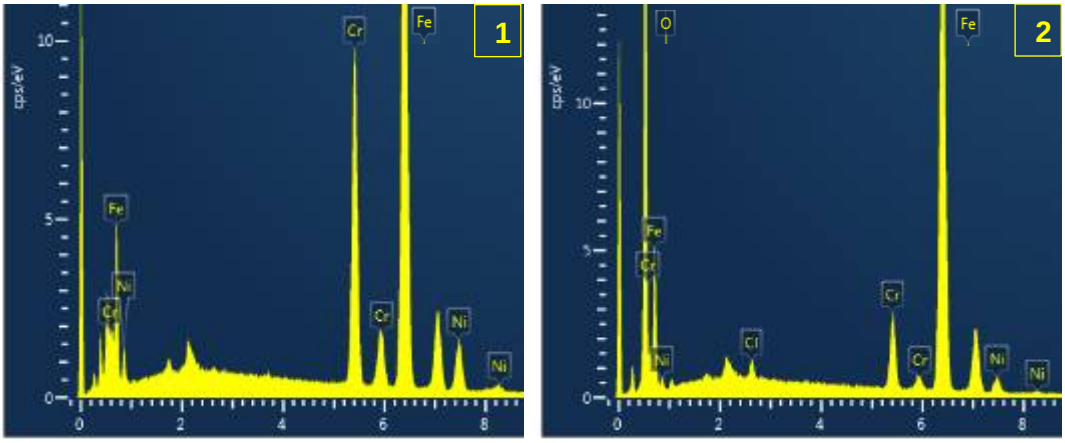

Figure 86. *EDS spectrum of the surface inside a pit on the SS-TK-NSi-IL-N sample. Reference point 1 and 2* ***Figure 85****.*

All the nitrided and thin coating samples suffered corrosion damage only by the nitriding edge effect (**Figure 87**). No differences on the coated samples' behaviour were observed regarding their silicon doping or interlayer thickness.

The corroded area has a similar morphology to that observed on the thick and nitrided coated samples, a wave-like directional pattern along the nitriding edge effect zone (**Figure 88**). The corrosion products display similar compositions as the ones analysed on the nitrided and thick coated samples. **Figure 89** shows the confocal mapping of this region as well.

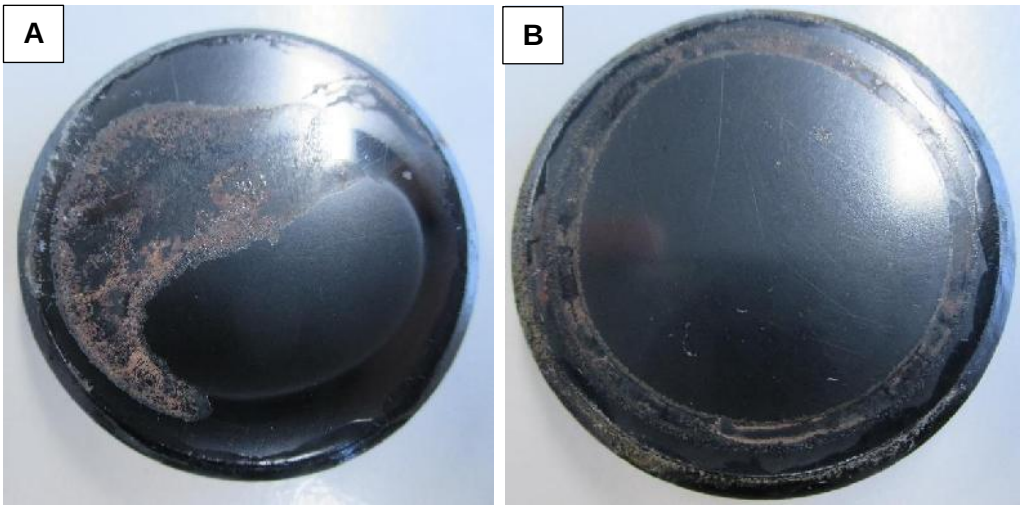

Figure 87. *A) SS-N-NIL-TN-SI 300-hour sample after the salt spray test. B) SS-TN-NSi-IL-N 300-hour sample after the salt spray test.*

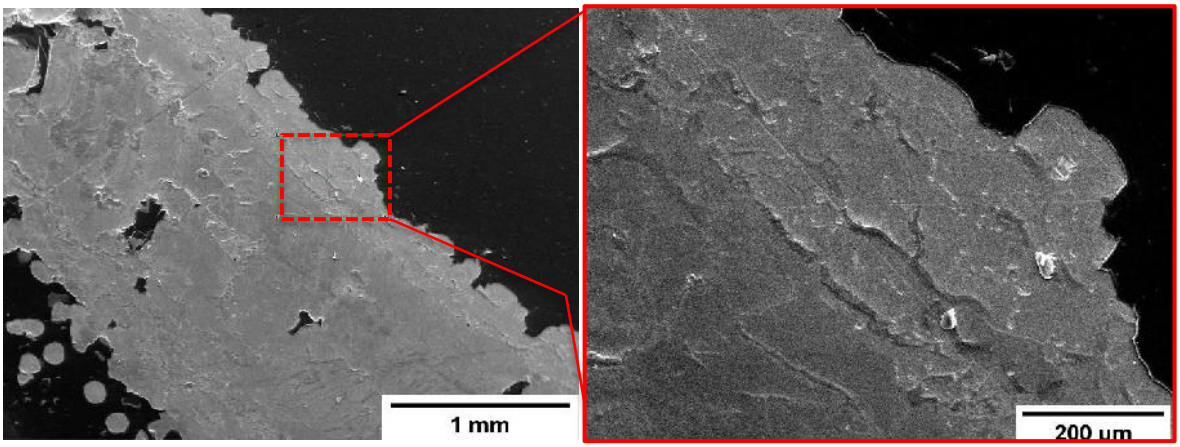

Figure 88. *SEM image showing the damage morphology in a SS-TN-NSi-IL-N sample.*

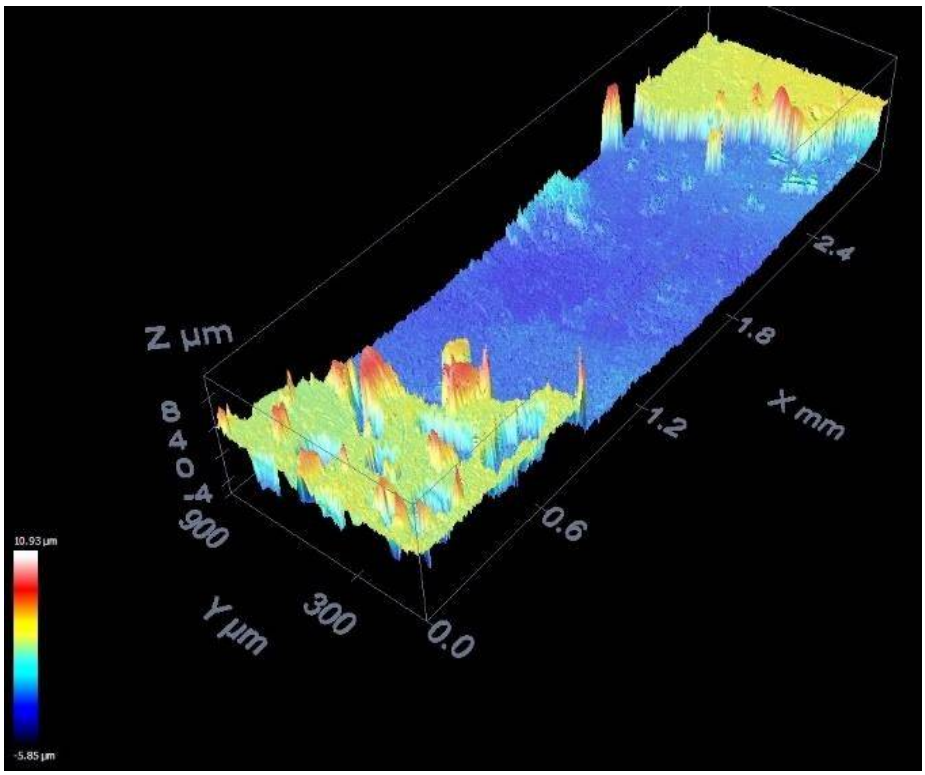

Figure 89. *Confocal 3-D scan showing damage morphology in a SS-TN-NSi-IL-N sample.*

The non nitrided substrate with thick and silicon doped coatings displayed a unique behaviour. It seems that the DLC cracking started on the coating's edges progressing concentrically inwards, as can be seen by comparing a sample at 200-hour exposition time and a sample at 300-hour exposition time (**Figure 90**). The thickness of the interlayer does not seem to have affected this behaviour.

The corroded area displays a wave-like concentric pattern, without any trace of the DLC coating (**Figure 91**). According to the EDS results, the wave-like pattern matches an increase in iron and oxygen, indicating the possible presence of iron oxides (**Figure 92**). The

confocal mapping of this effect is shown in **Figure 93**, where the irregular texture of the surface after the test can be seen.

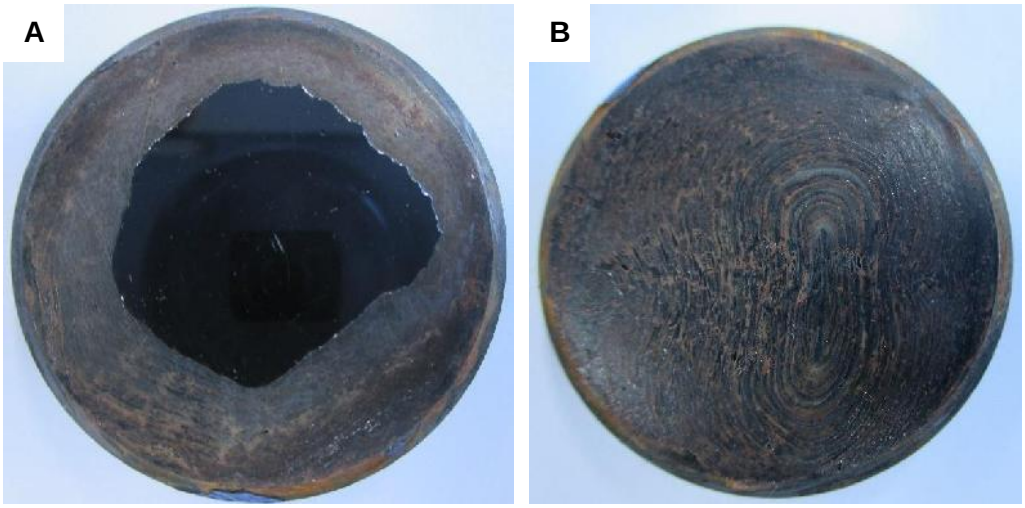

Figure 90. *A) SS-TK-Si-IL-P 200-hour sample. B) SS-TK-Si-IL-P 300-hour sample.*

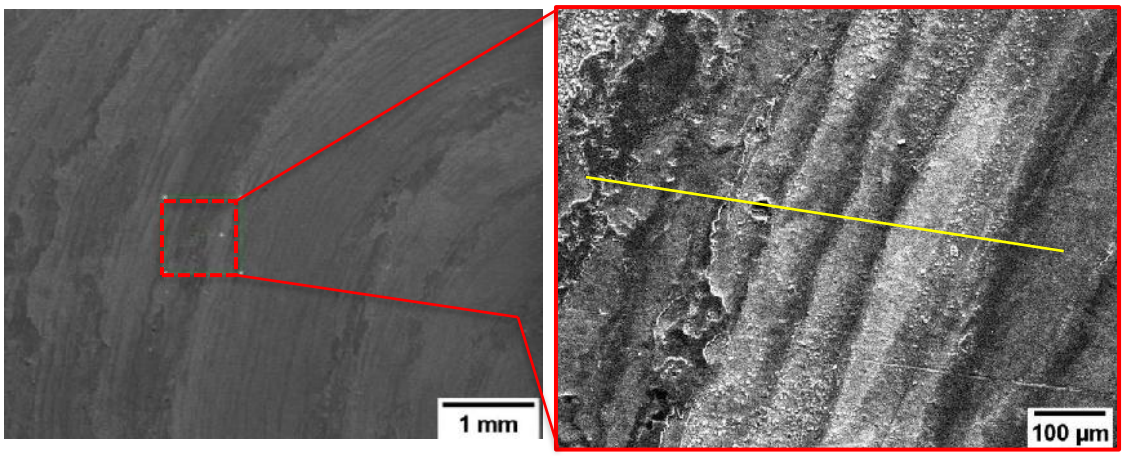

Figure 91. *SEM image showing the damage morphology in a SS-TK-Si-IL-P sample. An EDS line scan line is indicated in yellow.*

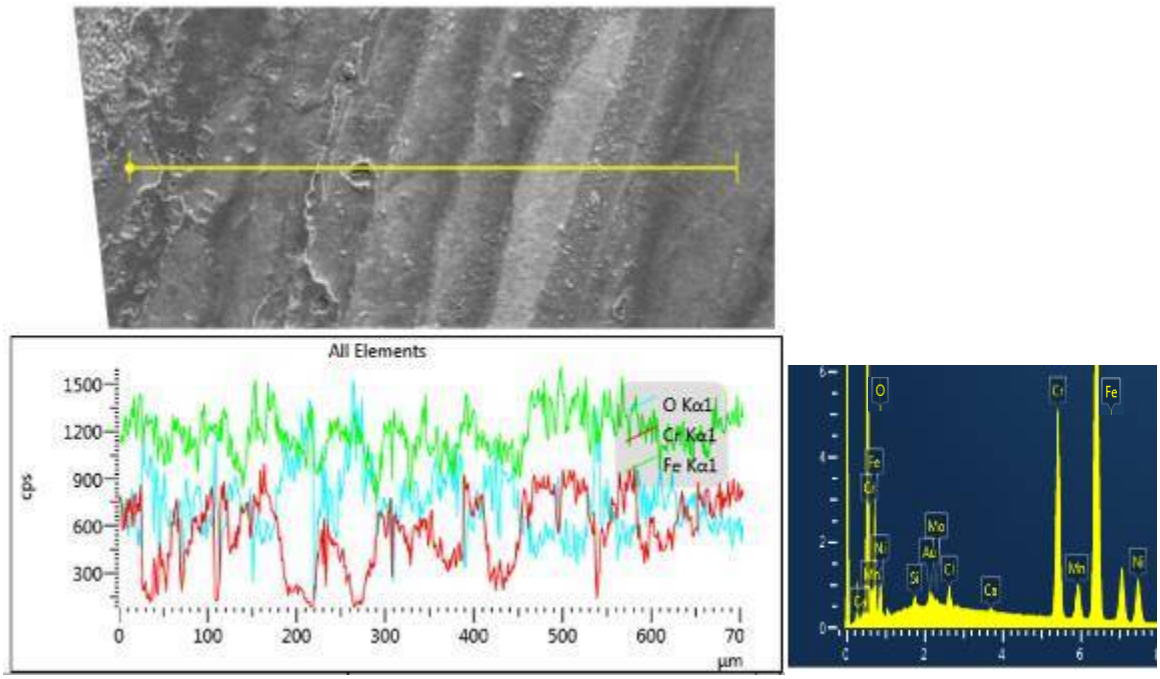

Figure 92. *EDS Linescan performed on the SS-TK-Si-IL-P sample.*

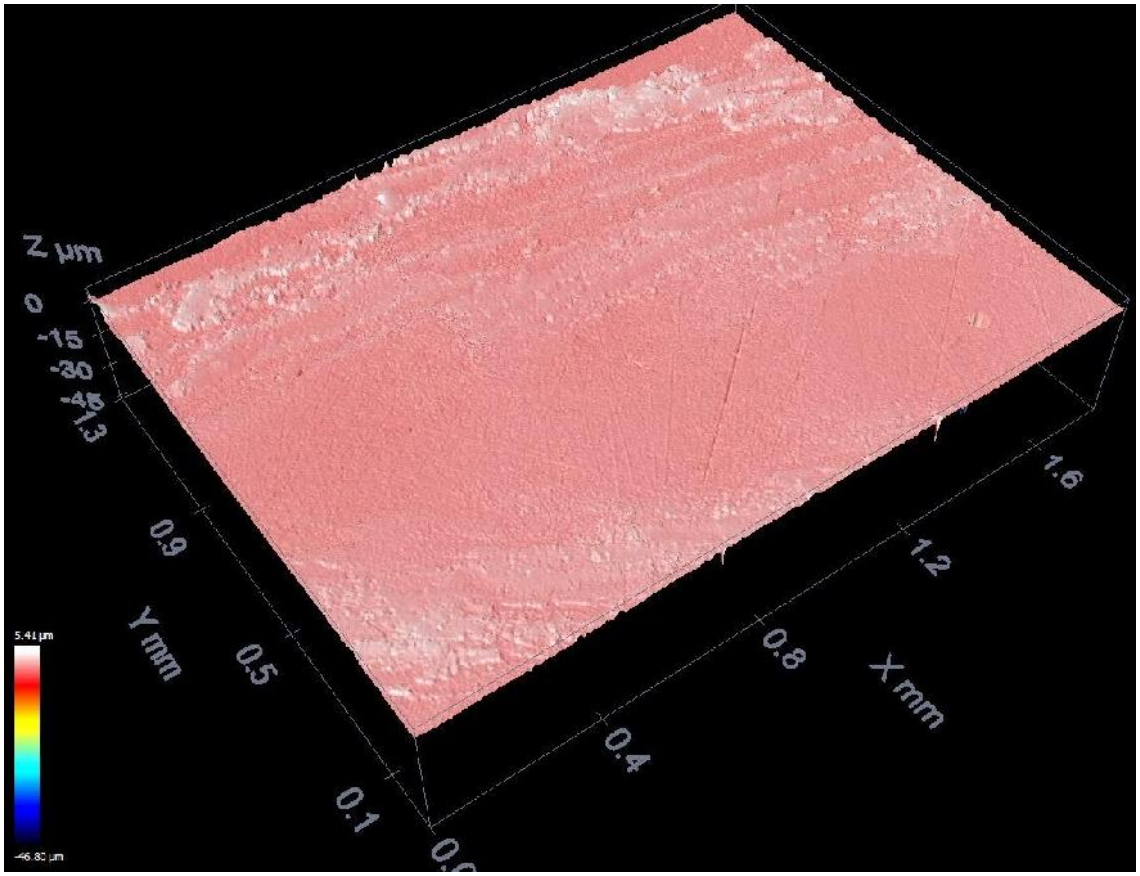

Figure 93. *Confocal mapping of SS-TK-Si-IL-P.*

The non nitrided substrate with thick and not silicon doped coatings exhibited a behaviour similar to the polished and thin samples. Multiple concentric cracking points could be observed after the test (**Figure 94**).

On the corroded area the same wave-like pattern as in the polished and thin samples could be observed, but with some DLC flakes still adhered to the substrate (Figure 95). The EDS results indicate the possible presence of iron and chromium oxides (Figure 96). On Figure 97, the confocal scan of this effect is seen as well, where the difference in heights between the DLC flakes and the revealed substrate can be appreciated.

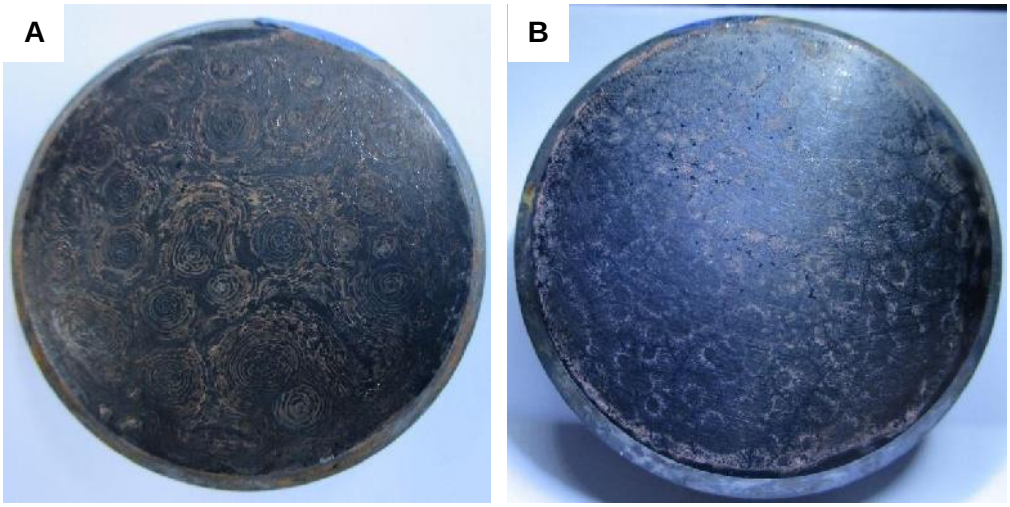

Figure 94. *A) SS-TK-NSi-IL-P sample after 100 hours in the salt spray test. B) SS-TN-NSi-NIL-P sample after 100 hours in the salt spray test.*

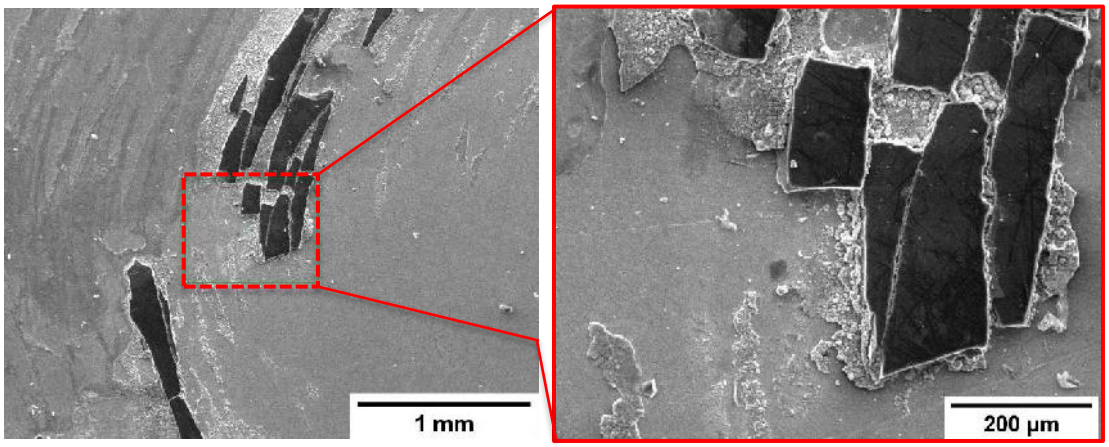

Figure 95. *SEM image showing the damage morphology in a SS-TK-NSi-NIL-P sample.*

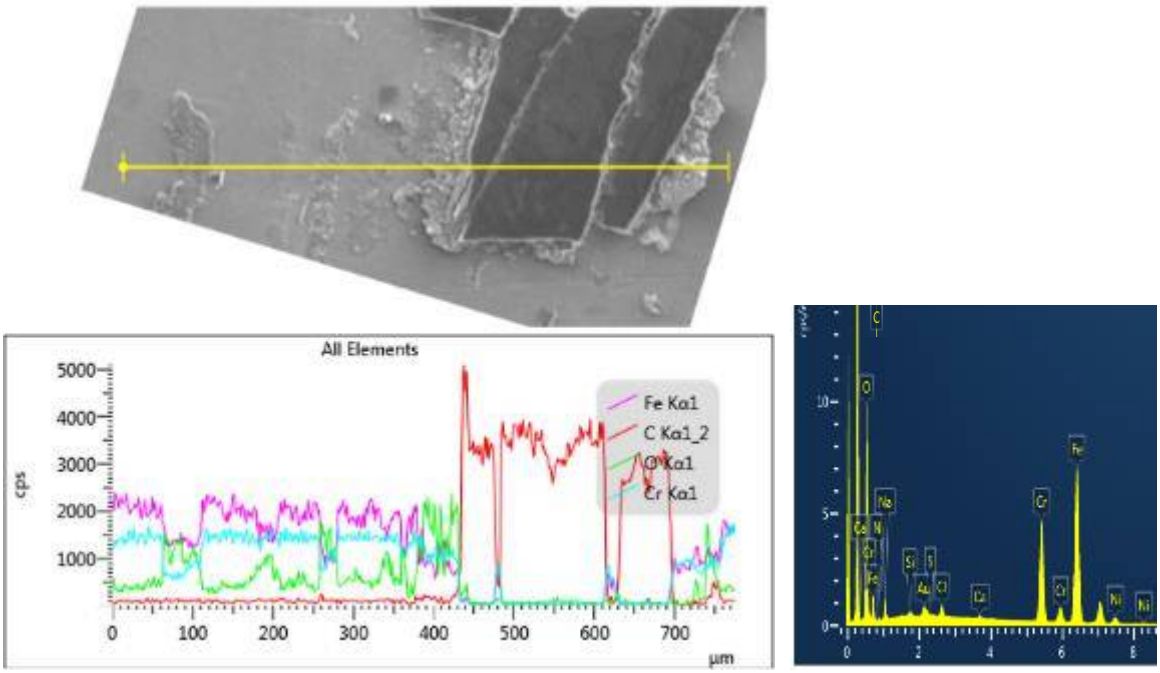

Figure 96. *EDS line scan performed on the SS-TK-NSi-NIL-P sample.*

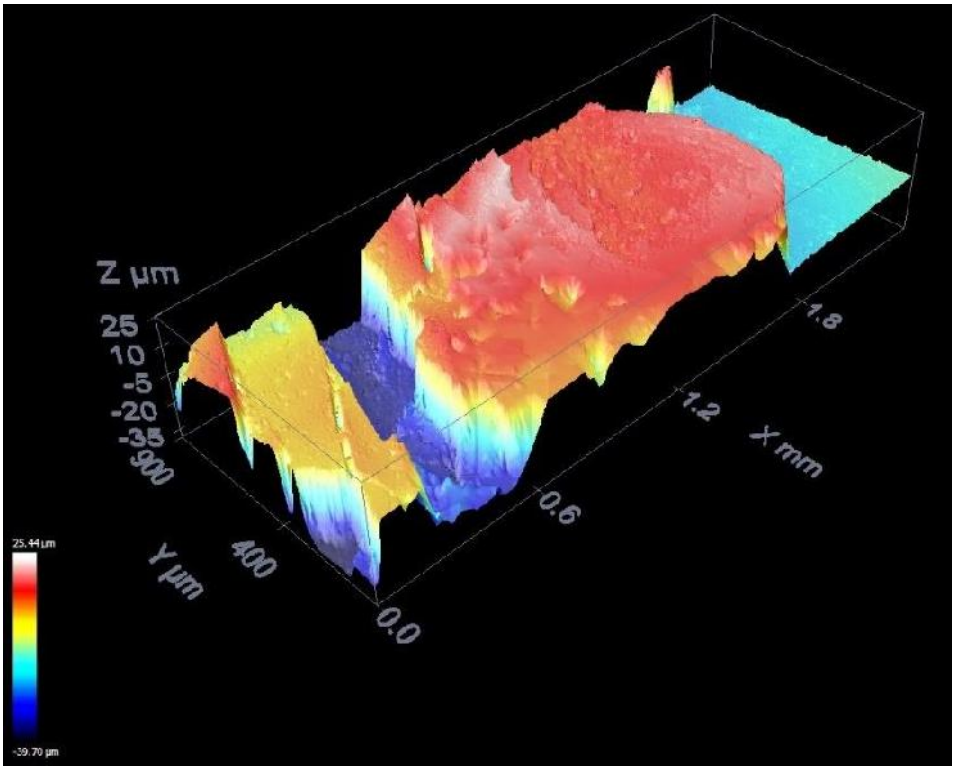

Figure 97. *Confocal mapping of SS-TK-NSi-NIL-P sample.*

4.2.3 Performance Ranking

The WPIM allowed to easily analyse qualitatively the impact the corrosive media had on the different samples. In **Figure 98** the final corrosion performance ranking is presented. It would seem that thick and silicon doped DLC coatings result in the best performance when

exposed to a corrosive media, followed by the substrate´s nitriding pre-treatment. It is worth noting that even when the nitriding edge effect on SS samples, makes them more susceptible of suffering corrosion damage, the substrate´s pre-treatment improves the DLC performance when exposed to corrosive media.

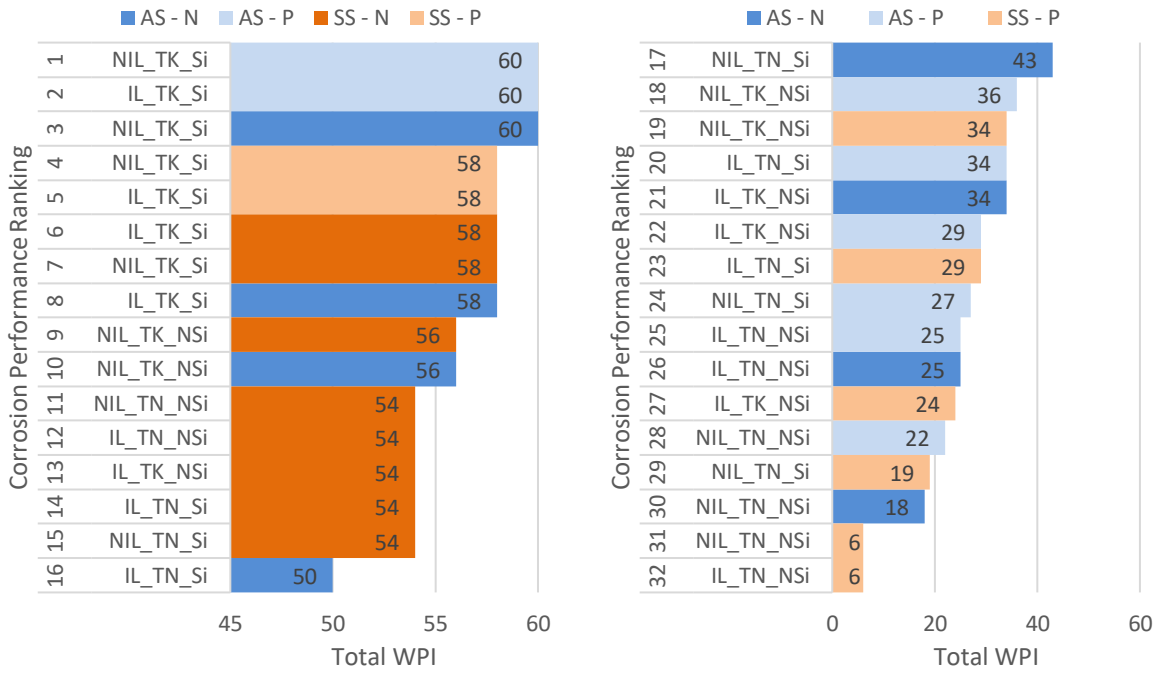

Figure 98. *Corrosion performance ranking final result.*

5 General Analysis

Regarding the different coatings' behaviour when exposed to a corrosive media, the performance ranking helps in identifying the best and worst combination of variables. The variables that appear to have a bigger impact are the coating thickness and its silicon doping, followed by the type of substrate and its pre-treatment. The silicon interlayer thickness did not display a consistent effect.

The DLC coating doping with 0.5%at Si provides a reduction of the film friction coefficient, especially in humid environments, and a hardness increase. Although the silicon doped coatings have a lower sp^3 bond fraction than non-silicon doped ones, the hardness increase is due to higher Si-C and C-C sp^3 bond fraction. In non-silicon doped coatings higher sp^3 bond fraction is due to a higher hydrogen content, since it also includes hydrogen terminated carbon sp^3 bonds that are not related to the diamond-like behaviour, thus lowering these type of coating's mechanical properties. In order to perform the silicon doping, lower reactor power was used, hence, a lower bias voltage. By lowering the bias voltage, a higher hydrogen content and lower defect density are achieved in the coating[50]. The lower defect density in the silicon doped coatings result in less pinhole defects that could connect the

metallic substrate with the corrosive media, thus explaining why these coatings displayed better corrosion resistance. **Figure 99** shows the best 8 coatings, according to the corrosion performance ranking, all of them are silicon doped and thick DLC coatings. A thicker coating reduces the chance of a passing-through defect exposing the metallic substrate to the corrosive media, meaning that thick and silicon doped DLC coatings could have a synergistic effect regarding the coating's pinhole defect density.

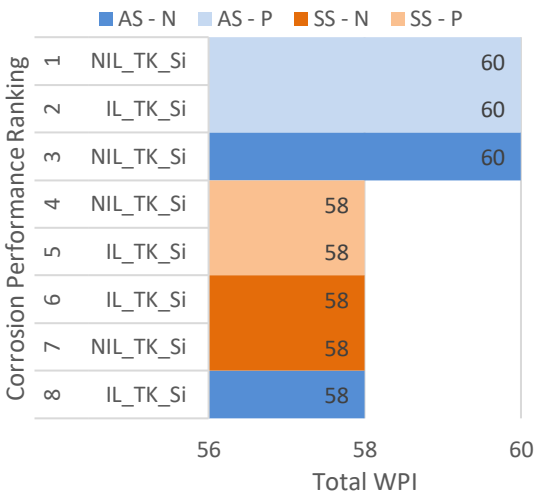

Figure 99. *Best eight variables combination, according to the corrosion performance ranking.*

The DLC coating thickness is a result of the PACVD deposition rate and the deposition time. Besides possibly reducing the formation of passing-through defects, thicker DLC coatings displayed an adherence increase of at least 100% in most cases (**Figure 100**). Thicker coatings have increased load carrying capacity, which results in a more homogeneous stress distribution than in thin films. This effective load distribution reduces the substrate/DLC interphase stress, delaying the coating detachment until higher loads are applied [17,60]. An improved adhesion could result in a higher capacity of the DLC to accommodate the stress produced by corrosion products formation, and its related volumetric expansion, on the substrate/film interphase, achieving less corrosion-induced coating delamination, and thus, less substrate area exposed to the environment. In Figure 100, this relation between adherence and corrosion resistance can be seen, where in all cases but one a better ranked coated sample has a higher adherence value.

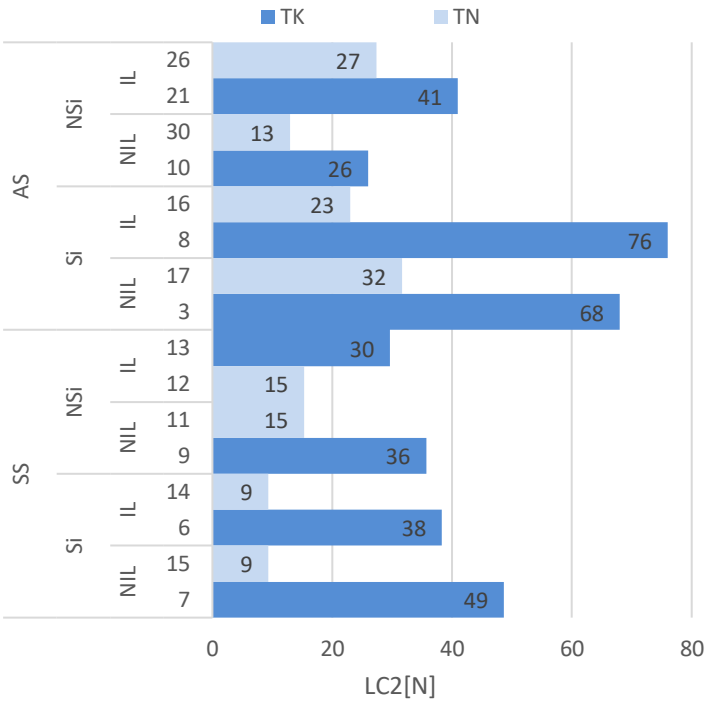

Figure 100. *Adherence (LC2) increase in nitrided (N) DLC coatings, besides sample related variables, the corrosion ranking position is also shown for comparison.*

The third condition that resulted in an improvement of the coated substrates corrosion behaviour is the substrate type and its plasma nitriding pre-treatment. It is a known fact that plasma nitriding on austenitic stainless steel performed below 420°C, like in our case, result in a corrosion resistance increase[61]. All the nitrided stainless steel substrates ended between the 16 best combinations, independently of their coating thickness and silicon doping, regarding their corrosion behaviour. This is consistent with the SS-N substrate having higher corrosion resistance, although, the plasma nitriding edge defect should be avoided, since it represents an inhomogeneity in the nitrided layer and it is a zone of preferential corrosion that compromises the coating's integrity. On the other hand, the AS substrate improves its corrosion resistance with plasma nitriding over 570°C[62], which explains why even the nitrided and coated samples suffer corrosion damage. Additionally, plasma nitriding pre-treatment results in an increase of the superficial roughness of both substrates, bigger for AS coated substrates than SS coated ones.

Finally, the silicon interlayer's thickness did not show to have any effect on the studied properties. This result was consistent along all the tests performed, whether they were corrosion tests or mechanical characterization.

6 Conclusion

6.1 Project conclusions

Thirty-two different DLC-coating/substrate systems were analysed in order to study and compare the proposed variables effect on their mechanical, tribological and corrosion properties.

It was possible to evaluate all the DLC-coating/substrate systems response to two different corrosive environments. In order to effectively compare the different exhibited behaviours, the weighted property index method (WPIM) was applied. The coating thickness and its silicon content resulted the ruling factors to achieve the best corrosion resistance. This effect was mainly related to their synergistic effect in decreasing the passing-through defect density of the DLC coating. The substrate's corrosion resistance also plays a major role, since plasma nitrided AISI 304 coated samples only suffered corrosion damage on the nitriding edge effect zone.

By curve fitting of the obtained Raman spectra from coatings with different silicon content, it was possible to estimate their molecular structure. Which allowed the understanding of the correlations between the DLC silicon coating, the associated PACVD process' bias voltage, and the resulting coating hydrogen content and sp^3 bonds fraction. The silicon doped coatings had lower hydrogen content and sp^3 bonds fraction, but since silicon substitution promotes the formation of Si-C and C-C sp^3 bonds, an increase in the coating hardness was measured. Additionally, the lower bias voltage in the silicon doped coating's deposition process was related to the mentioned decrease in the defect density.

The DLC coating/substrate systems mechanical and tribological characterization was performed. Besides the already mentioned hardness increasing effect of the silicon doping variable, the scratch testing adherence results and their fractographic behaviour was studied. The adherence between the substrate and the DLC coating increased with the coating's thickness, due to an increased load carrying capacity, and also with its superficial roughness, mainly related to the substrate roughness increase after the plasma nitriding process. Coating failure modes are related to the coating-substrate interaction under an applied load. When the DLC coating admits certain degree of deformation and the substrate is soft enough to allow it, the coatings develop ductile failure modes. On the other hand, hard coatings that are more restricted on the degree of deformation will result in brittle failure modes.

During our time in Austria, we designed and manufactured a confocal microscope compatible sample holder with a micrometric reference point that allowed us to precisely perform the topographic mapping of large-scale areas of the coated samples, before and after

the corrosion tests took place. Since this achievement was a trial-and-error process it allowed us to improve our understanding of this technique and correct several learning curve related errors.

6.2 Difficulties

Some difficulties were faced during the project development, due to a series of unexpected factors. The two main causes of these difficulties were the limited time we stayed in Wels, which did not let us complete every test planned, and the current COVID-19 pandemic lockdown, that did not allow us to finish the planned activities in the INTEMA facilities in Mar del Plata.

Firstly, a systematic study by Electrochemical Impedance Spectroscopy analysis was started in early March 2020, that could not be finished due to the lockdown. The EIS cell was designed by us in a CAD software and then manufactured (**Figure 101**), although, less than half of the runs were performed, but it had to be terminated as the INTEMA facilities were shut down in mid-March. This test would have allowed us to make more significant conclusions regarding corrosion behaviour of the samples and corroborate with further measurements the evidence seen in photographs and microscopic images. Additionally, the electrical conductivity of the coating with and without silicon doping could have been studied, since it was one of the original objectives of this final project. The impossibility of finishing the EIS tests forced us to change the project's scope and perform only a qualitative analysis on the corrosion resistance of the coated samples.

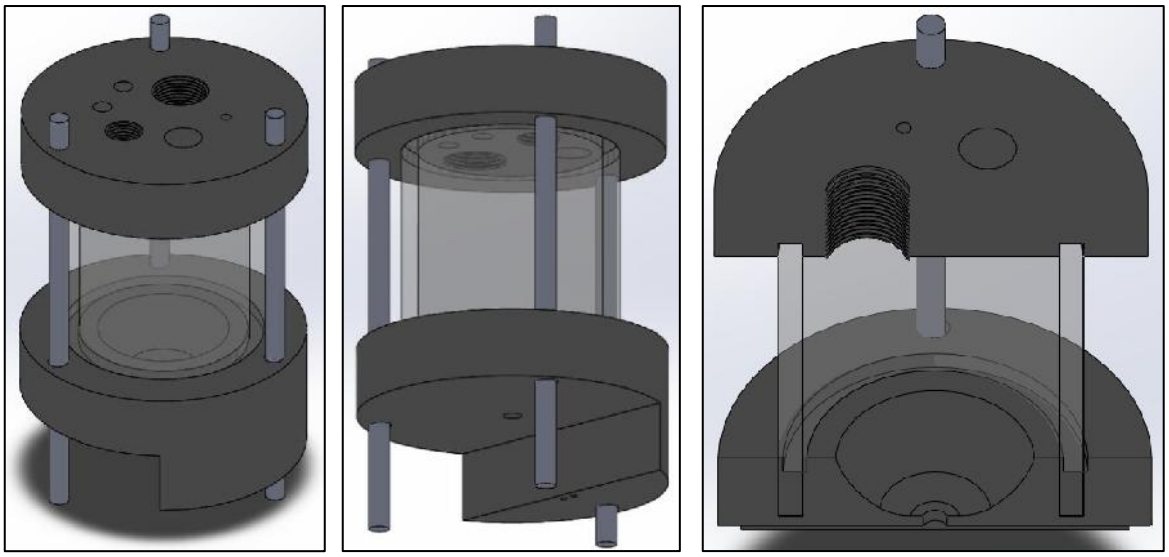

Figure 101. *Schematic CAD design of the manufactured electrochemical cell.*

Secondly, the confocal scanning on pin-on-disk test samples was expected to be done in more samples, for better statistical results. This could not be completed in time before our

return to Argentina, since some conclusions could be extracted from the partial tests performed, and with the friction coefficient being one of the most appealing properties of DLC coatings, the obtained results were presented anyway. A more thorough analysis could have been done with more samples scanned.

Lastly, the AISI 304 nitrided samples showed an unexpected plasma nitriding edge effect which resulted to be a defect susceptible of suffering preferential corrosion damage. This pre-treatment defect can be modified by varying some of its parameters, like the reactor vacuum pressure, but it is a phenomenon that it has yet to be understood in order to eliminate it.

6.3 Future work

Due to the large number of samples used and conditions tested, there are some issues that could be addressed in future investigations.

As mentioned in different parts of this work, the condition labelled as “no interlayer” has actually a thin interlayer of a few nanometres. This is done to avoid delamination, but it would be interesting to test the same conditions tested in our project in samples with truly no interlayer, in order to have a better comparison of the results.

In a similar way, the PACVD deposition process for the silicon doped coatings was done at a lower reactor power (150W) than in the case of the non-silicon doped ones (500W). This parameter greatly modifies the deposition rate of the DLC and the hydrogen content of the DLC, meaning that some variables that could be modified by the reactor power or coating chemistry could not be comparable. For example, a TK-Si sample needed a 30-hour process in order to achieve around 28 µm thickness while a TK-NSi sample took only 10 hours to achieve a similar value. In order to evaluate the silicon doping or reactor power effect on properties like, for example, coating thickness, a study with fixed reactor power should be designed.

As mentioned in section 6.2, Pin on Disk confocal scanning and EIS test could not be finished for this project. EIS could be done for a quantitative approach regarding corrosion resistance. A complete Pin on Disk test, on the other hand, would give a better mechanical characterization of the DLC films.

After analysing the Raman results, we realized that, in order to analyse the effect of silicon doping on the DLC molecular structure a reactor power value should be fixed. The reactor power affects the hydrogen content of the DLC, which affects its molecular structure, thus making more difficult to isolate and analyse the silicon addition effect.

6.4 Final Thoughts

In order to analyse all the variables possible combinations and provide consistent statistic data dispersion, over 300 samples were studied. This feat implied the development of advanced data management skills, curve fitting and image processing software skills. As well as the capability to learn and apply the wide range of techniques that were kindly made available for us by our colleagues in Upper Austria.

The experience we lived in the FHOÖ was invaluable and certainly marked us for life, everyone treated us kindly and patiently, and we made the most of it. It does not matter where life takes us from now on, we will never forget all the things we learned and the places and people that we met due to this final project.

The pursue of knowledge was the driving force that allowed us to overcome all kinds of obstacles in order to complete this Materials Engineering final project.

7 References

[1] Lifshitz, Y. (1999). Diamond-like carbon—present status. *Diamond and Related materials*, *8*(8-9), 1659-1676.

[2] Donnet, C., & Erdemir, A. (Eds.). (2007). *Tribology of diamond-like carbon films: fundamentals and applications*. Springer Science & Business Media.

[3] Vetter, J. (2014). 60 years of DLC coatings: historical highlights and technical review of cathodic arc processes to synthesize various DLC types, and their evolution for industrial applications. *Surface and Coatings Technology*, *257*, 213-240.

[4] Erdemir, A., & Donnet, C. (2006). Tribology of diamond-like carbon films: recent progress and future prospects. *Journal of Physics D: Applied Physics*, *39*(18), R311.

[5] Grill, A. (1999). Diamond-like carbon: state of the art. *Diamond and related materials*, 8, 428-434.

[6] Papakonstantinou, P., Zhao, J. F., Lemoine, P., McAdams, E. T., & McLaughlin, J. A. (2002). The effects of Si incorporation on the electrochemical and nanomechanical properties of DLC thin films. *Diamond and related materials*, *11*(3-6), 1074-1080.

[7] Choi, J., Kawaguchi, M., Kato, T., & Ikeyama, M. (2007). Deposition of Si-DLC film and its microstructural, tribological and corrosion properties. *Microsystem technologies*, *13*(8-10), 1353-1358.

[8] Lee, K. R., Kim, M. G., Cho, S. J., Eun, K. Y., & Seong, T. Y. (1997). Structural dependence of mechanical properties of Si incorporated diamond-like carbon films deposited by RF plasma-assisted chemical vapour deposition. *Thin Solid Films*, *308*, 263-267.

[9] Moolsradoo, N., & Watanabe, S. (2017). Influence of elements on the corrosion resistance of DLC films. *Advances in Materials Science and Engineering*, 2017.

[10] Dalibon, E. L., Trava-Airoldi, V., Pereira, L. A., Cabo, A., & Brühl, S. P. (2014). Wear resistance of nitrided and DLC coated PH stainless steel. *Surface and Coatings Technology*, *255*, 22-27.

[11] Cemin, F., Bim, L. T., Menezes, C. M., da Costa, M. M., Baumvol, I. J. R., Alvarez, F., & Figueroa, C. A. (2015). The influence of different silicon adhesion interlayers on the tribological behavior of DLC thin films deposited on steel by EC-PECVD. *Surface and Coatings Technology*, *283*, 115-121.

[12] Capote, G., Lugo, D. C., Gutiérrez, J. M., Mastrapa, G. C., & Trava-Airoldi, V. J. (2018). Effect of amorphous silicon interlayer on the adherence of amorphous hydrogenated carbon coatings deposited on several metallic surfaces. *Surface and Coatings Technology*, *344*, 644-655.

[13] Aghajani, H., & Behrangi, S. (2017). *Plasma nitriding of steels*. Springer International Publishing.

[14] Moriguchi, H., Ohara, H., & Tsujioka, M. (2016). History and applications of diamond-like carbon manufacturing processes. *Sei Technical Review*, *82*, 52-58.

[15] Hamedani, Y., Macha, P., Bunning, T. J., Naik, R. R., & Vasudev, M. C. (2016). Plasma-enhanced chemical vapor deposition: Where we are and the outlook for the future (pp. 247-280). *InTech.*

[16] Mattox, D. M., & Mattox, V. H. (2003). *Vacuum coating technology*. William Andrew Publishing, New York.

[17] Forsich, C., Dipolt, C., Heim, D., Mueller, T., Gebeshuber, A., Holecek, R., & Lugmair, C. (2014). Potential of thick aC: H: Si films as substitute for chromium plating. *Surface and Coatings Technology*, *241*, 86-92.

[18] Jones, D. (1996). *Principles and Prevention of Corrosion. Second edition.* Prentice-Hall.

[19] Olzon-Dionysio, M. C. (2010). Influences of plasma nitriding edge effect on properties of 316 L stainless steel. *Surface and Coatings Technology*, 204, 3623-3628.

[20] Matthews, A. E. (1994). Engineering applications for diamond-like carbon. *Diamond and related materials*, 3, 902-911.

[21] Santos, L. T.-A. (2006). DLC cold welding prevention films on a Ti6Al4V. *Surface and coatings technology*, 200, 2587-2593.

[22] Cramer, S. D., Covino, B. S., & Moosbrugger, C. (2005). *ASM handbook volume 13b: corrosion: materials* (Vol. 13). Ohio: ASM International.

[23] HORIBA technology. (n.d.). *What is Raman Spectroscopy?* Retrieved 31/10/2020, from *https://www.horiba.com/en_en/raman-imaging-and-spectroscopy/*

[24] Nano Photon Corporation (n.d.). Lesson 1. Basic of Raman scattering. Retrieved 8/12/2020, from https://www.nanophoton.net/lecture-room/raman-spectroscopy/lesson-1-1

[25] Cui, W. L. (2010). Quantitative measurements of sp3 content in DLC films with Raman spectroscopy. *Surface and Coatings Technology*, 205, 1995–1999.

[26] Choi, S. K. (1997). Deposition of diamondlike carbon films by plasma enhanced chemical vapour deposition. *Materials Science and Engineering*, 46, 133-136.

[27] PVD Coatings UK. (n.d.). *Coating thickness tester*. Retrieved 31/10/2020, from *https://web.archive.org/web/20090628230613/http:/pvd-coatings.co.uk/coating-thickness-tester.htm*

[28] Rupetsov, V., & Minchev, R. (2016, June). Experimental calo tester for the coating thickness measurement. In *15th International Scientific Conference Smolyan, Bulgaria* (pp. 188-191).

[29] Schuh, C. A. (2006). Nanoindentation studies of materials. *Materials today*, *9*(5), 32-40.

[30] Pharr, G. M., & Oliver, W. C. (1992). Measurement of thin film mechanical properties using nanoindentation. *Mrs Bulletin*, *17*(7), 28-33.

[31] McKeen, L. W. (2016). *Fatigue and tribological properties of plastics and elastomers*. William Andrew.

[32] Bruker Nano Surfaces. (n.d.). *Advanced Scratch Testing for Evaluation of Coatings.* Retrieved 31/10/2020, from *https://www.bruker.com/fileadmin/user_upload/8-PDF-Docs/SurfaceAnalysis/TMT/Webinars/Advanced-Scratch-Testing-for-Evaluation-of-Coatings-Slides.pdf*

[33] Li, D., & Herrmann, A. Industrial coating scratch and wear evaluation.

[34] Bull, S. (1991). Failure modes in scratch adhesion testing. *Surface and Coatings Technology*, 50, 25-32.

[35] Ghabchi, A., Sampath, S., Holmberg, K., & Varis, T. (2014). Damage mechanisms and cracking behavior of thermal sprayed WC–CoCr coating under scratch testing. *Wear*, *313*(1-2), 97-105.

[36] Gu, W., & Yao, Z. (2011). Evaluation of surface cracking in micron and sub-micron scale scratch tests for optical glass BK7. *Journal of mechanical science and technology*, *25*(5), 1167.

[37] Holmberg, K., Laukkanen, A., Ronkainen, H., Wallin, K., Varjus, S., & Koskinen, J. (2006). Tribological contact analysis of a rigid ball sliding on a hard coated surface: Part I: Modelling stresses and strains. *Surface and Coatings Technology*, *200*(12-13), 3793-3809.

[38] Corrosionpedia. (n.d.). *Salt Spray Testing*. Retrieved 31/10/2020, from *https://www.corrosionpedia.com/definition/1394/salt-spray-testing*

[39] Ascott Analytical. (n.d.). CCT Chambers – Salt Spray Mode – how it works. Retrieved 8/12/2020 from https://www.ascott-analytical.com/how-chambers-work/cct-chambers-salt-spray-mode-how-it-works

[40] Corrosionpedia. (n.d.). *Immersion Test*. Retrieved 31/10/2020, from *https://www.corrosionpedia.com/definition/1243/immersion-test*

[41] Evans, A. A., & Donahue, R. E. (2008). Laser scanning confocal microscopy: a potential technique for the study of lithic microwear. *Journal of Archaeological Science*, *35*(8), 2223-2230.

[42] Solomon, M. J.; Kogan, M. (2005). Confocal Optical Microscopy. Encyclopedia of Condensed Matter Physics.

[43] Girão, A. V., Caputo, G., & Ferro, M. C. (2017). Application of Scanning Electron Microscopy–Energy Dispersive X-Ray Spectroscopy (SEM-EDS). In *Comprehensive Analytical Chemistry* (Vol. 75, pp. 153-168). Elsevier.

[44] Thermofisher Scientific. (n.d.). *EDX Analysis with a Scanning Electron Microscope (SEM): How does it work?* Retrieved 31/10/2020, from *https://www.thermofisher.com/blog/microscopy/edx-analysis-with-sem-how-does-it-work*

[45] Findik, F., & Turan, K. (2012). Materials selection for lighter wagon design with a weighted property index method. *Materials & Design*, *37*, 470-477.

[46] All Metals and Forge Group. (n.d.). *AISI / SAE 4140 alloy steel.* Retrieved 31/10/2020, from *https://www.steelforge.com/alloy-steel-4140/*

[47] Sinha, A., Wu, C. & Liu, G. (2016). Nomenclature: Steel. In: R. Colás and G. Totten, ed., *Encyclopedia of Iron, Steel, and Their Alloys*. CRC Press, 2434-2488.

[48] All Metals and Forge Group. (n.d.). *Stainless Steel 304 & Stainless Steel 304L forgings.* Retrieved 31/10/2020, from *https://www.steelforge.com/stainless-304-stainless-304l/*

[49] Gasco Owens, A., Brühl, S., Simison, S. N., Forsich, C., & Heim, D. (2015). Comparison of tribological properties of stainless steel with hard and soft DLC coatings.

[50] Casiraghi, C. F. A. R. J., Ferrari, A. C., & Robertson, J. (2005). Raman spectroscopy of hydrogenated amorphous carbons. *Physical Review B*, *72*(8), 085401.

[51] Ferrari, A. C., & Robertson, J. (2004). Raman spectroscopy of amorphous, nanostructured, diamond–like carbon, and nanodiamond. *Philosophical Transactions of the Royal Society of London. Series A: Mathematical, Physical and Engineering Sciences*, *362*(1824), 2477-2512.

[52] Singh, R. K., Xie, Z. H., Bendavid, A., Martin, P. J., Munroe, P., & Hoffman, M. (2008). Effect of substrate roughness on the contact damage of DLC coatings. *Diamond and related materials*, *17*(6), 975-979.

[53] Salvadori, M. C., Martins, D. R., & Cattani, M. (2006). DLC coating roughness as a function of film thickness. *Surface and Coatings Technology*, *200*(16-17), 5119-5122.

[54] Delfín, F. A., Brühl, S. P., Forsich, C., & Heim, D. (2018). Carbon based DLC films: Influence of the processing parameters on the structure and properties. *Matéria (Rio de Janeiro)*, *23*(2).

[55] Wu, W. J., & Hon, M. H. (1997). The structure and residual stress in Si containing diamond-like carbon coating. *Thin Solid Films*, *307*(1-2), 1-5.

[56] Fujimoto, S., Ohtake, N., & Takai, O. (2011). Mechanical properties of silicon-doped diamond-like carbon films prepared by pulse-plasma chemical vapor deposition. *Surface and coatings Technology*, *206*(5), 1011-1015.

[57] Lee, K. R., Kim, M. G., Cho, S. J., Eun, K. Y., & Seong, T. Y. (1997). Structural dependence of mechanical properties of Si incorporated diamond-like carbon films deposited by RF plasma-assisted chemical vapour deposition. *Thin Solid Films*, *308*, 263-267.

[58] Hofmann, D., Kunkel, S., Bewilogua, K., & Wittorf, R. (2013). From DLC to Si-DLC based layer systems with optimized properties for tribological applications. *Surface and Coatings Technology*, *215*, 357-363.

[59] Donnet, C. (1998). Recent progress on the tribology of doped diamond-like and carbon alloy coatings: a review. *Surface and Coating technology,* 100, 180-186.

[60] Dalibón, E. L., Escalada, L., Simison, S., Forsich, C., Heim, D., & Brühl, S. P. (2017). Mechanical and corrosion behavior of thick and soft DLC coatings. *Surface and Coatings Technology*, *312*, 101-109.

[61] Liang, W. (2003). Surface modification of AISI 304 austenitic stainless steel by plasma nitriding. *Applied surface science*, *211*(1-4), 308-314.

[62] Ebrahimi, M., Sohi, M. H., Raouf, A. H., & Mahboubi, F. (2010). Effect of plasma nitriding temperature on the corrosion behavior of AISI 4140 steel before and after oxidation. *Surface and Coatings Technology*, *205*, S261-S266.